MULTI-REGIME TURBULENT COMBUSTION MODELING USING LARGE EDDY SIMULATION/PROBABILITY DENSITY FUNCTION

A Thesis

Submitted to the Faculty

of

Purdue University

by

Shashank S. Kashyap

In Partial Fulfillment of the

Requirements for the Degree

of

Master of Science

August 2019

Purdue University

West Lafayette, Indiana

THE PURDUE UNIVERSITY GRADUATE SCHOOL
STATEMENT OF THESIS APPROVAL

Dr. Haifeng Wang, Chair

School of Aeronautics and Astronautics

Dr. Li Qiao

School of Aeronautics and Astronautics

Dr. Terrence R. Meyer

School of Mechanical Engineering

Approved by:

Dr. Wayne Chen

Head of the School Graduate Program

I would like to dedicate this thesis to my parents, S V Satyanarayana and Sudha S Narayana as well as my brother, Siddarth S Kashyap.

ACKNOWLEDGMENTS

This journey of completing my thesis would not be complete by thanking all the people who were involved in many capacities to support, guide and encourage me.

I would like to thank my parents and my brother who have constantly encouraged me throughout my Masters studies. They have taught me to be strong during hard times and remain thankful for everything life has offered till now. They have always pushed me to strive for the best results but also enjoy the journey all along.

Secondly, this thesis would not be possible without my advisor, Dr. Haifeng Wang. I would like to especially thank him for having the confidence in me and including me to be part of his research group: CEPL (Computational Energy and Propulsion Lab). His constant guidance and criticism has always pushed me in the right direction as well as deliver the right results. I would like to also thank Dr. Terrence Meyer and Dr. Li Qiao for agreeing to be part of my advisory committee. I am also very grateful for my colleagues in the research group: Dr. Chao Han (graduated), Pei Zhang, Tejas Pant, Jie Tao, Menglin Ni (graduated), Tianfang Xie, Abhinand Ayyaswamy and Dr. Meng Xia. Their experience and support has made my thesis journey smooth and enjoyable. I would like to especially thank Pei Zhang for helping me understand the research code and answering any constant questions I had with the research.

I would like to thank the Department of Computer Science in Purdue University for financially supporting my graduate studies. This research would not be possible without the computational resources and technical support provided by ITaP (Information Technology at Purdue) Research Computing.

This acknowledgment would be incomplete without thanking all the people, who were either directly or indirectly involved in supporting and encouraging me through this amazing journey of Masters studies.

TABLE OF CONTENTS

Page

LIST OF FIGURES

Figure Page

Figure Page

Figure Page

SYMBOLS

$\bar{\rho}$	large eddy simulation mean density
$\widetilde{u}_i$	resolved velocity in the i^{th} direction
x_i	spatial coordinate in i^{th} direction
t	time
T_{ij}	residual turbulent stress
S_{ij}	strain rate tensor
δ_{ij}	Kronecker delta
μ_t	residual turbulent eddy viscosity
Δ	turbulence resolution scale
$\widetilde{T}$	resolved temperature
$\widetilde{f}$	joint composition probability density function
Φ	composition space
Ψ	sample space of Φ
Γ	molecular diffusivity
Γ_t	residual turbulent eddy diffusivity
Sc	Schmidt number
X^*	particle location
m^*	particle mass
N_{pc}	number of particles per grid cell
Ω	mixing frequency
C_ϕ	model constant for mixing frequency
B_j	model constant for EMST
γ	model constant for EMST
χ_α	scalar dissipation rate for species α

$\phi_\alpha''^2$	sub-filter scale variance for species α
Ω_{NP}	mixing frequency for non-premixed combustion
Ω_P	mixing frequency for premixed combustion
Ξ_D	flame wrinkling factor for premixed flames
δ_{th}	thermal thickness of laminar premixed flames
α_D	model constant for premixed PDF model
S_L	laminar flame speed
φ	local equivalence ratio
FI	flame index
θ	parameter for regime identification
Ω_{MR}	mixing frequency for multi-regime combustion
D	jet diameter
ξ	mixture fraction
Re	Reynolds number
x	axial distance in computational domain
r	radial distance in computational domain

ABBREVIATIONS

LES	Large Eddy Simulation
PDF	Probablity Denisty Function
DNS	Direct Numerical Simulation
RANS	Reynolds Averaged Navier-Stokes
CMC	ConditionalMoment Closure
MCurl	Modified Curl
IEM	Interaction by Exchange with the Mean
EMST	Euclidean Minimum Spanning Trees
ISAT	In-Situ Adapative Tabulation
DRM	Dimension Reduced Mechanism
P	Premixed
NP	Non-premixed
FI	Flame Index

ABSTRACT

Kashyap, Shashank S. M.S., Purdue University, August 2019. Multi-regime Turbulent Combustion Modeling using Large Eddy Simulation/Probability Density Function. Major Professor: Haifeng Wang.

Combustion research is at the forefront of development of clean and efficient IC engines, gas turbines, rocket propulsion systems etc. With the advent of faster computers and parallel programming, computational studies of turbulent combustion is increasing rapidly. Many turbulent combustion models have been previously developed based on certain underlying assumptions. One of the major assumptions of the models is the regime it can be used for: either premixed or non-premixed combustion. However in reality, combustion systems are multi-regime in nature, i.e., co-existence of premixed and non-premixed modes. Thus, there is a need for development of multi-regime combustion models which closely follows the physics of combustion phenomena. Much of previous modeling efforts for multi-regime combustion was done using flamelet-type models. As a first, the current study uses the highly robust transported Probability Density Function (PDF) method coupled with Large Eddy Simulation (LES) to develop a multi-regime model. The model performance is tested for Sydney Flame L, a piloted methane-air turbulent flame. The concept of flame index is used to detect the extent of premixed and non-premixed combustion modes. The drawbacks of using the traditional flame index definition in the context of PDF method are identified. Necessary refinements to this definition, which are based on the species gradient magnitudes, are proposed for the multi-regime model development. This results in identifying a new model parameter β which defines a gradient threshold for the calculation of flame index. A parametric study is done to determine a suitable value for β, using which the multi-regime model performance is assessed for

Flame L by comparing it against the widely used non-premixed PDF model for three mixing models: Modified Curl (MCurl), Interaction by Exchange with Mean (IEM) and Euclidean Minimum Spanning Trees (EMST). The multi-regime model shows a significant improvement in prediction of mean scalar quantities compared to the non-premixed PDF model when MCurl mixing model is used. Similar improvements are observed in the multi-regime model when IEM and EMST mixing models are used. The results show potential foundation for further multi-regime model development using PDF model.

1. INTRODUCTION AND LITERATURE REVIEW

1.1 Need for combustion research

The energy demand for the world is ever increasing and is only expected to keep rising at an enormous rate. According to an article by International Energy Agency [1], the global energy demand increased by 2.3% in 2018, which was the fastest rate recorded over the last decade and natural gas as the primary choice of energy source. Energy generation through combustion, to this day, remains as the primary choice for the global energy demand. Figure 1.1, taken from the BP Energy Outlook 2019 report [2], shows the history as well as the projection of demand of fuels in the time period 1970-2040. Arguably, energy from natural gas, coal and oil, show a constant increasing demand over the decades.

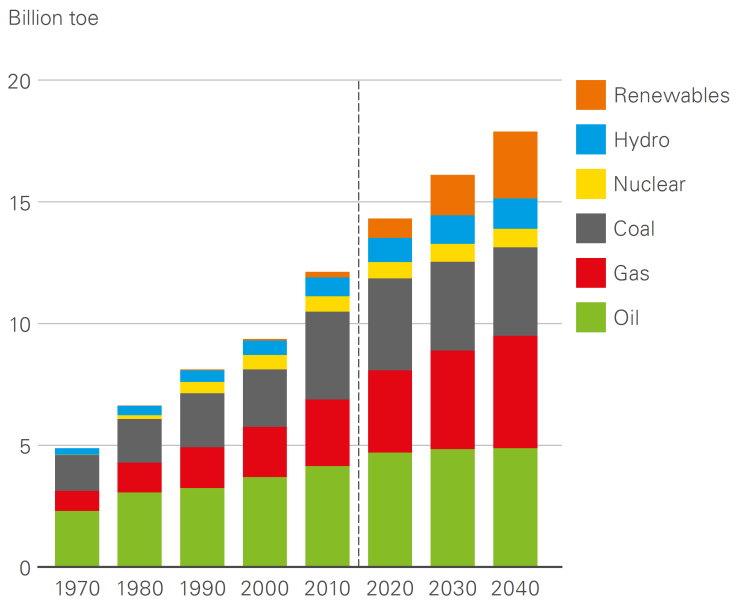

Fig. 1.1. Distribution of energy sources 1970-2040

Though many alternative sources of energy are emerging, energy from fossil fuels remain quite abundant and is considered the primary source currently as well in the foreseeable future. Combustion research in the past was focused on delivering high efficiency and maximum power. With recent discoveries of the adverse environmental impacts of fossil fuels, much of the research has been focused on delivering high efficiency as well as clean combustion. Research on renewable sources of energy such as wind, solar, nuclear etc., is flourishing at a high rate because of its environment-friendly capabilities as well as concerns about deplenishing fossil fuel resources. Though this is justified, combustion research still needs to be constantly developing considering that it will remain a primary source of energy for a substantial period of time. Though renewable sources of energy have shown promise in generating sustainable energy, it still has a long way to go to completely supply the world energy demands. On the other hand, combustion of fossil fuels deliver high energy from a small quantity which can easily support the global energy requirements. Thus, it becomes imperative to understand combustion to increase its efficiency as well as develop ways to harness it in an environmental friendly manner. Considering this, combustion research still has a long way to go to completely understand the physics and chemistry behind it.

1.2 Overview of Turbulent Combustion Modeling

Combustion research focuses on understanding the underlying chemical reactions and the fluid dynamics of the flow. Experimental research of combustion has been done for many years and still continues to grow as an important way of understanding it. Though, a new form of research using computational methods is emerging with the advent of computers and parallel programming. Computational Fluid Dynamics (CFD) [3] is a new field of research where the physics of complex flows can be predicted by solving the fundamental fluid equations and using advanced numerical techniques.

CFD research has become an integral part of the design and development process. Turbulent combustion modeling comes under the umbrella of CFD research, where the computational models developed are used to predict the highly turbulent flow field as well as the combustion process. Turbulent combustion modeling has become a broad field with focus on developing models to understand various combustion phenomena such as gaseous combustion, spray combustion, coal combustion, soot etc. Various components of turbulent combustion modeling [4] include:

- Predicting the *fluid properties* of the flow which are characterized by various turbulent scales. This includes understanding transfer properties (heat transfer, turbulent as well as molecular transport etc.), that consequently affect mixing of reactants. This can be useful in designing efficient combustion applications.
- Developing *detailed reaction mechanisms* which can accurately predict the combustion species and reactions, which will help us in understanding the production of pollutants.
- Developing models that effectively *couple the turbulence and chemistry* to accurately predict the overall physics of the problem.

Various canonical or laboratory flames are an important way of understanding the fundamentals of turbulent combustion. Under the collaborative efforts of TNF workshop [5], many fundamental flames have been identified for the purpose of experimental as well as modeling studies. Many different types of turbulent combustion models have been developed, each model with it's own limitations as well as advantages. The models developed tend to get more diversified with new research and applications, with minor refinements and changes to the existing models. The performance of the models developed are assessed by comparing the simulation results to experimental data. The models developed have underlying assumptions depending on combustion regime, chemical reaction time scale, turbulent length scale etc. [4]

Since turbulence plays a vital role in the chemistry, the starting point for turbulent combustion models would be understanding of turbulence models which can be coupled with various combustion models. Direct Numerical Simulation (DNS) [6, 7] is a model where the governing equations are resolved for all turbulent scales - as small as Kolmogorov scale. This technique can be computationally quite expensive for high Reynolds number flow. Reynolds Averaged Navier-Stokes (RANS) [8] turbulence model is a statistical based model which solves for only the mean field, while the fluctuating components are modeled. Large Eddy Simulation (LES) [9–11] turbulence model uses a filter to solve only large scale eddies with the smaller eddies being modelled. These turbulence models can be coupled to various combustion models depending on the specific study. There are various combustion models already developed and each of these models have different underlying assumptions. Lower order models include Finite Rate Chemistry [12], Eddy Break-up models [13] etc., while higher order models include flamelet models, Probability Density Function (PDF) [14] Models, Conditional Moment Closure (CMC) [15] models etc. Section 1.3 provides an overview of the models developed based on the type of combustion regime. With many different models developed under different contexts, there is a lack of a universal model that closely follows combustion physics and has accurate predictions.

1.3 Combustion Regimes and Modeling

Combustion involves reaction between multiple reactant species to generate products depending on various factors. The reactants can be thought of having two major component: a fuel and an oxidizer. Depending on the nature in which the fuel and oxidizer undergo combustion, it can be fundamentally divided into three categories or regimes - non-premixed, premixed and partially-premixed. Sections 1.3.1, 1.3.2 and 1.3.3 provide an overview of these combustion regimes and corresponding relevant modeling techniques.

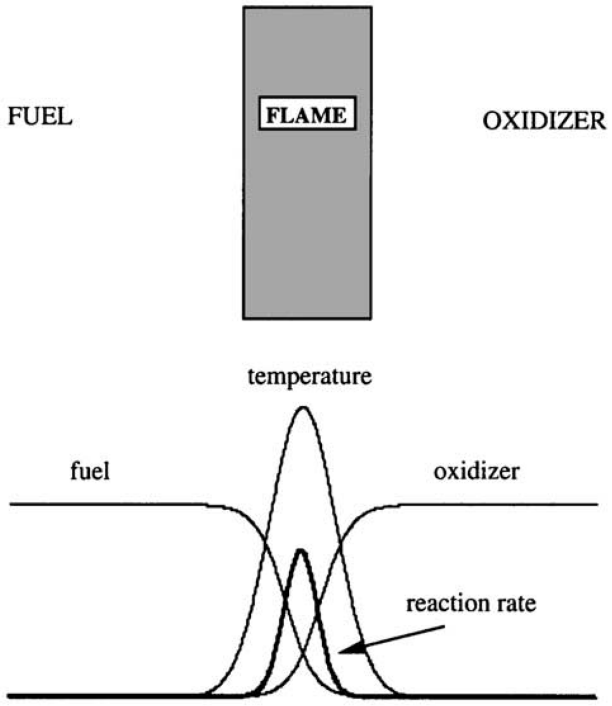

Fig. 1.2. Structure of non-premixed combustion [4]

1.3.1 Non-premixed Combustion Regime

In non-premixed combustion, the reactants i.e. fuel and oxidizer are introduced separately before combustion. Thus, combustion occurs at the interface or point of contact between the fuel and the oxidizer. Non-premixed flames are also called diffusion flames since the reactants diffuse into each other across the flame surface. Figure 1.2 shows a basic sketch of a diffusion flame. The extent of combustion is largely affected by the extent of mixing between the fuel and the oxidizer in the reaction zone. Thus, the gradients of fuel and oxidizer are in the opposite direction since they are approaching each other. Non-premixed combustion is largely mixing controlled due to turbulence effects but with a weak dependence on chemical reactions.

Flamelet models [11, 16] and PDF models [14, 17] have been widely used to study non-premixed flames. The non-premixed flamelet models developed are strictly applicable to non-premixed combustion regime though theoretically, the PDF models

can be applied to any combustion regime since it does not make any strong assumptions based on the regime. Yang *et al.* [18] used LES/PDF modeling to study non-premixed CO_2/H_2 temporally evolving flame. Xu and Pope [19] used the joint velocity-composition PDF model to study non-premixed turbulent jet flame [20]. *et al.* [21] used the LES/PDF model to study flow and turbulence fields to study pulsed jet flame based on Sydney Flame L [22]. These models are developed and tested for non-premixed flames and does not consider the co-existence of different regimes within the flames.

1.3.2 Premixed Combustion Regime

In premixed combustion, the fuel and oxidizer are already in a mixture form before entering the reaction zone. Unlike non-premixed combustion, where the reaction occurs at the interface of fuel and oxidizer, in premixed combustion, the reaction occurs everywhere. Since the combustion happens in the mixture from a certain point, a flame front exists which propagates towards the reactant mixture. This flame front is assumed to move at a speed called the laminar flame speed S_L. Figure 1.3 shows a sketch of a simple premixed flame. The flame front is present at the centre with products on one side and reactants on the other. There is a steep temperature gradient in the flame front region, where the reaction rate is maximum. In essence, since the fuel and oxidizer are already mixed, the gradients are in the same direction.

Though flamelet models were developed originally for non-premixed combustion, it was later extended to study premixed combustion based on premixed set of equations [23, 24] . The transported PDF model was also used to study premixed combustion in various studies [25]. Studies done by Lindstedt and Vaos [26], and Stollinger and Heinz [27] on premixed PDF modeling were done using the Reynolds Averaged Navier Stokes (RANS) models. Recently, Wang *et al.* [28], proposed a premixed PDF model in the context of Large Eddy Simulation (LES) turbulence model by improving the subfilter scale mixing frequency term. These models are developed exclusively for

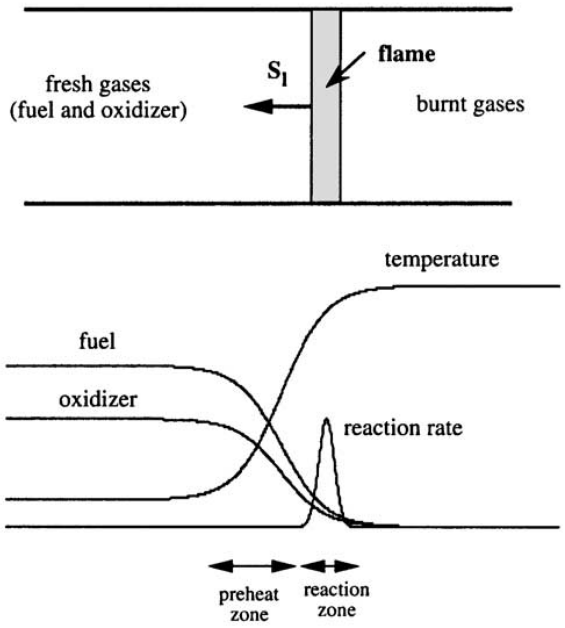

Fig. 1.3. Structure of premixed combustion [4]

premixed flames, though in reality, combustion phenomena is never truly premixed in nature within the domain. Thus, there is a gap in the models and the actual physics in combustion.

1.3.3 Partially Premixed/ Multi-regime Combustion

In practical applications, the notion of completely premixed or completely non-premixed combustion regime does not exist. It is argued that combustion is a combination of premixed as well as non-premixed combustion modes in the reaction zone. Figure 1.4 shows an ideal sketch of a partially premixed flame. The fuel and oxidizer emerge from the inlets as a non-premixed flame. As we go downstream of the flame, any unburnt reactants undergo mixing and result in a premixed combustion mode downstream. This type of flame is referred to as *triple flame* which has been reported in some studies [29].

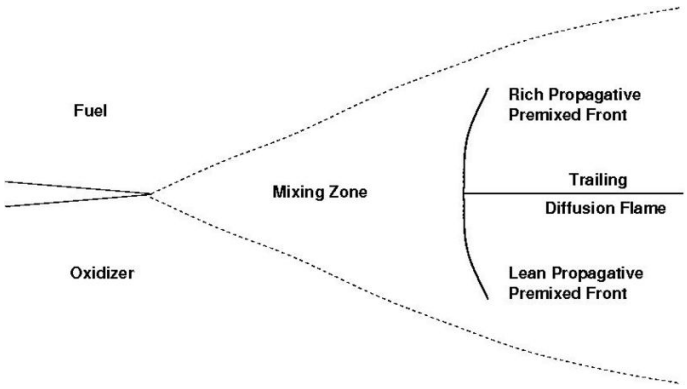

Fig. 1.4. Structure of partially premixed combustion in a *triple flame* [30]

Turbulent lifted jet flames have partially premixed combustion regimes at the base of the flame, which has been studied quite extensively [31]. This type of regime can be observed in fuel injectors, gas turbines etc. DNS simulation of a turbulent lifted flame, as seen in Figure 1.5, 1.5 by Mizobuchi *et al.* [32], showed the presence of regions of partially premixed flame fronts at the base of lifted flame. Simulations done by [33] on swirling combustors show the presence of both premixed and non-premixed regimes.

Thus, it becomes quite necessary to develop models that closely follow the physical aspects of partially premixed combustion regimes. Multi-regime modeling has thus become an important and trending research topic in combustion. It involves using techniques to differentiate non-premixed as well as premixed regimes, and combining the properties of these individual regimes accordingly to represent multi-regime concept. Yamashita *et al.* [34] performed a DNS analysis of a turbulent jet flame and introduced the concept of flame index, a technique based on gradients of fuel and oxidizer to identify premixed combustion mode from non-premixed mode. The study showed the presence of collection of premixed, non-premixed and partially premixed front. Section 2.9 gives a more detailed explanation on definition and properties of flame index. This concept of flame index has been used for many further studies or inspired new techniques to develop partially premixed models. Domingo *et al.* [35]

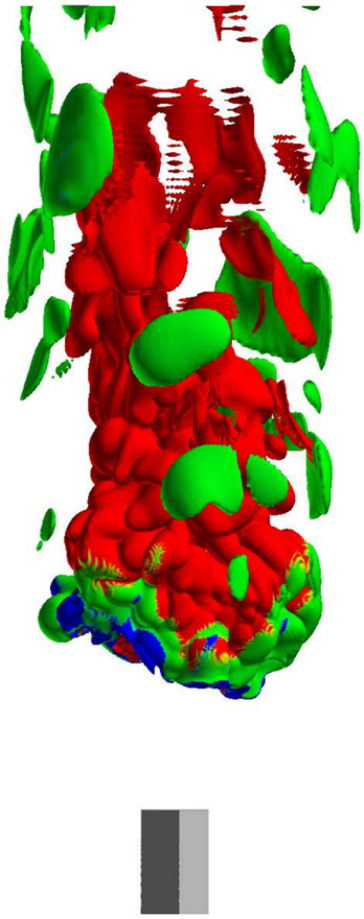

Fig. 1.5. DNS simulation of turbulent lifted flame done by Mizobuchi *et al.* [32]. Surface colors show the presence of different combustion regimes. Red: rich premixed, blue: lean premixed, and green: diffusion.

initially proposed a partially premixed flamelet model in LES with small modifications to the definition of flame index. Another study by Domingo *et al.* [36] proposed a partially premixed model based on DNS by combining the burning rates from premixed and non-premixed regimes. Fiorina *et al.* [37] studied the chemical structure of partially premixed and diffusion counterflow flames using FPI flamelet tabulation. The study was limited to a one dimensional flame with detailed chemistry mechanism. Knudsen and Pitsch [38] proposed a general flamelet transformation to distinguish between premixed and non-premixed combustion modes, which fundamentally differs

from the traditional flame index used in studies. This resulted in developing a new multi-regime flamelet model by Knudsen and Pitsch [39]. The flamelet solutions from premixed and non-premixed solutions were combined based on the values of a new regime indicator. Nguyen *et al.* [40] proposed a multidimensional flamelet-generated manifolds for partially premixed combustion. These models use flamelet-type models, which are fundamentally different from PDF models. Thus, there is a lack of multi-regime model development in PDF context.

1.4 Motivation

The previous studies for multi-regime modeling are all limited to flamelet combustion model with no study reported using transported PDF model. Transported PDF model does not make any underlying major assumptions like the flamelet models, making it a more robust combustion model. The PDF model is considered more advantageous since the reaction source term in the PDF equation comes in a closed form. The PDF model has been well studied for non-premixed combustion [17,18,21]. Many different models were proposed for the premixed PDF model considering the enhancement of small scale mixing due to chemistry. Recently, Wang *et al.* [28] proposed a modeling framework to simulate turbulent premixed jet flames using the PDF model with modifications to the mixing frequency term. Thus two separate frameworks for PDF model is identified for non-premixed and premixed combustion. With the lack of a multi-regime model in the LES/PDF context, the existing PDF models [21] [28] can be extended to develop a partially premixed combustion model. The main motivation of this work is to attempt to develop a new multi-regime model for turbulent jet flames using LES/PDF technique and assess its performance compared to the widely used traditional non-premixed PDF model.

1.5 Objectives

The main objectives for this study are as follows:

- To develop a systematic approach for multi-regime modeling by combining previously developed PDF models in the LES/PDF context.
- To identify the non-premixed/premixed combustion regimes in a turbulent jet flame and assess the validity of using the traditional regime identification definition.
- To assess the performance of the multi-regime PDF model in comparison to the widely used traditional non-premixed PDF model for a turbulent jet flame.
- To identify the advantages and limitations of the multi-regime model.

1.6 Major Research Contributions

Multi-regime combustion modeling has been gaining a lot of interest in the combustion community recently. With most of modeling efforts concentrated on a single combustion regime, multi-regime modeling research still has many areas to be explored. Previous studies on multi-regime or partially premixed combustion modeling has been limited to flamelet-type models. The current study uses the highly robust transported PDF model coupled with LES turbulence solver, which has never been done before. A complete framework has been presented for a LES/PDF multi-regime model using the previously developed PDF models for the individual premixed and non-premixed regimes. Using the concept of flame index, a thorough investigation is done to identify the combustion regime in the domain. Any necessary refinements to the standard definition of flame index are identified and employed for further model development. Multi-regime model parameters are recognized and a parametric study is done to understand the importance of this quantity. Model performance is assessed by using the turbulent piloted jet flame, Sydney Flame L, as a test case. The results of the multi-regime model is compared against the widely used non-premixed PDF model to understand its performance for different types of mixing models (MCurl, IEM and EMST).

1.7 Thesis Outline

The thesis is mainly divided into four chapters. Chapter 1 provides a brief introduction about the importance of combustion research and the advent of turbulent combustion modeling. It talks about the basic combustion regimes and a brief literature review is presented on the previous modeling efforts for each combustion regime with an emphasis on multi-regime/partially premixed regime. Finally, the motivation, objectives and major research contributions for the current study are presented.

Chapter 2 provides a complete mathematical framework for developing a multi-regime model using LES as the turbulence solver coupled with transported PDF model as the combustion solver. The concept of flame index, which is used as a regime identification technique in the current study, is introduced.

Chapter 3 provides information about the experimental as well as the computational setup for Sydney Flame L, which is used to assess the performance of the multi-regime model. The first section in this chapter provides an overview of the burner configuration and flame conditions used in the experimental setup performed by Masri *et al.* [41]. The second section outlines the computational details such as mesh, boundary conditions and numerical schemes used.

Finally, Chapter 4 presents the results of the current study. The first section presents results using the traditional non-premixed PDF model to understand the limitations of the model. The second section contains the results of regime identification using traditional flame index definition and talks about further refinements required for this definition in the context of PDF model for a more accurate identification. The third sections presents the results of the multi-regime model in comparison to the traditional non-premixed model to identify its advantages and limitations. Important conclusions and future work for this research work are presented.

2. MODELLING FRAMEWORK

This chapter includes the mathematical framework used to model multi-regime turbulent combustion flows. The various sections include governing equations to model turbulence, combustion and the theoretical framework behind modeling multi-regime combustion.

2.1 Overview of Framework

In this study, Large Eddy Simulation (LES) turbulence model was used to calculate the velocity and turbulence field. This turbulence model was coupled with Transported Probability Density Function (PDF) model to calculate the combustion fields. This coupled LES/PDF method has been previously used in many studies to model piloted turbulent jet flames [21, 42]. A detailed reaction mechanism (DRM19) with In-Situ Adapative Tabulation (ISAT) mechanism is used to calculate the chemical reactions because of it's accurate and computationally fast advantages. The transported PDF method is solved using the Monte-Carlo Particle method, which involves closure of the micro-mixing term in composition space using one of the following mixing models in this study: Interaction by Exchange with the Mean (IEM) [43], Modified Curl (MCURL) [44] model and Euclidean Minimum Spanning Trees (EMST) [45] model.

The LES/PDF method has been previously used to model non-premixed turbulent jet flames [21, 42]. The model was also extended to study premixed piloted jet flames by modifying the sub-filter scale mixing frequency term [28]. The key idea behind this study is to blend the mixing frequency term defined individually for non-premixed as well as premixed combustion regime to develop a multi-regime combustion model. The combustion regime is identified using the concept of flame index and the mixing frequency terms are blended depending on the value of flame index in the domain.

2.2 Turbulence Modeling

Turbulent flows are characterized by a wide range of turbulence scales and extend down till Kolmogorov scale. Large scale eddies contain the most turbulent kinetic energy and this energy cascades down till the small scales. Hence, to accurately model turbulent flows, all the scales of the flow have to be resolved to capture the contribution of the entire spectrum. This can be done using Direct Numerical Simulation (DNS) [6,7] approach, where the governing equations for the flow are solved for all scales. Computations of such small scale turbulent features vastly increases the computational cost. Thus, this method can be computationally very expensive for high Reynolds number flow, even with current computational resources. To overcome these limitations, Large Eddy Simulation (LES) [9–11] turbulence model was developed, in which larger three-dimensional turbulent motions are computed explicitly, while the small scales turbulence is modeled. In this way, LES is capable of capturing the large-scale flow features (which contain majority of turbulent kinetic energy), making it widely popular and of practical interest.

In LES, a cut-off is defined to separate the large scale eddies from small scale ones by defining a *filtering* operation. This *filtering* operation is defined to decompose the velocity $\mathbf{u}(\mathbf{x}, t)$ into a resolved, $\overline{\mathbf{u}}(x, t)$ (filtered) component and a subgrid-scale, $u'(\mathbf{x}, t)$ (SGS) component. This can be implemented by using a spatial filter, $G(\mathbf{x}, \Delta\mathbf{x})$, which is applied to the Navier-Stokes equation. Considering a quantity, Φ (which can density, velocity components, scalars, etc.), the filtered values, $\overline{\Phi}$ can be obtained by,

$$\Phi(\mathbf{x}, t) = \int \Phi(\mathbf{x}', t) G(\mathbf{x}, \mathbf{x}' - \mathbf{x}) d\mathbf{x}'. \tag{2.1}$$

Usually, the filter-function ($G(\mathbf{x}, \Delta\mathbf{x})$) can take various forms, but the most common ones used are box and Gaussian filters. A characteristic LES filer-width, Δ is

defined for the filtering process, which in practice, is often defined using the grid-size [9].

In reacting flows, the density of the flow field is not constant and hence, Favre-averaging is considered for the various quantities. Favre-average of a quantity, $\widetilde{\Phi}$ is defined as,

$$\widetilde{\Phi} = \frac{\overline{\rho\Phi}}{\overline{\rho}}, \tag{2.2}$$

where $\overline{\rho}$ is the filtered density of the flow field. After applying the LES spatial filtering to the Navier-Stokes equation, we get the following modeled governing equations,

$$\frac{\partial\overline{\rho}}{\partial t} + \frac{\partial(\overline{\rho}\widetilde{u}_j)}{\partial x_j} = 0, \tag{2.3}$$

$$\frac{\partial\overline{\rho}\widetilde{u}_i}{\partial t} + \frac{\partial(\overline{\rho}\widetilde{u}_i\widetilde{u}_j)}{\partial x_j} = -\frac{\partial\overline{P}}{\partial x_i} + \frac{\partial}{\partial x_j}(2\mu\widetilde{S}_{ij}) + \frac{\partial T_{ij}}{\partial x_j}, \tag{2.4}$$

where "$\sim$" denotes Favre filtering and "—" denotes spatial filtering. $\widetilde{S}_{ij}$ is the traceless strain rate tensor given by, $\widetilde{S}_{ij} = (\partial\widetilde{u}_i/\partial x_j + \partial\widetilde{u}_j/\partial x_i)/2 - \delta_{ij}(\partial\widetilde{u}_k/\partial x_k)/3$ and $T_{i,j} = \overline{\rho}\widetilde{u_i}\widetilde{u_j} - \overline{\rho}\widetilde{u_iu_j}$, is the residual turbulent stress. This term needs closure and is modeled by the eddy viscosity model [9] given by,

$$T_{ij} = \overline{\rho}\widetilde{u_i}\widetilde{u_j} - \overline{\rho}\widetilde{u_iu_j} = 2\mu_t\widetilde{S}_{ij} + \frac{1}{3}T_{kk}\delta_{ij}, \tag{2.5}$$

where δ_{ij} is the Kronecker delta and μ_t is the turbulent eddy viscosity. The residual turbulent eddy viscosity is specified by the Smagorinsky model [46],

$$\mu_t = C_\mu\overline{\rho}\Delta^2|\widetilde{\mathbf{S}}|, \tag{2.6}$$

where $|\widetilde{\mathbf{S}}| = \sqrt{S_{ij}S_{ij}}$ and C_μ is a model constant which is determined by the dynamic procedure [47]. The LES filter size, Δ (or the turbulence resolution scale) is specified same as the local grid size [21].

The molecular viscosity are approximated using the equation (2.7), as done by previous studies [48]. This reduces the computational cost of calculating the transport properties.

$$\mu = \rho\nu_0\Big(\frac{\widetilde{T}}{T_0}\Big)^{\alpha}, \tag{2.7}$$

where $\nu_0 = 1.1613 \times 10^{-5}$, $T_0 = 300$ K, α=1.1721.

2.3 Turbulent Combustion Modelling

In addition to solving the turbulence field, the combustion field needs to be solved for a reacting flow problem. This involves solving the temperature and various species consumed as well as formed during the combustion process. This includes using a chemical reaction scheme to estimate combustion reactants and products. Additionally, turbulence plays an important role in chemical reactions by promoting mixing between reactants and transfer phenomena affecting the different species. This turbulence-chemistry interaction needs to be considered while modeling reacting flows. The key challenge in turbulent combustion modeling is estimating the reaction rate or burning rate for the chemical reactions.

Many models such as the flamelet-like model, eddy-break up model, transported PDF model etc., have been previously developed to study turbulent jet flames. The flamelet models [11] [16] are based on the assumption that the turbulent combustion quantities lie in a one-dimensional manifold defined by the mixture fraction (ξ). The solutions to the governing equations are obtained by using a presumed-PDF approach. These type of models are usually restrictive because of the underlying assumption of mixture fraction dependence, cannot be used to solve problems with more than two

streams and more accurate for fast-chemistry/low turbulence problems. However, the transported PDF model [14] does not make any underlying assumptions, making it a more robust model to solve turbulent combustion problems with finite-chemistry and interaction with turbulence.

2.4 Transported PDF Model

A complete methodology for using the PDF model was developed by Stephen B. Pope [14] to solve turbulent reactive flows. In the composition PDF model, we define the composition space $\Phi = f(\phi_1, \phi_2, ..., \phi_n)$ for n components. This composition space includes all the species mass fractions that are being considered and the enthalpy. Using this composition space, Φ, a joint- PDF is defined as $\widetilde{f}(\Psi; \mathbf{x}, t)$ with $\Psi = (\psi_1, \psi_2, ..., \psi_n)$ being the sample phase variable corresponding to Φ. The transport equation for this joint composition PDF [21], $\widetilde{f}(\Psi; \mathbf{x}, t)$ is,

$$\begin{aligned} &\frac{\partial \overline{\rho}\widetilde{f}}{\partial t} + \frac{\partial}{\partial x_j}(\overline{\rho}\widetilde{u}_j\widetilde{f}) + \frac{\partial}{\partial \psi_\alpha}[\overline{\rho}\widetilde{f}S_\alpha(\psi)] - \frac{\partial}{\partial x_j}\left[\overline{\rho}\Gamma\frac{\partial \widetilde{f}}{\partial x_j}\right] \\ &= -\frac{\partial}{\partial x_j}\left(\overline{\rho}\widetilde{f}\widetilde{u_j''|\psi}\right) - \frac{\partial^2}{\partial \psi_\alpha \psi_\beta}\left[\widetilde{f}\left(\overline{\rho\Gamma\frac{\partial \phi_\alpha}{\partial x_j}\frac{\partial \phi_\beta}{\partial x_j}|\psi}\right)\right], \end{aligned} \tag{2.8}$$

where $\widetilde{u}_j$ is the resolved velocity and Γ is the molecular diffusivity. The molecular diffusivity is calculated [48] by using a similar form as the molecular viscocity μ in the equation (2.7) as follows,

$$\Gamma = \Gamma_0\left(\frac{\widetilde{T}}{T_0}\right)^\alpha, \tag{2.9}$$

where $\Gamma_0 = \nu_0/Sc = 2.293 \times 10^{-5}\ m^2 s^{-1}$, T_0=300 k and α=1.660. Equal molecular diffusivity and unity Lewis number are assumed following the common practice in many studies [9, 48].

The first two terms on the left hand side represent the change of joint PDF $\widetilde{f}(\Psi;\mathbf{x},t)$ due to the residual velocity. The third term on the left hand side of equation (2.8) is source terms due to chemical reaction and it appears in the closed form, which is one of the biggest advantages of Transported PDF method. The two terms on the right hand side of equation (2.8) are unclosed and need some models to solve the transport equation. The first term on the right hand side is the spatial flux of the PDF due to residual velocity, which is usually modeled by the gradient diffusion hypothesis [9],

$$-\frac{\partial}{\partial x_j}\left(\overline{\rho}\widetilde{f}\widetilde{u"_j|\psi}\right) = \frac{\partial}{\partial x_j}\left(\overline{\rho}\Gamma_t\frac{\partial\widetilde{f}}{\partial x_j}\right), \tag{2.10}$$

where Γ_t is the residual turbulent eddy diffusivity, which is obtained from $\overline{\rho}\Gamma_t = \mu_t/Sc_t$ with the Schmidt number $Sc_t = 0.4$. The second term on the right hand side of the equation (2.8) represents the molecular mixing in the composition space due to the conditional scalar dissipation. The closure of this term has been one of the most crucial aspects of transported PDF model. Several mixing models have been developed and can be categorized into the following: the IEM (Interaction by Exchange with Mean) [43] model, the MCurl [44] (Modified Curl) model, and the EMST [45] (Euclidean Minimum Spanning Tree) model.

The PDF transport equation is a very high dimensional equation and its solution by traditional finite-difference or finite-volume methods are not realizable [14]. Thus, special solution schemes have been developed, both in Eulerian and Lagrangian context. The Monte-Carlo particle method [14] is usually used to solve the Transported PDF equation by using the concept of notional Lagrangian particles. The transported PDF method can also be solved by introducing notional Eulerian fields [49,50] as well. This method was developed more recently compared to the traditional particle-based PDF model.

This study uses the Monte-Carlo particle method to solve the transported PDF equation using the in-house research code HPDF [48]. The method involves a col-

lection of random particles within the physical domain and the scalar space. These discrete set of particles can be used to represent the joint PDF and the evolution of this joint PDF can be described by the change of particle properties. In composition PDF method, each particle carries properties like the physical location $\mathbf{X}^*(t)$, particle mass m^*, velocity $\widetilde{\boldsymbol{u}}^*(t)$, diffusivities Γ^*, mixing frequencies Ω^*, which can be obtained from the LES field data at time t. The particles follow a set of Stochastic Differential Equations (SDE) [21] shown below,

$$d\mathbf{X}^*(t) = \left[\widetilde{\boldsymbol{u}} + \frac{\nabla[\overline{\rho}(\Gamma + \Gamma_t)]}{\overline{\rho}}\right]^* dt + [2(\Gamma + \Gamma_t)^*]^{\frac{1}{2}} d\,\boldsymbol{W}, \tag{2.11}$$

$$d\boldsymbol{\phi}^*(t) = \boldsymbol{M}(\boldsymbol{\phi}^*, \Omega^*)dt + \boldsymbol{S}(\boldsymbol{\phi}^*)dt, \tag{2.12}$$

where $d\,\boldsymbol{W}$ is the incremental Wiener process, $\boldsymbol{M}(\boldsymbol{\phi}^*, \Omega^*)$ stands for mixing and $\boldsymbol{S}(\boldsymbol{\phi}^*)$ is the reaction source term. The superscript "$*$" represents the quantity at the particle location given by $d\mathbf{X}^*(t)$. The nth moment in a given cell with N_{pc} particles can be calculated using the composition value $\boldsymbol{\phi}^*$, and the mass ${m_i}^*$, of the ith particle as [21],

$$\widetilde{\boldsymbol{\phi}}^n = \frac{\sum_{i=1}^{N_{pc}} {m_i}^* \boldsymbol{\phi}^*}{\sum_{i=1}^{N_{pc}} {m_i}^*}. \tag{2.13}$$

These moments can be used to construct the resolved scalar fields, which represent the thermo-chemical properties in a given cell. These properties are used for closure of the LES equations, making the system fully-coupled.

2.5 Detailed Reaction Mechanism using ISAT

In the solution of the PDF Transport equation, the chemical source term, $\boldsymbol{S}(\boldsymbol{\phi}^*)$ needs to be calculated. This involves using a reaction mechanism scheme which typically includes the reacting species, elementary reactions and the reaction properties

associated with the corresponding elementary reactions. In this study, a reduced chemical mechanism DRM19 [51] with 19 reacting species and 84 reactions is used to describe the chemical reactions in the system. This mechanism scheme is based on GRI Mech 1.2 [52] and can closely reproduce the same combustion process as that of GRI Mech 1.2.

The chemical source term is calculated using ISAT (In Situ Adaptive Tabulation) [53] approach, which was developed to accelerate the calculations of the detailed chemistry. In contrast to Direct Integration, ISAT significantly speeds up the computational time by 100-1000 times [53], which can be particularly advantageous while using higher order models like the transported PDF model.

2.6 PDF Mixing Models

This section provides an overview of different mixing models: the IEM model, MCurl model and the EMST model, developed for Transported PDF model and used in this study. The mixing of PDF particles are represented by the term $\boldsymbol{M}(\boldsymbol{\phi}^*, \Omega^*)$. This unknown mixing term requires a model for closure caused by the conditional mean scalar dissipation rate. A mixing model causes decay of the sub-filter scale variance due to sub-filter scale dissipation effect. The models depend on mixing frequency Ω which determines the rate of change by mixing. The mixing frequency is dependent on C_ϕ, which is an important model parameter of the PDF model. The main focus of this paper is the blending of this mixing frequency model developed for a turbulent non-premixed flame and a premixed flame. Sections 2.7 and 2.8 will include details for modeling of this mixing frequency value for non-premixed and premixed combustion regime.

2.6.1 IEM Mixing Model

IEM (Interaction by Exchange with the Mean) mixing model was developed by Villermaux and Devillon [43]. In this type of model, the sub-filter scale mixing process

is done by advancing the particles in a grid cell towards the mean value. This can be done using the following equation,

$$\frac{d\Phi_i(t)}{dt} = -\Omega(\Phi_i - \widetilde{\Phi}), \tag{2.14}$$

where Ω is the mixing frequency which is used to descibe the rate of mixing of particles, Φ_i is the scalar of i th particle and $\widetilde{\Phi}$ is the Favre averaged composition of the ensemble of particles of a particular cell. Since IEM model relaxes the composition towards the mean of all particles in the cell, it lacks the localness property [54].

2.6.2 MCurl Mixing Model

Modified Curl mixing model is based on Curl's mixing model [44,55]. In the MCurl model, the mixing is performed by randomly selecting n pairs of particles. Considering a pair of equal- weighted particles (p,q), the mixing is performed according to the equations,

$$\Phi^{(p,new)} = \Phi^{(p)} + \frac{1}{2}a(\Phi^{(q)} - \Phi^{(p)}), \tag{2.15}$$

$$\Phi^{(q,new)} = \Phi^{(q)} + \frac{1}{2}a(\Phi^{(p)} - \Phi^{(q)}), \tag{2.16}$$

where a is a random number uniformly distributed in (0,1), *new* is the new composition of the particle. The particles that are not selected during mixing are not changed. The n selected pairs of particles are controlled by the model parameter C_ϕ to ensure the same variance decay rate as that in IEM model.

2.6.3 EMST Mixing Model

The EMST (Euclidean Minimum Spanning Tree) mixing model is a complicated particle-interaction model developed by Subramaniam and Pope [45]. This model was developed since the IEM model and MCurl models are non local in composition space.

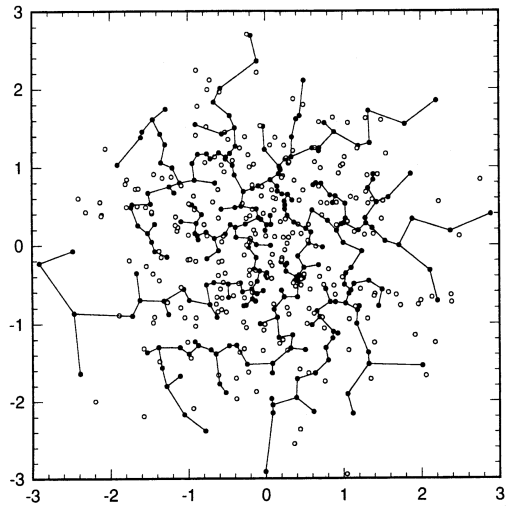

Fig. 2.1. EMST tree constructed from an ensemble of 512 particles where open circles are in non-mixing state [45]

In EMST model, based on particle weight and edge weights, a selected subset of particles in the scalar space form a Euclidean minimum spanning tree, as shown in Figure 2.1. The EMST model performs mixing of the selected particles by the equation,

$$m_p \frac{d\Phi_p}{dt} = -\gamma \sum_{j=1}^{n_s-1} B_j[(\Phi_p - \Phi_n)\delta_{p,n_j} + (\Phi_p - \Phi_{m_j})\delta_{p,m_j}], \tag{2.17}$$

where the j th edge of the tree connects the particle pair (m_j, n_j), B_j and γ are model constants. The parameter γ determines determines the sub-filter scale variance decay which is caused by mixing and is therefore, related to the mixing frequency Ω.

2.7 PDF Modeling of Non Premixed Flames

For all the mixing models discussed in the previous sections, a model for mixing frequency Ω, needs to be supplied to the transported PDF model. This sections describes the equations used to define a non-premixed mixing frequency model. The mixing frequency determines the decay rate of the sub-filter scalar variance due to mixing and is also closely linked to the scalar dissipation rate. Using the equation (2.14) in IEM Model, the equation for filtered scalar dissipation rate of can be obtained as,

$$\frac{d\widetilde{\phi_\alpha''^2}}{dt} = -2\Omega\widetilde{\phi_\alpha''^2} = \chi_\alpha, \tag{2.18}$$

where $\chi_\alpha = 2\Gamma|\widetilde{\nabla\phi_\alpha}|^2$ is the filtered scalar dissipation rate of ϕ_α, $\phi_\alpha''^2$ is the sub-filter scale variance and $|\nabla\phi_\alpha|$ is the magnitude of gradient of the composition α. Thus, a model for Ω can be formulated as,

$$\Omega = \frac{\chi_\alpha}{2\widetilde{\phi_\alpha''^2}}. \tag{2.19}$$

Substituting the commonly used model [56] for $\chi_\alpha = 2(\Gamma + \Gamma_t)|\nabla\phi_\alpha|^2$ (Under the assumption that the sub-filter scale dissipation and production are balanced) and the sub-filter scale variance being often modeled as [57], $\phi_\alpha''^2 = C_\nu\Delta^2|\nabla\widetilde{\phi}_\alpha|^2$, where C_ν is a model constant, a model for mixing frequency Ω can be developed as,

$$\Omega_{NP} = \frac{C_\phi(\Gamma + \Gamma_t)}{2\Delta^2}, \tag{2.20}$$

where $C_\phi = 4/C_\nu$ is a mixing parameter and NP stands for non-premixed. Various studies have been conducted to specify the value for C_ϕ [58] for different choice of canonical flames.

This model for mixing frequency Ω_{NP} is found to perform well for turbulent non-premixed combustion, as reported in various studies [17,19]. Turbulent non-premixed combustion is solely mixing controlled due to large scale turbulent eddies and hence, can be parameterized by a single conserved scalar mixture fraction. This model does not account for the effect of chemical reaction on sub-filter mixing. Thus, when the flame front is smaller than that turbulence resolution scale Δ, this model fails to consider the effect of flame characteristics [28].

2.8 PDF Modeling of Premixed Flames

The traditional model for mixing frequency Ω_{NP} works quite well for turbulent non-premixed combustion but needs additional improvements when it comes to turbulent premixed combustion. In turbulent premixed combustion, not only is it mixing controlled due to resolved turbulence field but also reaction controlled, where the flame propagation affects the scalar mixing. In premixed combustion, the flame front in wrinkled sue to coupling between turbulence and reaction, which consequently enhances mixing. A mixing frequency frequency model was previously developed [28] for LES/PDF modeling of turbulent premixed flames by considering locally enhanced mixing due to reaction. This new sub-filter scale mixing frequency considers the effect of chemical reaction by improving the scalar dissipation rate model χ_α.

When the thermal flame thickness, δ_{th} is less than the turbulence resolution scale Δ, DNS data [59] shows that the scalar dissipation rate based on equilibrium assumption under-predicts the scalar dissipation rate. Dunstan *et al.*. [60] proposed the following model for the scalar dissipation rate in premixed flames,

$$\chi_\alpha = 2\Gamma|\nabla\widetilde{\phi}_\alpha|^2 \cdot \Xi_D, \tag{2.21}$$

where Ξ_D is the flame wrinkling factor. A power law model is often used for modeling Ξ_D, which is proposed [60] to be a power law function of the ratio Δ/δ_{th} as,

$$\Xi_D = \left(\frac{\Delta}{\delta_{th}}\right)^{\alpha_D}, \tag{2.22}$$

where α_D is a model constant and δ_{th} is the laminar flame thickness. According to DNS data [59, 60], this model is applicable when flame front is under-resolved ($\Delta > \delta_{th}$). When $\Delta \to 0$, which is the DNS limit, this model for χ_α gives an inconsistent DNS limit of $\lim_{\Delta\to 0} \chi_\alpha = 0$, while the correct limit is $\lim_{\Delta\to 0} \chi_\alpha = 2\Gamma|\nabla\widetilde{\phi}_\alpha|^2$. To rectify this, Wang *et al.* [28] proposed a scaling factor $F(\Delta/\delta_{th})$ to replace Ξ_D in equation (2.22),

$$\chi_\alpha = 2\Gamma|\nabla\widetilde{\phi}_\alpha|^2 \cdot F(\Delta/\delta_{th}), \tag{2.23}$$

with $F(\Delta/\delta_{th})$ modeled as:

$$F\left(\frac{\Delta}{\delta_{th}}\right) = \begin{cases} \left(\frac{\Delta}{\delta_{th}}\right)^{\alpha_D} & \text{if } \Delta \geq \delta_{th}, \\ 1 & \text{if } \Delta < \delta_{th}. \end{cases} \tag{2.24}$$

The comparison between the above formula for the scaling factor and the curve fit from the DNS data [60] for a premixed flame is shown in Figure 2.2 , taken from [28], proving that the model for F correctly captures the asymptotic behavior in comparison to the DNS fit. The value for model parameter, α_D, varies for different flames and as well as spatially in a given flame, though DNS studies [59,61] have found that α_D varies between 0.86 and 1.42 in some different flames. Following previous studies from Wang *et al.* [28], a value of $\alpha_D = 2$ is used in the following study as well.

Considering the new model for χ_α from Eq 2.22 and the definition of mixing frequency from Eq 2.23, the new model for premixed combustion can be obtained as,

$$\Omega_P = \frac{C_\phi(\Gamma + \Gamma_t)}{2\Delta^2} \cdot F\left(\frac{\Delta}{\delta_{th}}\right), \tag{2.25}$$

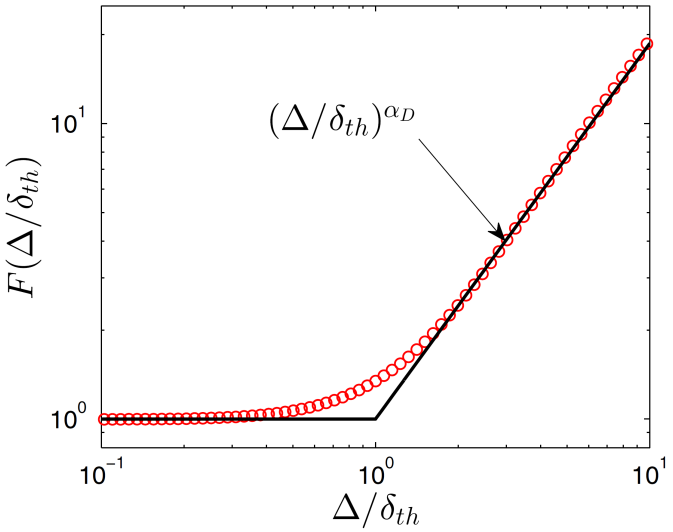

Fig. 2.2. Scaling factor F against Δ/δ_{th} [28]. Solid line: F defined by Eq. 2.24, Circles: curve fit from DNS data [60]

with $F(\Delta/\delta_{th})$ being modeled according to equation (2.24) and P stands for premixed regime. This new model differs from the non-premixed mixing frequency model only with respect to the length scale. The length scale for premixed mixing frequency model needs to be reduced when the flame front is under-resolved (when $\Delta < \delta_{th}$) and the mixing frequency reduces to,

$$\Omega = \frac{C_\phi(\Gamma + \Gamma_t)}{2\delta_{th}^2}. \tag{2.26}$$

This new model also requires the value for laminar flame thickness, which is calculated as $\delta_{th} = \Gamma_u/S_L(\varphi)$ [28], where Γ_u is the molecular diffusivity of the unburnt reactant and $S_L(\varphi)$ is the laminar flame speed as a function of local equivalence ratio φ. For methane-air flames at 300 K and 1 atm, the laminar flame speed can be obtained from one-dimensional laminar flame propagration calculations [62], for which the results are shown in Figure 3.2, taken from [62]. The value of laminar flame speed

S_L used is solely for calculating the value of δ_{th} but does not mean that the local flame front propagates at speed S_L. The local equivalence ratio φ is calculated based on resolved species mass fractions.

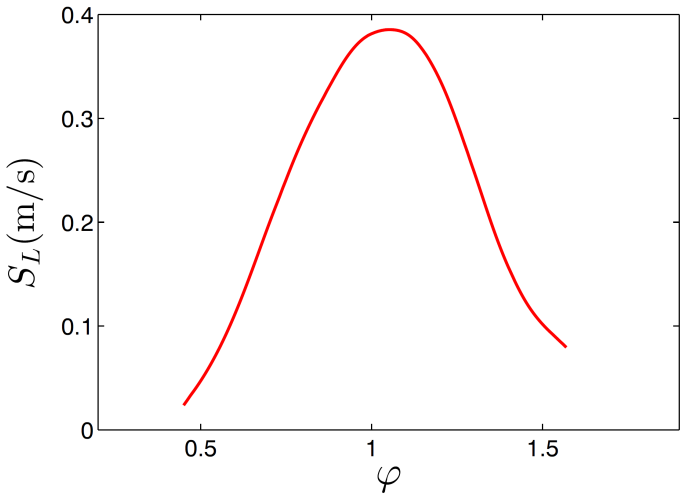

Fig. 2.3. Laminar methane-air flame speed S_L against equivalence ratio ϕ at 300 K and 1 atm [62]

2.9 Regime Identification

After having identified different models for the premixed as well as non-premixed combustion regimes, it becomes important to devise a way to identify the combustion regime spatially in a flame. Many different methods have been developed and studied previously to identify the combustion regime [34, 38, 63, 64], though the most popular approach is using flame index (FI). The concept of flame index was first introduced by Yamashita *et al.* [34] to study the structure of a turbulent diffusion flames. Flame index can be defined as follows,

$$FI = \frac{\nabla\widetilde{Y}_O \cdot \nabla\widetilde{Y}_F}{(|\nabla\widetilde{Y}_O||\nabla\widetilde{Y}_F| + \epsilon)}, \tag{2.27}$$

where $\nabla\widetilde{Y}_O$ is the gradient of resolved mass fraction of the oxidizer species and $\nabla\widetilde{Y}_F$ is the gradient of resolved mass fraction of the fuel species. The dot product of these two gradients are normalized by their respective magnitudes. A small value of ϵ is added to the denominator to prevent division by zero. Considering this definition, when FI tends to a value of -1 locally, we can identify it as non-premixed combustion mode. When FI tends to a value of +1, it can be identified as premixed combustion mode. Additionally, with this definition of flame index, we get values ranging between -1 and +1, which can be associated with the degree of a particular combustion mode as well.

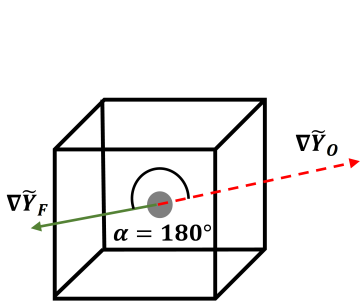

(a) Non-premixed ($\theta = 0$)

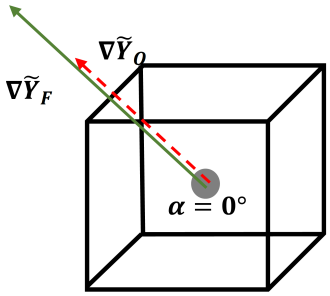

(b) Premixed ($\theta = 1$)

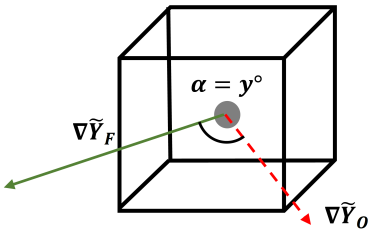

(c) Partially premixed ($0 < \theta < 1$)

Fig. 2.4. Orientations of gradients of oxidizer and fuel in a given grid cell. Red dotted line: Gradient of oxidizer, Green solid line: Gradient of fuel.

Essentially, flame index is cosine of the angle between the gradient of fuel and oxidizer. When the angle between the two gradients is 180 °, the cosine value is -1 and a non-premixed combustion is identified at the given grid cell. When the angle between the two gradients is 0 °, the two vector are aligned and the cosine value is 1, resulting in detection of premixed combustion mode in a given grid cell. Any angle between 0 ° and 90 °, will result in a greater proportion of premixed combustion mode, while any angle between 90 ° and 180 ° will result in a greater proportion of non-premixed combustion mode. The value of flame index we obtain is sensitive to not only the orientation of gradients but also to the magnitude of gradients as well. A simple transformation can be made to change the FI range from (-1,1) to (0,1) as follows,

$$\theta = \frac{1}{2} \times (1 + FI). \tag{2.28}$$

Thus, a value of $\theta = 0$ corresponds to non-premixed combustion mode and $\theta = 1$ corresponds to premixed combustion mode. Figure 2.9 shows the three scenarios a given grid cell can have: completely premixed, completely non-premixed and partially premixed.

The standard definition of flame index based on gradients of mass fraction has been subject to modifications and refinements in other specific studies. Fiorina *et al.* [37] observed that, in a 1-D counterflow flame, discrepancies are observed when the definition predicts a premixed combustion mode even in regions where it is diffusion controlled combustion. Hence, a slight modification was made to account for relative significance of diffusion of oxidizer for the counterflow flame. Domingo *et al.* [35] suggested modifications considering sub-grid scale effects in the definition of flame index using LES method. In another study conducted by Domingo *et al.* on DNS analysis of partially premixed combustion in spray flames [36], the flame index is calculated where the heat release rate is larger than a threshold value. These

modifications and refinements are all limited to flamelet modeling but there are no previous studies relevant to PDF modeling.

In the current study, the standard definition of flame index in equation (2.27) was initially used to identify combustion regime. Results from this definition showed that it requires further refinement to provide a more accurate prediction of the combustion regimes. Section 4.2 provides the results and further discussions about the refinement to the definition of flame index pertaining to PDF model.

2.10 Multi-regime Modelling using LES/PDF

Multi-regime modeling of combustion involves the following core aspects:

- Modeling of individual combustion regimes, i.e., premixed as well as non-premixed combustion modes.
- A careful method of identifying the combustion modes in the flow field.
- Finally, combining the individual combustion regime models depending on the extent to which each combustion mode exists locally.

Having identified PDF models that describe individual combustion modes and the method of flame index to quantify the extent of these combustion modes, it becomes necessary to carefully combine these quantities to develop a multi-regime PDF model. Much of efforts to study multi-regime models has been done using the flamelet models. In the multi-regime flamelet model developed by Knudsen and Pitsch [39], the flamelet solutions from non-premixed regime and the premixed regime are linearly blended using a weighting coefficient used to identify the combustion regime. In the DNS studies of partially premixed combustion by Domingo *et al.* [35], a similar linear blending concept is used to define the burning rate for a partially premixed flame. Following this concept, a similar linear blending approach is used to define the multi-regime PDF model in this study. Considering the mixing frequency model developed

for non-premixed combustion Ω_{NP} defined in Section 2.7 and mixing frequency model developed for premixed combustion Ω_P defined in Section 2.8 and the flame index parameter θ, the mixing frequency for the multi-regime model can be defined as,

$$\Omega_{MR} = \theta \times \Omega_P + (1 - \theta) \times \Omega_{NP}, \tag{2.29}$$

where Ω_{MR} is the mixing frequency for the multi-regime model. This new model combines the values of individual mixing frequencies defined for premixed as well as non-premixed combustion mode depending on the value of θ. When the value of θ is 0, i.e., non-premixed combustion mode, the value of Ω_{MR} is the same as Ω_{NP} and when the value of θ is 1, i.e., premixed combustion mode, the value of Ω_{MR} is the same as Ω_P. For intermediate values of θ, the value of Ω_P and Ω_{NP} are blended accordingly to get the new Ω_{MR}. This new mixing frequency will be used for particle mixing in the solution of PDF equation.

3. MODEL VALIDATION

3.1 Experimental Setup

In this section, the experimental setup of the flame used to validate the multi-regime model is described. The model is validated against Sydney Flame L, a flame belonging to the the Sydney piloted series of flames [41, 65], developed at University of Sydney. These are methane-air flames with increasing jet velocity, which causes local extinction leading to global blow-off downstream of the flame. Many different piloted jet flames have been studied extensively through experiments to understand turbulent combustion phenomena and obtain key velocity as well as scalar data quite accurately. The Sydney piloted jet flame series include flames L, B and M, studied by Masri *et al.* [41, 65]. A similar flame burner is also used in Sandia piloted jet flame series D,E and F [22].

3.1.1 Sydney Flame L Burner Configuration

The Sydney piloted flame burner has a central fuel jet with a diameter of $D = 7.2$ mm. This central jet is supplied with pure methane CH_4. The jet tube is surrounded by a pilot tube with an outer diameter of 18 mm. The wall thickness of the fuel tube is 0.26 mm and the pilot tube is 0.2 mm. This setup of jet and pilot tube is placed at the center of a small square wind tunnel. The fuel tube is a stainless steel tube of length 550 mm and the squared co flow wind tunnel has sides of 0.3 m with a concentration ratio of 9:1 [65].

Fig. 3.1. Sydney piloted jet flame [66]

3.1.2 Flame Conditions

The jet tube of Sydney Flame L is supplied with pure methane CH_4 with a temperature of 300 K and a bulk velocity of 41 m/s. The peak velocity on the centerline was found to be 49.9 m/s and a Reynolds Number $Re = 17900$. The pilot tube is supplied with a stoichiometric mixture of C_2H_2, H_2 and air with $C - H$ mole ratio the same as methane. The pilot gas mixture exits the tube at a temperature of 300 K and a bulk velocity of 3 m/s. The burnt gas out from the pilot has a measured bulk velocity of 22.8 m/s and average temperature of 2600 K, under the assumption of 5% heat loss to the burner walls. Additionally, the burner also is supplied with a coflow of air around the pilot tube with a speed of 15 m/s at a temperature of 300 K.

The flow field and scalar data for the flame is collected through Spontaneous Raman Scattering [65] and a complete set of experimental data is available for model validation [66]. The stoichiometric mixture fraction for methane-air flames is $\xi_{st} = 0.055$

3.2 Computational Setup

This section provides a compete overview of the computational setup of Sydney Flame L done to study the multi-regime model. The setup consists of defining a proper computational domain, a sufficiently spaced grid to obtain accurate simulations, appropriate boundary conditions to closely replicate experimental setup and finally, using the suitable numerical techniques to solve the governing equations. The simulation was performed using an in house coupled LES/HPDF FORTRAN solver developed by Wang *et al.* [42, 48]. The code is second order accurate is space as well as time. Turbulent combustion simulations, in general, are computationally very intensive. The transported PDF method is especially quite computationally expensive and hence, the code also has parallel computing capability to scale up the simulations using the Open Message Passing Interface (Open MPI) flavor.

3.2.1 Computational Domain and Mesh

A cylindrical domain is chosen for the simulation, which is a very common choice for piloted turbulent jet flames. Following studies by Zhang *et al.* [21], a domain size chosen of $[0, 60D] \times [0, 20D] \times [0, 2\pi]$ in the axial x, radial r, and azimuthal θ directions respectively, is chosen. Here, $D = 7.2\ mm$, which is the diameter of the fuel jet inlet. The governing equations are cast into corresponding cylindrical coordinate system. This domain size is proved to be sufficient large is all directions to capture the physics of Sydney Flame L quite accurately. The radial direction size of $20D$ is large enough to avoid inaccurate results due to entertainment of air. The experimental data for scalars are available at axial distances of $x/D = 10, 20$ and 30.

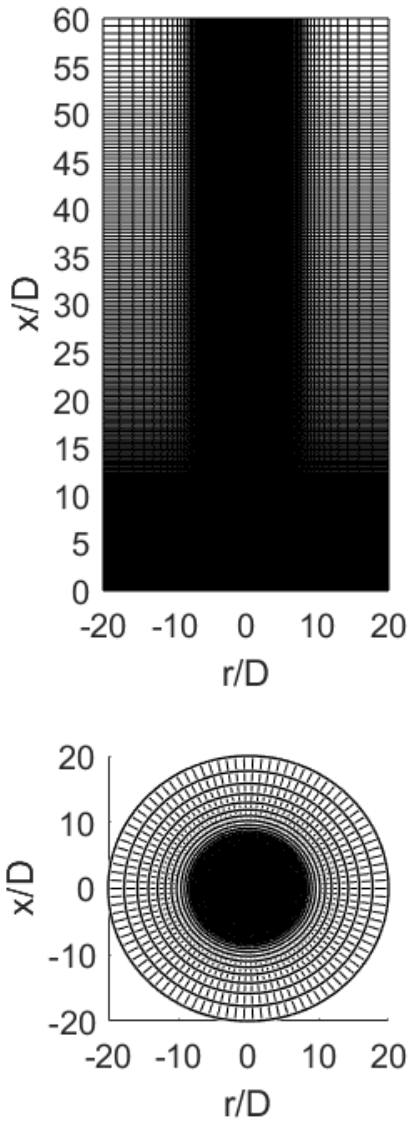

Fig. 3.2. Computational grid used for current study: $256 \times 108 \times 48$ grid cells in x, r and θ directions respectively

The domain is divided into non-uniform $256 \times 108 \times 48$ grid cells in x, r and θ directions respectively. A grid independent analysis is not performed in this study since the specified grid size was found to be sufficient to obtain an accurate statistically stationary flame as found in the study by Zhang *et al.* for Sydney Flame L using the

HPDF code [21]. The figure shows the grid used in the current simulation in the $x-r$ plane and the $r-\theta$ plane. The effect of turbulence and chemistry is predominant along the planes closer to jet and pilot tube inlet. Thus, the grid is refined to capture the physics of the flame accurately. Additionally, the grid is refined further in the interface between jet and pilot exit planes to resolve the mixing layer, where the effects of shear stress is predominant.

The domain is decomposed in the axial and radial direction only for the purpose of parallelization of the code. For the specified grid size of $256 \times 128 \times 48$, the domain is decomposed into 128 blocks along axial direction and 4 blocks along the radial direction. Thus, the simulation was run on 512 cores and for a wall time of approximately of 38 hours for each case ($\sim$ 20,000 core hours).

3.2.2 Boundary Conditions

Appropriate boundary conditions are essential to a numerically and physically accurate computational simulations. The boundary conditions can largely affect the convergence of the simulations as well. The inlet boundary conditions are specified for the fuel tube, pilot tube and co-flow inlet. The fuel inlet boundary condition is specified as a velocity profile to consider the inflow turbulence effects. This profile is obtained from a separate simulation of of fully-developed turbulent piper flow with same Reynolds number as the fuel jet, which is around $Re = 17000$ [21, 42]. The specified velocity profile gives a mean bulk velocity of 41 m/s, which is the experimental inflow condition. The fuel inlet is specified with a mixture fraction of $\xi = 1$ since pure methane is used in Flame L, and a temperature of $T = 300\ K$.

A constant velocity of 3 m/s is specified for the pilot tube inlet. The composition at this boundary is a mixture of C_2H_2, H_2 and air with $C-H$ mole ratio the same as methane, which corresponds to an equivalence ratio of 1 (stoichoimetric conditions).

The co-flow inlet is specified with a parabolic velocity profile from the pilot tube wall with a boundary layer thickness of $1.94D$ or 0.01397 m and a mean axial velocity

of 15 m/s. The composition and temperature of the co-flow boundary is the same as that of standard air. Figure 3.3 shows the mean velocity profile at the inlets along the radial direction. For the boundaries at $r/D = 30$ and $x/D = 60$, an outflow boundary condition is specified, which prevents backflow.

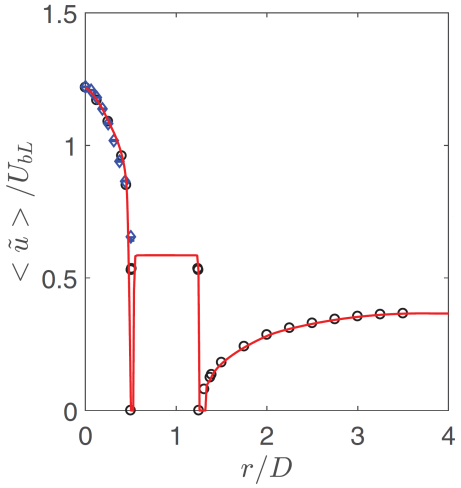

Fig. 3.3. Red line: Profile of velocity at the bottom boundary of computational domain, taken from [21]

3.2.3 Numerical Schemes and Parameters

The flow field LES equations are solved using a finite volume method and a second-order central difference scheme is used to discretize the LES equations. A semi-implicit iterative solution scheme is employed for time advancement to obtain a statistically stationary simulation. A constant non-dimesional time step size of $\Delta = 0.015$ is used for the semi-implicit scheme. A constant time step size is critical for ISAT computations [53]. The Courant-Friedrichs-Lewy (CFL), which affects the stability of the simulation, is adjusted throughout the iterations of the simulations to ensure convergence.

For the PDF model, number of particles per cell $N_{pc} = 30$ is used. This number was based on previous studies on Flame L by Wang et al. [42], where a sensitiv-

ity analysis was performed for N_{pc}. The evolution of particles are solved using the stochastic differential equations (SDE) in equations (2.11) and (2.12). First order time splitting scheme, TMR [48], is used to integrate the SDEs. T stands for substep of particle transport in physical space, M stands for substep of mixing in composition space, and R represents substep of chemistry. The chemical calculations are done using ISAT, with an error tolerance of 10^{-4} [21].

4. RESULTS AND DISCUSSIONS

This chapter provides a complete set of results for the given study. The results for the traditional non-premixed PDF model using the MCurl mixing model is presented first to provide an overview of Sydney Flame L and assess it's performance. Instantaneous contour plots of the flow and scalar fields is included to asses the model performance on a qualitative level. Time averaged results of the mean scalar quantities are compared with the experimental data at locations $x/D = 10, 20$ and 30. Additionally, conditional mean values in the mixture fraction space are compared with experimental data as well.

Section 4.2 includes results of regime identification using flame index in the given study. The need for refinement of the traditional definition in the PDF model context is justified with appropriate results and reasons. An essential model parameter β is identified in this section for the purpose of refining the definition of flame index.

4.1 Traditional Non-premixed Model

Before the results for multi-regime model are presented, results from the traditional non-premixed model is presented to understand its performance. The traditional non-premixed PDF model uses the default mixing frequency model, as described in Section 2.7. Sydney Flame L is characterized by significant local extinction and hence, the IEM and MCurl mixing models tend to produce a non-burning flame due inherent properties of non-localness, as pointed out in [21, 45]. In this section, MCurl mixing model is used to perform the simulation using the non-premixed model. Figure 4.1 show the instantaneous contours of mixture fraction (ξ), temperature (T), OH mass fraction ($\widetilde{Y}_{OH}$) and CO mass fraction ($\widetilde{Y}_{CO}$). From the contours of temperature we can observe that the flame tends to extinguish and does not yield a burning

flame beyond $x/D = 15$. The production of CO and OH, which are usually indicative of the flame front, are also limited beyond $x/D = 15$.

Figures 4.2 and 4.3 the radial profiles of the mean quantities at $x/D = 10, 20$ and 30. Upstream of the flame, i.e., at $x/D = 10$, the old traditional non-premixed models are fairly accurate with the experimental data. Though at axial distances of $x/D = 20$ and 30, the non-premixed model tends to deviate from the experimental data. This can especially observed for mean temperature $\widetilde{T}$, temperature variance $\widetilde{T}''$ and carbon species elements. In general, the traditional non-premixed PDF model using MCurl mixing model tends to under-predict the mean quantities for the flow field and the scalars, especially downstream of the flame.

The Transported PDF model can be studies from a statistical point of view as well. To understand the turbulence chemistry interaction, the mean quantities can be plotted on the mixture fraction space or conditioned over the mixture fraction. Figure 4.4] shows the conditional means of temperature, mass fractions of O_2, CO_2, H_2O, CO and H_2 at axial locations $x/D = 10, 20$ and 30. The traditional non-premixed model tends to under-predict the scalar quantities at downstream locations, which is similar to the observations in the plot of mean quantities.

There are some discrepancies observed especially in the mass fractions of CO and CO_2, in both physical space (mean) and the mixture fraction space (conditional mean) on the fuel rice side. Wang *et al.* [42] lists the following as the possible causes - (i) no consideration of differential-diffusion effect, (ii) uncertainty in the inflow boundary condition and (iii) uncertainty in CO measurements.

The aforementioned results show that the traditional non-premixed model using MCurl model tends to under predict the flow field and scalars compared to the experimental data. This can be possibly due to the lack of consideration of multi-regime effects. If a multi-regime model is considered, burning could be promoted due the presence of premixed component in the calculations [28].

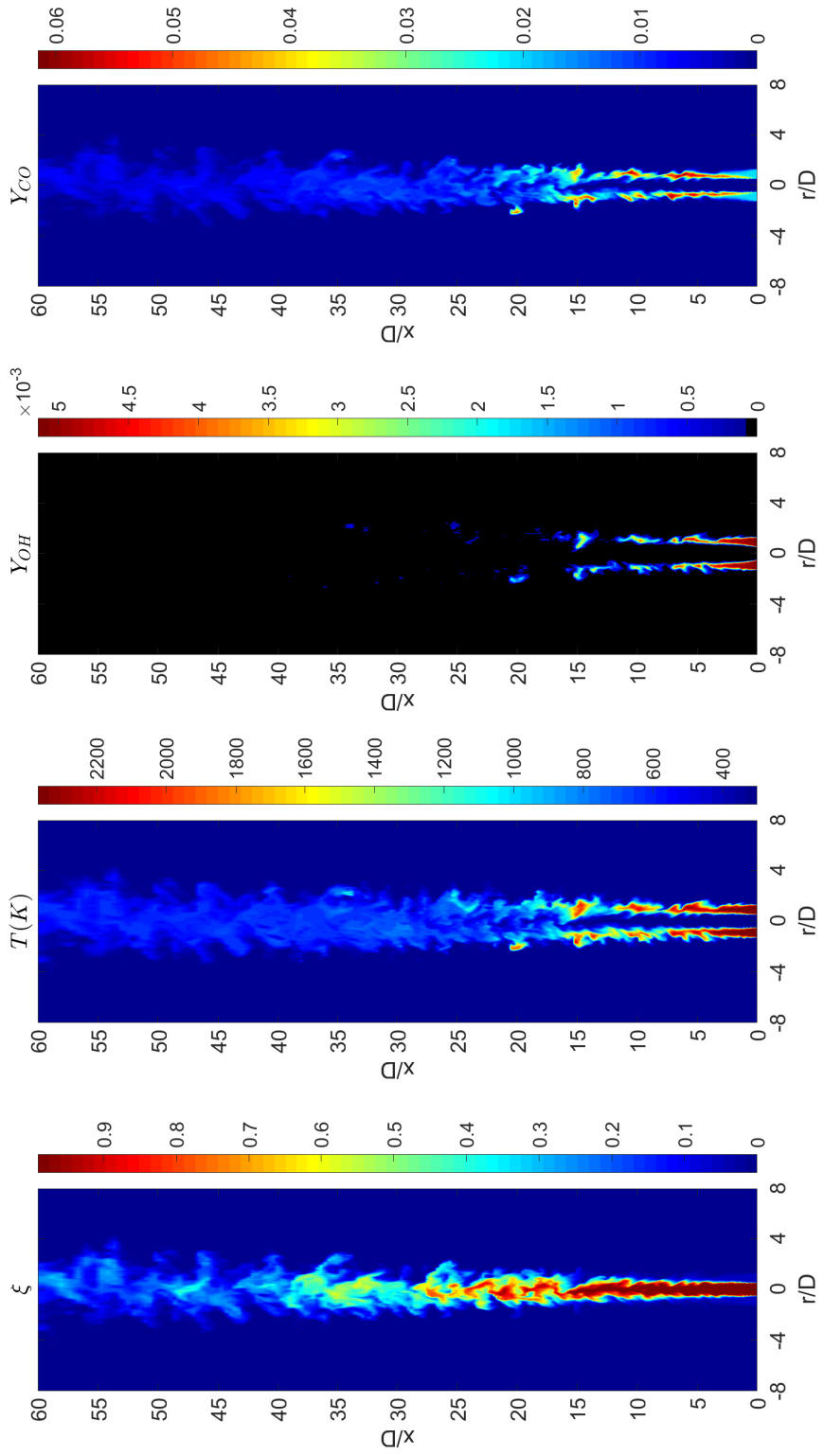

(a) Mixture Fracture, ξ (b) Temperature, T (K) (c) OH Mass Fraction, Y_{OH} (d) CO Mass Fraction, Y_{CO}

Fig. 4.1. Instantaneous contours of scalars using traditional non-premixed model.

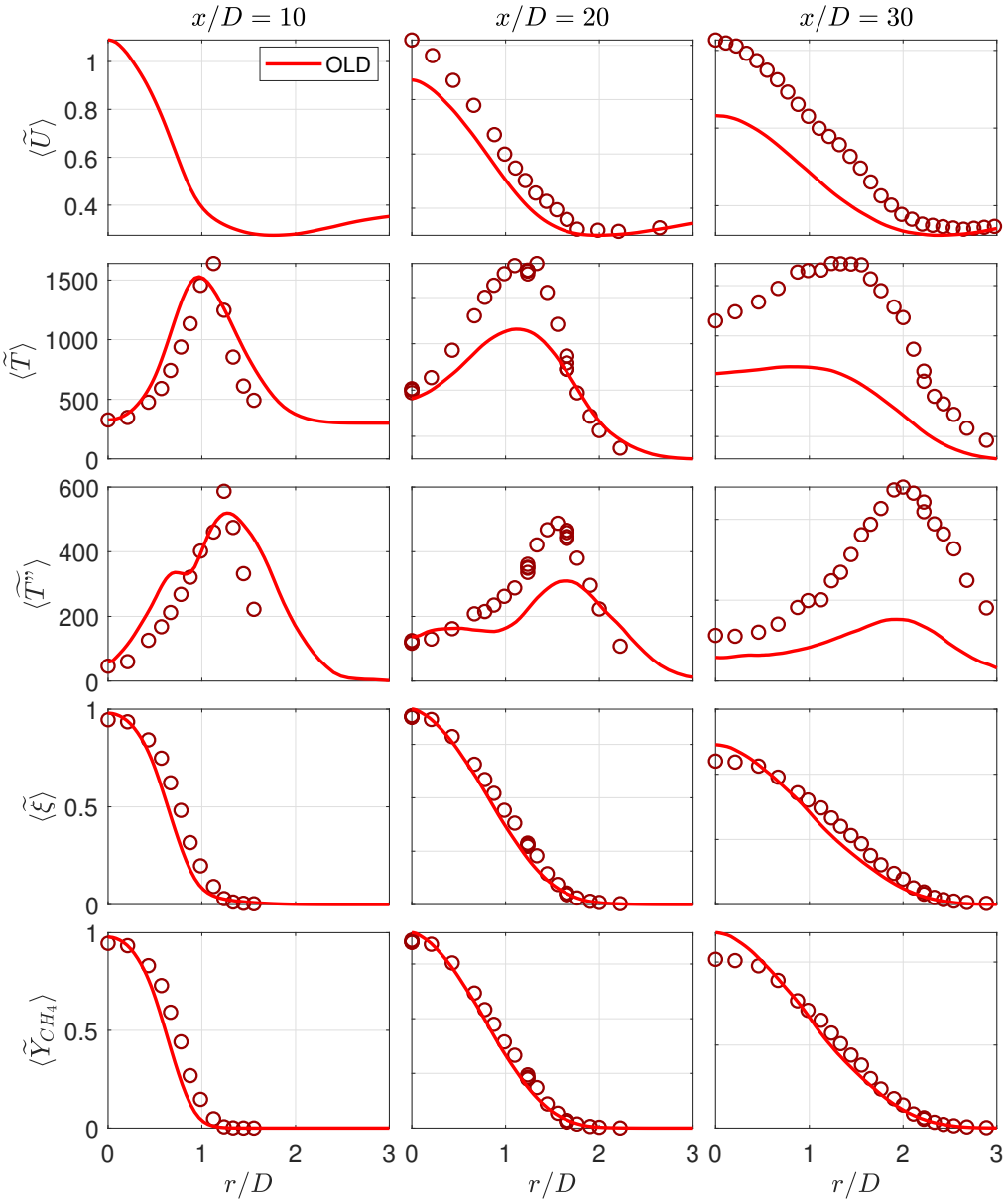

Fig. 4.2. Radial profiles of mean axial velocity $\widetilde{U}$, mean temperature $\widetilde{T}$, temperature variance $\widetilde{T}''$, mean mixture fraction $\widetilde{\xi}$ and mass fraction of $\widetilde{Y}_{CH_4}$ from the old traditional non-premixed model. Circle: experimental data and red line: simulation results

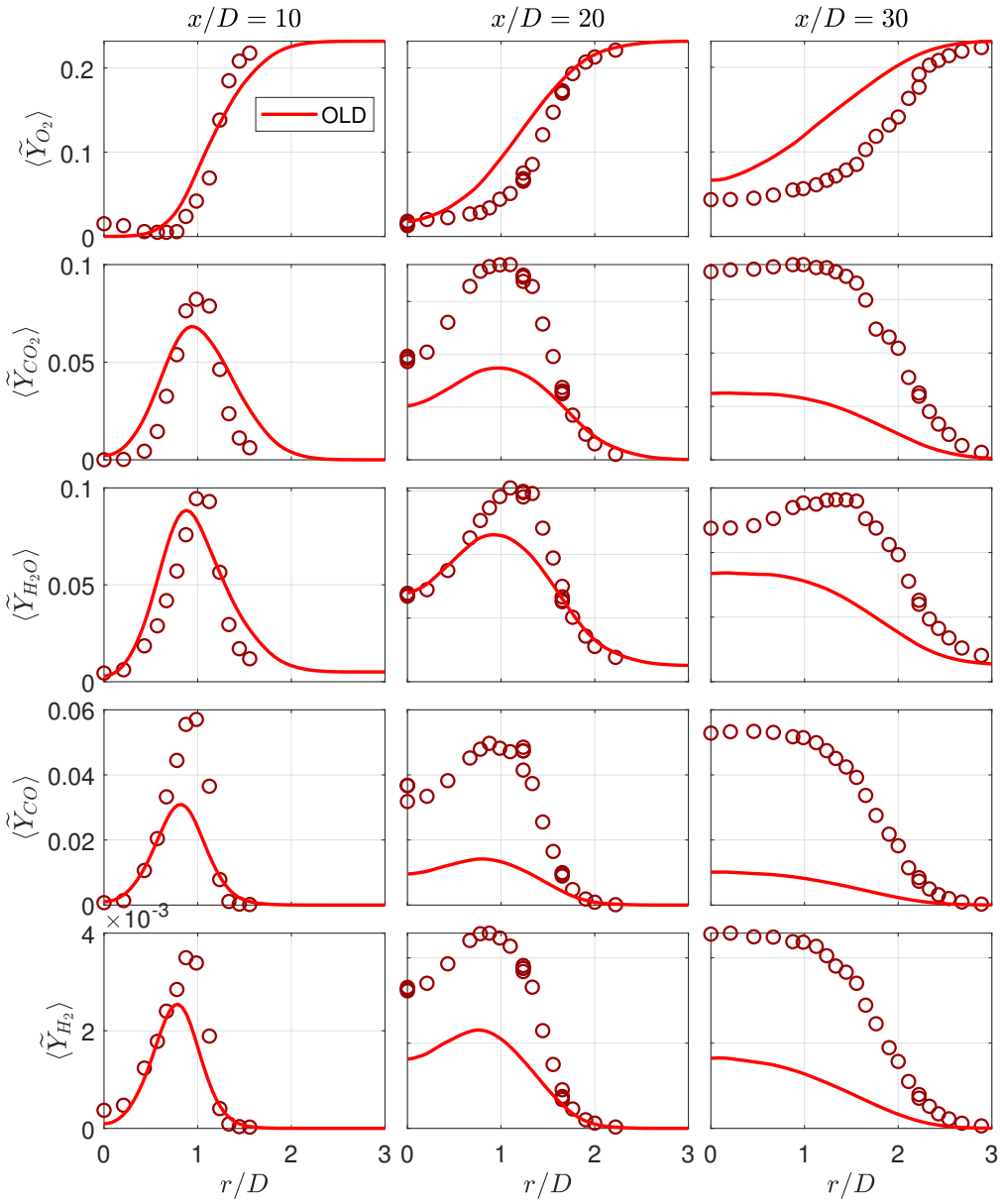

Fig. 4.3. Radial profiles of mean mass fractions of $\widetilde{Y}_{O_2}$, $\widetilde{Y}_{CO_2}$, $\widetilde{Y}_{H_2O}$, $\widetilde{Y}_{CO}$ and $\widetilde{Y}_{H_2}$ from the old traditional non-premixed model

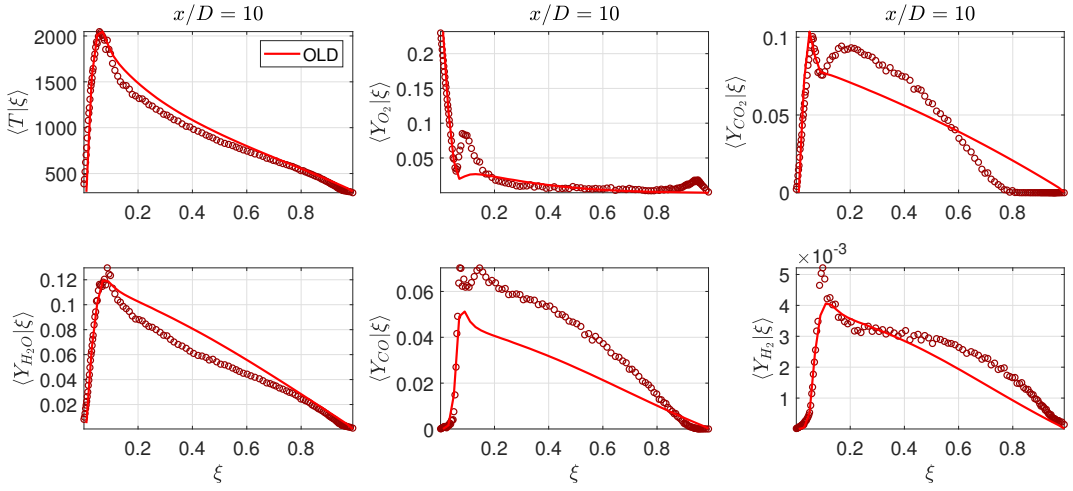

(a)

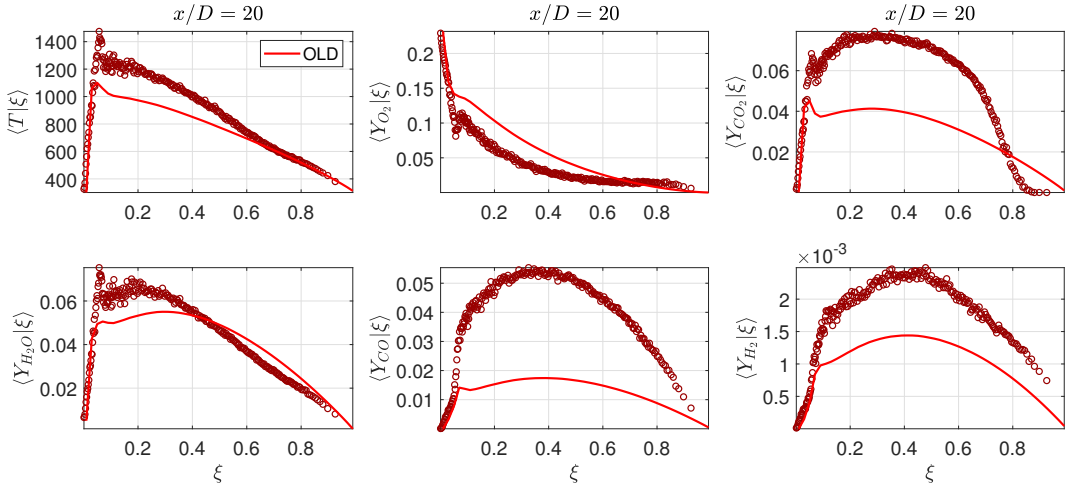

(b)

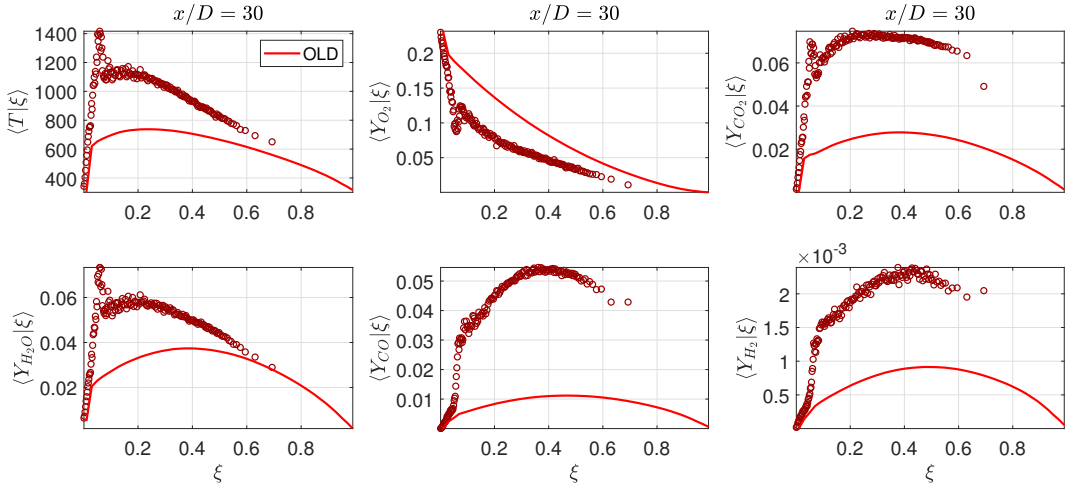

(c)

Fig. 4.4. Conditional means of scalars in the mixture fraction space at $x/D = 10, 20$ and 30 from the old traditional non-premixed model.

4.2 Regime Identification and Refinements

4.2.1 Results from Traditional Flame Index definition

The following section discusses the results of regime identification in Sydney Flame L. As outlined in Section 2.9, flame index is used as technique to identify the combustion regime. After the simple linear transformation of flame index as shown in equation (2.28), the parameter θ can be used to identify the combustion regime. A value of $\theta = 0$ corresponds to non-premixed combustion mode while a value of $\theta = 1$ corresponds to premixed mode. Any value between 0 and 1 corresponds to a partially-premixed mode in a given grid cell.

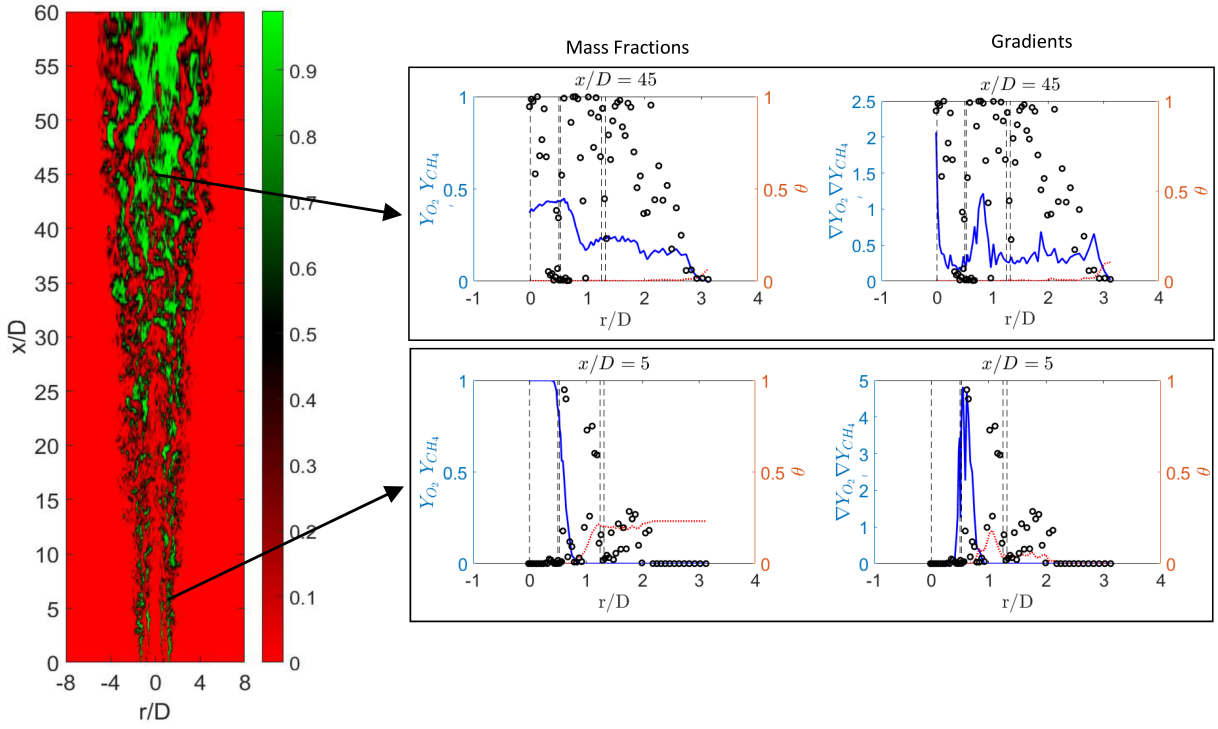

Fig. 4.5. Contour plot of θ (Left). Radial profiles of mass fractions and gradients of O_2 and CH_4 at $x/D = 5$ (bottom right) and at $x/D = 5$ (top right). The left axis of the plots are gradient magnitudes or mass fractions while the right axis is θ. Red dotted line: oxygen, blue solid line: methane, black circle: θ.

Figure 4.5 shows the contour plot of θ in the computational domain using the traditional definition of flame index as specified in equation (2.27). The red color corresponds to $\theta = 0$ (non-premixed or not burning), while green color corresponds to $\theta = 1$ (premixed). Qualitatively, we can observe that the traditional flame index definition tends to predict many regions with premixed combustion mode. Closer examination of these results show the possibility of false detection with the traditional definition. We know that Sydney Flame L is a non-premixed flame and we can expect a non-premixed combustion mode upstream of the flame, i.e., closer to the jet. But Figure 4.5 shows that the definition is predicting premixed mode (green region) even upstream of the flame. Similar observations are made downstream of the flame where the combustion is predominantly in premixed combustion mode. Considering two axial locations in these regions, $x/D = 5$ and $x/D = 45$, we can plot radial profiles of mass fraction, magnitude of gradients and θ, as shown in the right side of Figure 4.5. We can observe that even though the magnitude of gradients of oxygen is very small, a premixed combustion mode is detected $\theta = 1$. We can additionally plot the PDF distribution of θ in burning regions of the flame i.e $T > 300\ K$, as shown in Figure 4.6.

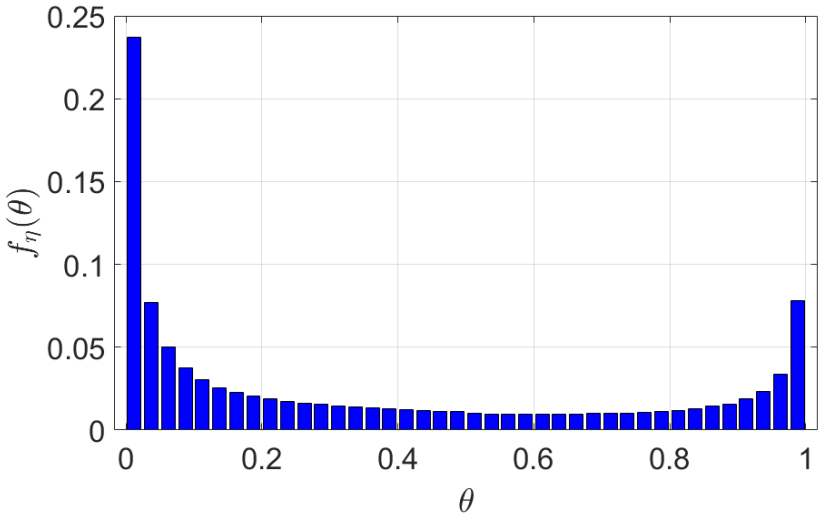

Fig. 4.6. PDF distribution of θ with bin size of $\Delta\theta = 0.02$, using the traditional flame index definition.

We can see from Figure 4.6 that using the traditional flame index gives a bi-modal distribution of θ. It tends to predict more regions of premixed modes. It can be argued that this bi-modal distribution is not accurate since we know that Sydney Flame L is a non-premixed flame and we should expect more non-premixed combustion modes and lesser premixed mode regions.

4.2.2 Refinement of Flame Index Definition

The above results and reasons point to the conclusion that the current definition of flame index is not accurate and need further refinement specific to PDF model. Looking at Figure 4.5, we can see that even small variations of mass fraction (or small magnitude of gradients), result in $\theta = 1$ or premixed combustion. These small variations can be attributed two aspects of PDF model: (i) presence of statistical errors in the PDF model and (ii) highly non-linear equations resulting in small variations in small grid sizes. Thus, it can be argued that we need to eliminate false detection of premixed mode in these regions of small gradient magnitudes. We must look closely into the small gradient magnitudes which tend to result in premixed combustion mode. As it was pointed before from Figure 4.5, the traditional definition detects premixed combustion mode even upstream of the flame, which is not possible since Sydney Flame L is a non-premixed flame and a proper detection will result in $\theta = 0$ or non-premixed mode upstream of the flame. Thus we need to take a closer look at the results of flame index in upstream locations of the flame. Figure 4.7 shows the PDF distribution of gradient magnitudes of oxygen at locations $x/D < 10$ which result in $\theta > 0.5$. We can observe that there are unusually greater number of very small gradient magnitudes that result in $\theta > 0.5$. This points to the possibility that the false detection reported earlier is caused due to the presence of very small gradient magnitudes that are causing $\theta > 0.5$.

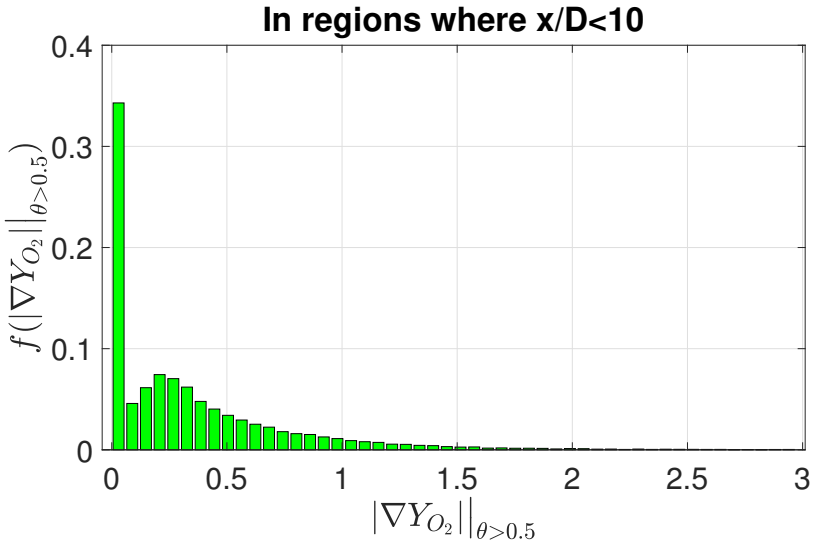

Fig. 4.7. PDF distribution of $|\nabla \widetilde{Y}_{O_2}|$ with bin size of $\Delta|\nabla \widetilde{Y}_{O_2}| = 0.0594$ conditioned that it results in $\theta > 0.5$ or premixed modes. The region is limited to $x/D < 10$

On zooming into the distribution of only the small gradients of oxygen, we get a distribution as shown in Figure 4.8. Again, the small gradients are conditioned on $\theta > 0.5$ or resulting in premixed combustion mode. We can observe the presence of very small gradients that are causing θ to be greater than 0.5. This points to the possibility of eliminating these gradients for a more accurate prediction of combustion regimes. Thus, we can choose a threshold value to eliminate these small gradients. Since this becomes an arbitrary number, we need to choose a general value independent of a particular scenario. Figure 4.8 shows a green region, which corresponds to the range of gradient values that are greater than 0.25% of the maximum gradient value and less than 1% of the maximum gradient value of oxygen in the entire computational domain. We can see that by using a threshold value in this range, we are eliminating those small gradients that produce $\theta > 0.5$. This range of 0.25% and 1% of $max(|\nabla \widetilde{Y}_{O_2}|)$ was chosen since it was small enough to not completely eliminate essential gradients and also large enough to eliminate small gradients resulting in false detection.

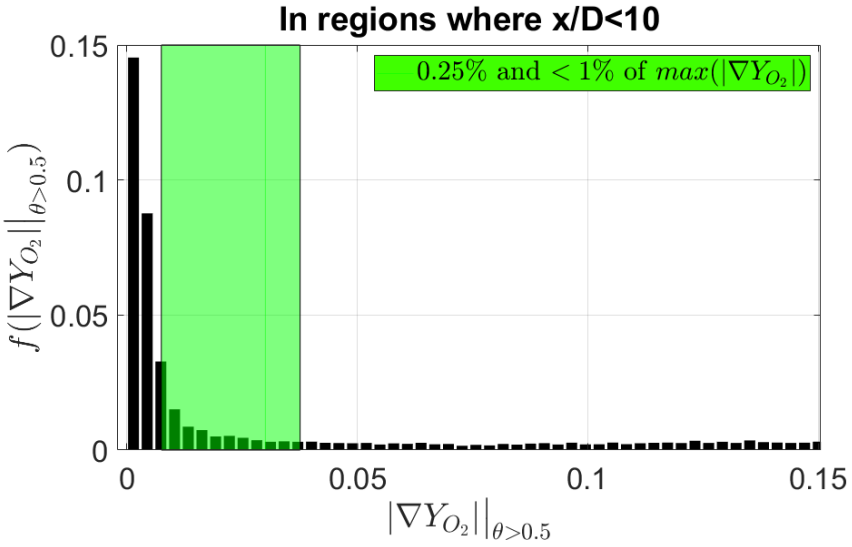

Fig. 4.8. PDF distribution of $|\nabla\widetilde{Y}_{O_2}|$ with bin size of $\Delta|\nabla\widetilde{Y}_{O_2}| = 0.003$ conditioned that it results in $\theta > 0.5$ or premixed modes. The region is limited to $x/D < 10$ and the distribution in zoomed in at very small values of gradient. The green translucent are gradient values that are greater than 0.25% and less than 1% of $max(|\nabla\widetilde{Y}_{O_2}|)$

.

The above discussion was based on gradients on oxygen but the same can be applied to the gradients on methane as well. Thus, we can refine the definition of flame index by applying a threshold to the magnitude of the gradients of oxidizer and the fuel. From Figure 4.8, we identified that a threshold value in the range of 0.25% to 1% of $max(|\nabla\widetilde{Y}_{O_2}|)$ was reasonable enough to use. We denote this new threshold parameter as β, where β is percentage value. By including this threshold to the definition of flame index, θ can be defined as,

$$\theta = \begin{cases} 0 & \text{when } |\nabla\widetilde{Y}_F| < \beta\%(max|\nabla\widetilde{Y}_F|), \\ & |\nabla\widetilde{Y}_O| < \beta\%(max|\nabla\widetilde{Y}_O|), \\ 0.5 * \left(1 + \frac{\nabla\widetilde{Y}_O \cdot \nabla\widetilde{Y}_F}{(|\nabla\widetilde{Y}_O||\nabla\widetilde{Y}_F|+\epsilon)}\right) & \text{otherwise.} \end{cases} \tag{4.1}$$

The value of β needs to be carefully chosen so as to not over-eliminate the small gradients. For the purpose of this study, we select $\beta = 0.25\%$, 0.5%, 1% as values to

perform a parametric study and choose a threshold that provides better predictions. Figure 4.9 shows the detection of combustion regime using $\beta = 0.5\%$.

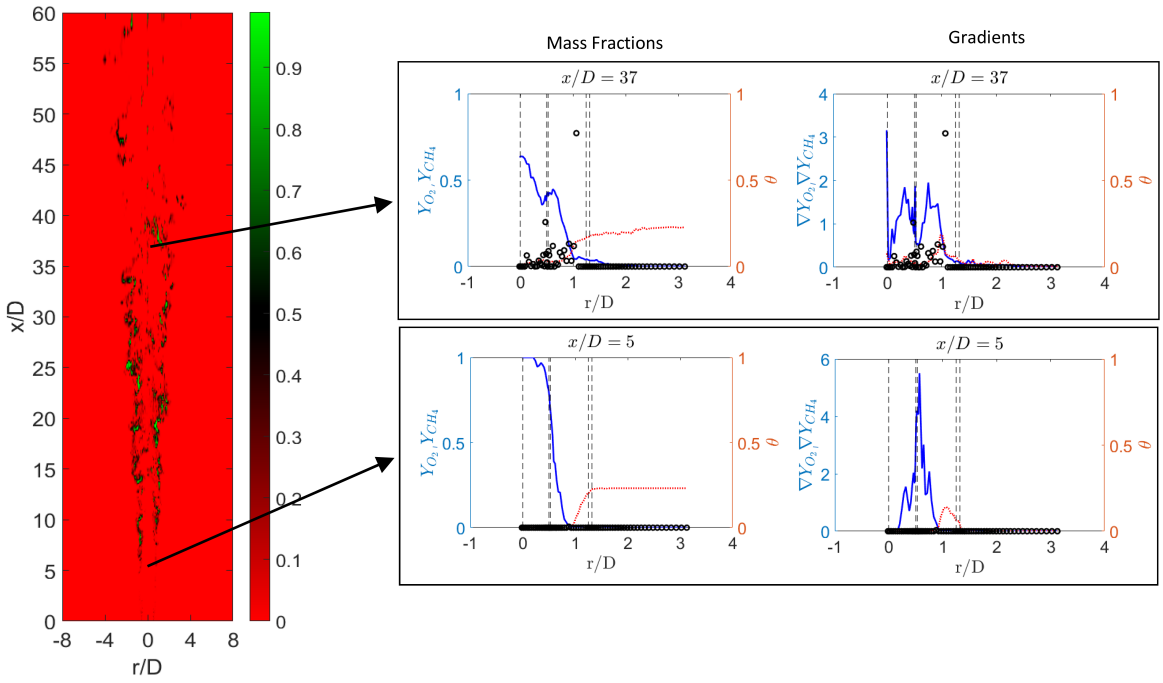

Fig. 4.9. Contour plot of θ (Left) using $\beta = 0.5\%$. Radial profiles of mass fractions and gradients of O_2 and CH_4 at $x/D = 5$ (bottom right) and at $x/D = 5$ (top right). The left axis of the plots are gradient magnitudes or mass fractions while the right axis is θ. Red dotted line: oxygen, blue solid line: methane, black circle: θ.

Compared to the detection as seen in Figure 4.5, the detection by using a gradient threshold parameter β provides better results of combustion regime. The false detection of premixed mode upstream of the flame is eliminated. Additionally, the large premixed regions observed completely downstream of the flame is also eliminated. Thus, we can argue that this gradient threshold parameter β, becomes an important model parameter. Figure 4.10 shows the PDF distribution of θ using the new definition from equation (4.1) in burning regions ($T > 300\ K$).

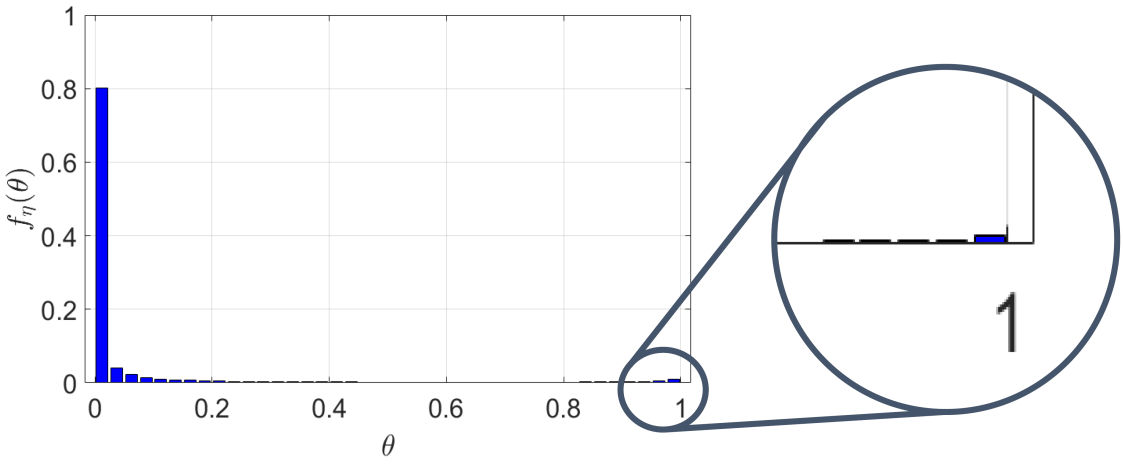

Fig. 4.10. PDF distribution of θ with bin size of $\Delta\theta = 0.02$, using the new flame index definition and $\beta = 0.5\%$.

The new distribution can be arguably called a more reasonable distribution. It represents the combustion modes in Sydney Flame L, which can be said to have predominantly non-premixed fronts with small regions of premixed fronts. Thus, this new model parameter β which determines the gradient threshold, can be used for the multi-regime model. With three values of $\beta = 0.25\%$, 0.5%, 1% selected, we can perform a parametric study to determine the optimum value.

4.3 Performance of the Multi-regime Model

This section presents the results for Sydney Flame L using the multi-regime LES/PDF model. The first part presents a parametric study procedure to determine an appropriate value for the gradient threshold parameter β. The second part shows a comparative study between the multi-regime model and the traditional non-premixed model for all the three mixing models: Mcurl, IEM and EMST.

4.3.1 Parametric Study for Multi-regime Model Parameter β

With the new definition of flame index from equation (4.1) which considers the parameter β and the blending technique as described in Section 2.10, we have a complete multi-regime model for LES/PDF. However, in the previous section, we established that $\beta = 0.25\%$, 0.5%, 1% are reasonable as well as appropriate for a more accurate regime identification. In Section 4.1, results from the traditional non-premixed model was presented using the MCurl mixing model. Thus, to determine the appropriate value of β, we follow the procedure outlined below,

- Using the MCurl mixing model, we perform a parametric study to find the optimum value for β such that it closely matches the experimental data.
- We then assess the performance of the multi-regime model compared to traditional non-premixed model for EMST as well as IEM model using this particular value of β.

Figure 4.11 shows the contour plots of instantaneous temperatures using four values of β: 0%, 0.25%, 0.5% and 1%. A value of $\beta = 0\%$ essentially corresponds to the traditional flame index definition as seen in equation (2.27), without any gradient threshold filtering. We observe a monotonic trend of decreasing extinction level as the value of β is increased. For $\beta = 0\%$, we observe a complete burning flame without any significant local extinction.

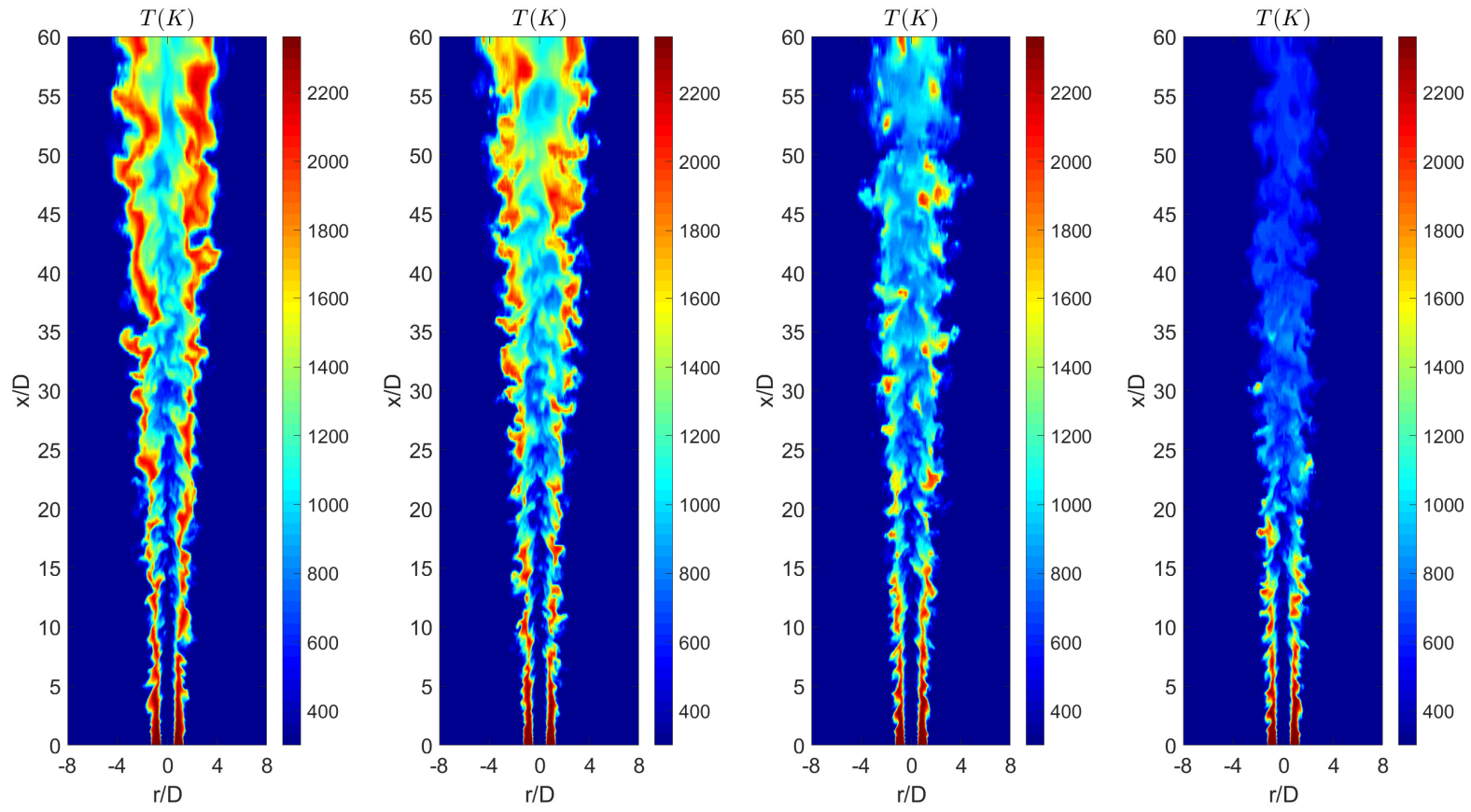

(a) $\beta = 0\%$ (b) $\beta = 0.25\%$ (c) $\beta = 0.5\%$ (d) $\beta = 1\%$

Fig. 4.11. Contours of temperature for the multi-regime model using $\beta = 0\%$, 0.25%, 0.5% and 1%. Mixing model: MCurl

For $\beta = 0\%$, the regime identification parameter θ detects premixed combustion regime in most regions of the flame, as seen in Figure 4.5. Thus, the premixed PDF mixing frequency model, described in Section 2.8 is used in all these grid cells. As we know, the premixed PDF model tends to promote mixing due to reaction and consequently results in higher temperature. As we increase the value of β, we eliminate over-detection of premixed combustion modes in the flame, which limits the inclusion of premixed PDF mixing frequency model in the grid cells and hence, results in lower temperatures. The contours provide just a qualitative assessment of using different values of β. We need to compare the results with the experimental data to determine the optimal value of β. Figures 4.12 and 4.13 show the mean or time-averaged values of the flow field and scalars at $x/D = 10, 20$ and 30. We can observe that $\beta = 0.5\%$ provides the closest agreement with the experimental data. For mean temperature $\langle\widetilde{T}\rangle$, temperature variance $\langle\widetilde{T''}\rangle$, mean mass fraction of $\langle\widetilde{O_2}\rangle$ and mean mass fraction of $\langle\widetilde{H_2O}\rangle$, we see that a value of $\beta = 0.5$ is much closer to the experimental data compared to other values.

Figure 4.14 shows the conditional means of the scalars in the mixture fraction space at $x/D = 10, 20$ and 30 using different values of β. The difference in using different values of β can be better observed in the mixture fraction space, especially at downstream locations $x/D = 20$ and $x/D = 30$. This is expected since upstream of the flame, we do not detect an premixed combustion mode from the refined flame index definition and hence only the non-premixed model used in all the different cases of β in the multi-regime model. We can see that the multi-regime model closely matches the experimental data for $\langle T|\xi\rangle$ and $\langle O_2|\xi\rangle$ using $\beta = 0.5\%$.

In both the plots of mean values in physical space and conditional mean in mixture fraction space, we can see a monotonic trend where increasing values of β result in under-prediction of quantities. For $\beta = 0\%$, the scalars are over predicted by a large extent because of more mixing due to reaction in the grid cells. Even using a value of $\beta = 0.25\%$ i.e. filtering all gradients of oxygen and methane less than 0.25% of maximum corresponding gradient value in the domain, results in over-prediction.

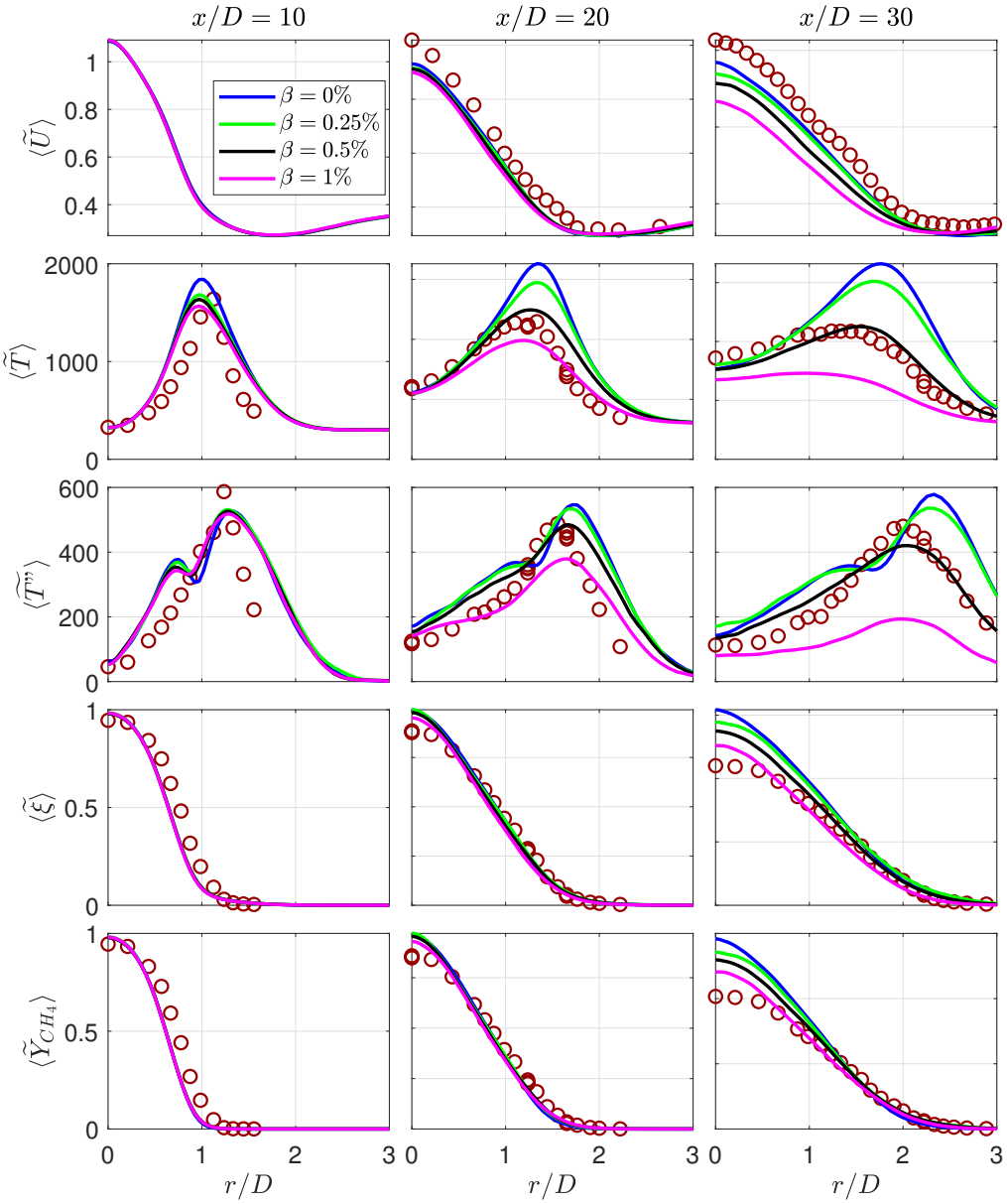

Fig. 4.12. Radial profiles of mean axial velocity $\widetilde{U}$, mean temperature $\widetilde{T}$, temperature variance $\widetilde{T}''$, mean mixture fraction $\widetilde{\xi}$ and mass fraction of $\widetilde{Y}_{CH_4}$ from the multi-regime model using $\beta = 0\%$, 0.25%, 0.5% and 1%. Mixing model: MCurl

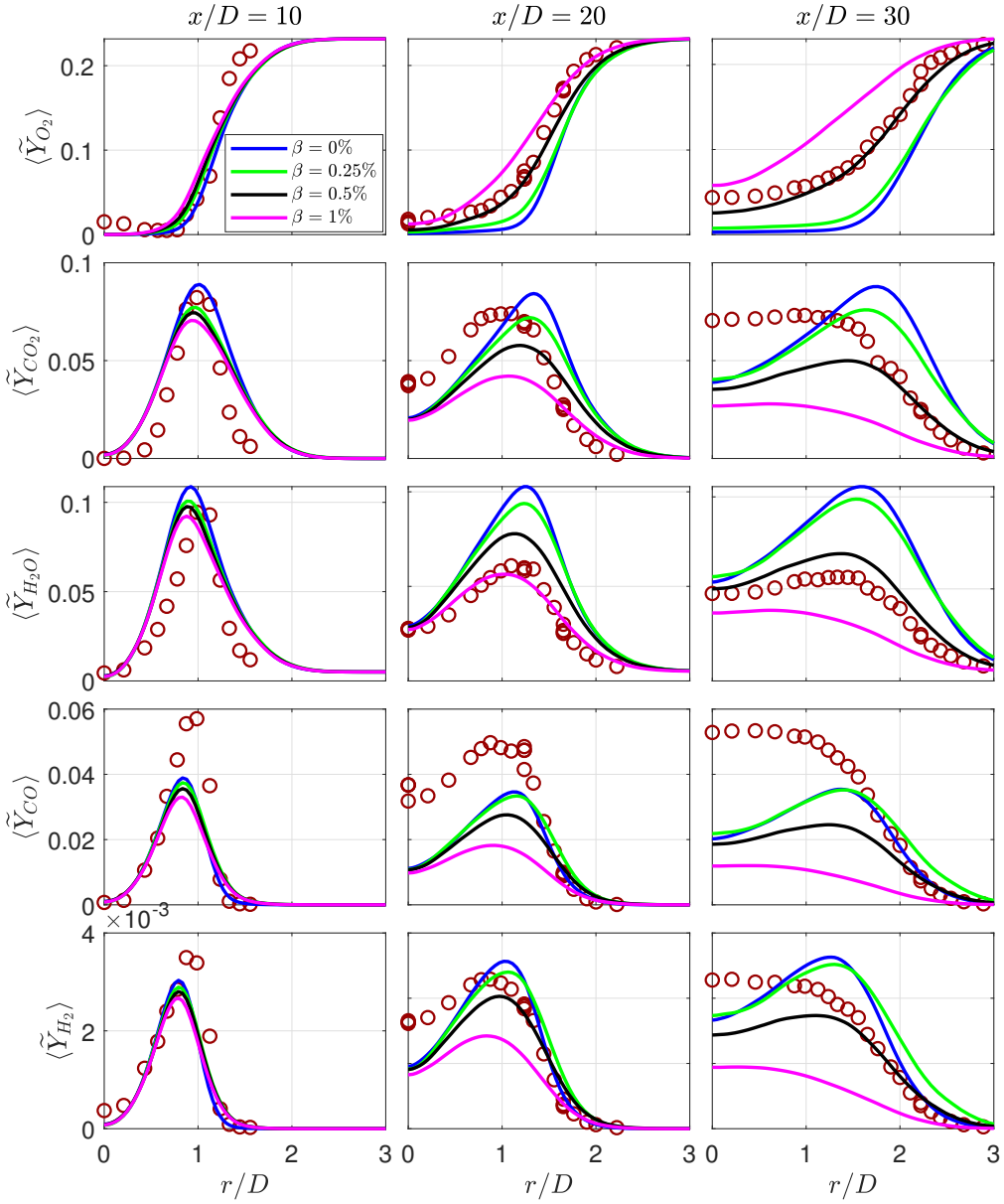

Fig. 4.13. Radial profiles of mean mass fractions of $\widetilde{Y}_{O_2}$, $\widetilde{Y}_{CO_2}$, $\widetilde{Y}_{H_2O}$, $\widetilde{Y}_{CO}$ and $\widetilde{Y}_{H_2}$ from the multi-regime model using $\beta = 0\%$, 0.25%, 0.5% and 1%. Mixing model: MCurl

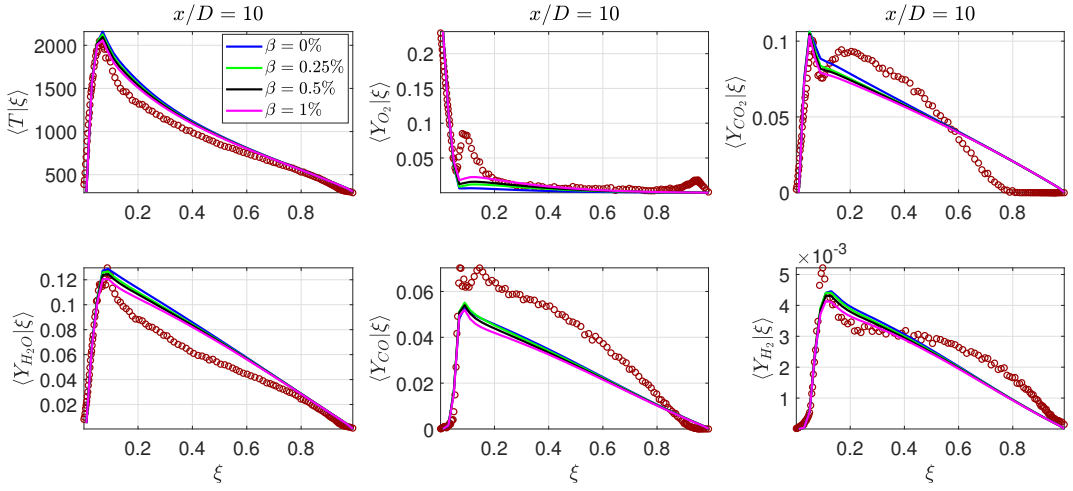

(a)

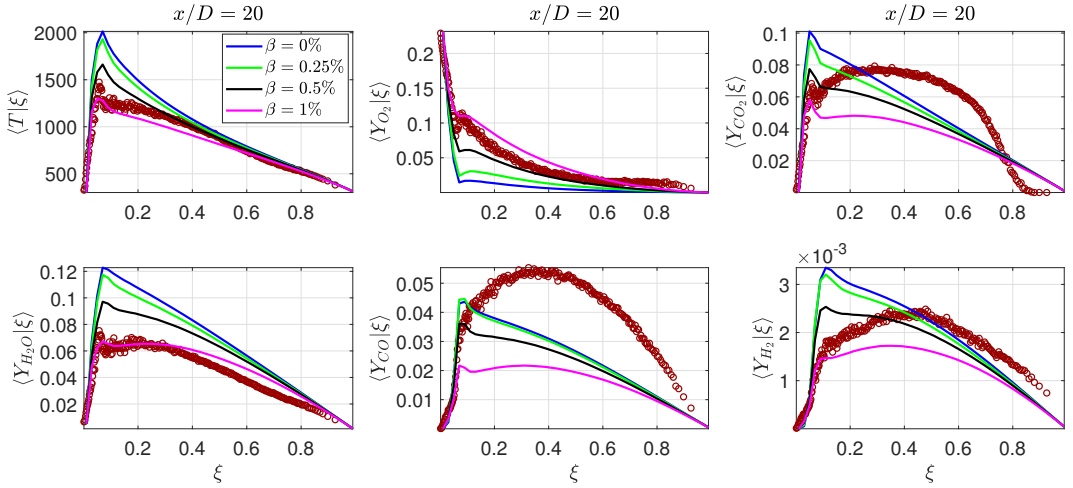

(b)

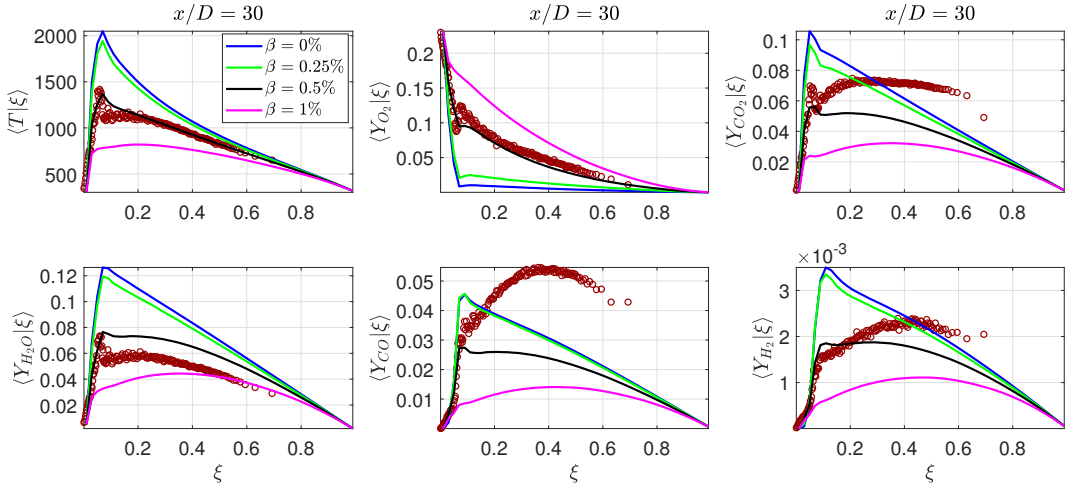

(c)

Fig. 4.14. Conditional means of scalars in the mixture fraction space at $x/D = 10, 20$ and 30 from the multi-regime model using $\beta = 0\%$, 0.25%, 0.5% and 1%. Mixing model: MCurl.

This suggests that not all small gradients which results in detecting premixed mode are eliminated and hence, premixed modes are over-detected in the domain. But a value of $\beta = 0.5\%$ is sufficiently small as well as large enough to produce a proper detection of premixed combustion mode. A value of $\beta = 1\%$ results in under-detection of premixed combustion modes since it tends to eliminate more gradients than expected. Thus, $\beta = 0.5\%$ can arguably called an optimum value for proper detection of combustion regime and resulting in better prediction using the multi-regime model. Section 4.3.2 presents the results for a comparative study between the multi-regime model using $\beta = 0.5\%$ and the traditional non-premixed model.

4.3.2 Comparative Study of Multi-regime vs Non-premixed Model

This section presents the performance of the multi-regime model using $\beta = 0.5\%$ when compared to the traditional non-premixed model. Section 4.1 discusses the results of the traditional non-premixed model using MCurl mixing model and Section 4.3.1 shows results from the parametric study to determine an optimum value of β using MCurl mixing model. To appreciate the superiority of the multi-regime model, results are presented by comparing it to the widely-used traditional non-premixed model. The results are shown for all three mixing models: MCurl, IEM and EMST. Qualitative comparison can be made based on the contour plots of key instantaneous quantities while qualitative comparison can be made using mean profiles in physical space and conditional mean profiles in mixture fraction space. Additionally, particle scatter plots in the mixture fraction space can be used to assess the extinction at different axial locations for the old non-premixed model, multi-regime model and experimental data.

MCurl Mixing Model

Figures 4.15, 4.16 and 4.17 show a comparison between the instantaneous contour plots of the scalars. We see that the multi-regime model produces a burning flame

with local extinction while the non-premixed model tends to completely extinguish the flame. The radial profiles shown in Figures 4.18 and 4.19 show that the multi-regime model using MCurl has a much better prediction than the old non-premixed model. This trend can also be observed in the conditional mean plots in the mixture fraction space show in Figure 4.20. The improvements in predictions of time-averaged as well as conditional means of temperature and temperature variance show that the multi-regime model using MCurl is much more accurate. Particle scatter plots between temperature and mixture fraction at axial locations can tell us about extinction as well as burning level of the flame. Figure 4.11 shows the particle scatter plot between temperature and mixture fraction. The scatter plot from the multi-regime model closely matches the experimental data, while the non-premixed plot shows extinction at $x/D = 30$.

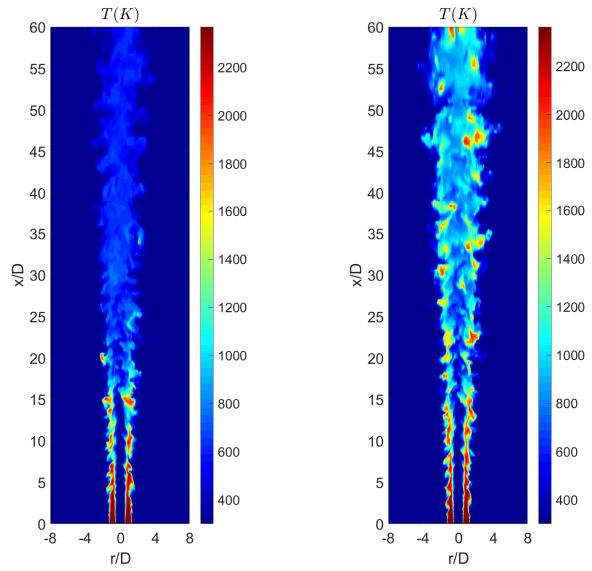

(a) (b)

Fig. 4.15. MCurl: Comparison of instantaneous temperature between (a) old non-premixed model and (b) multi-regime model with $\beta = 0.5\%$

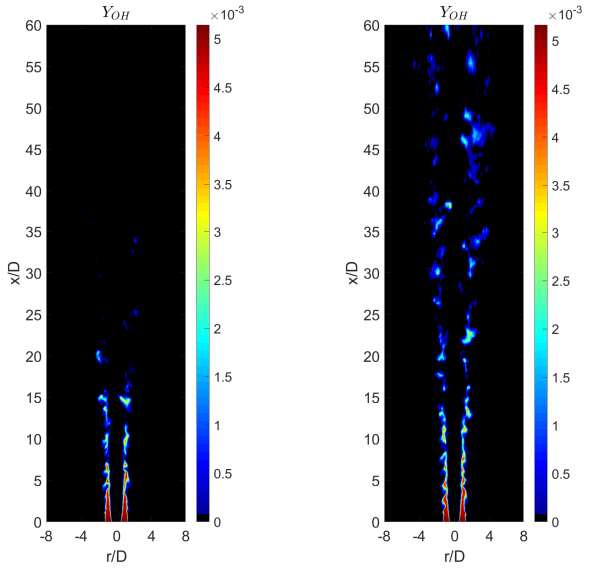

(a) (b)

Fig. 4.16. MCurl: Comparison of instantaneous Y_{OH} between (a) old non-premixed model and (b) multi-regime model with $\beta = 0.5\%$

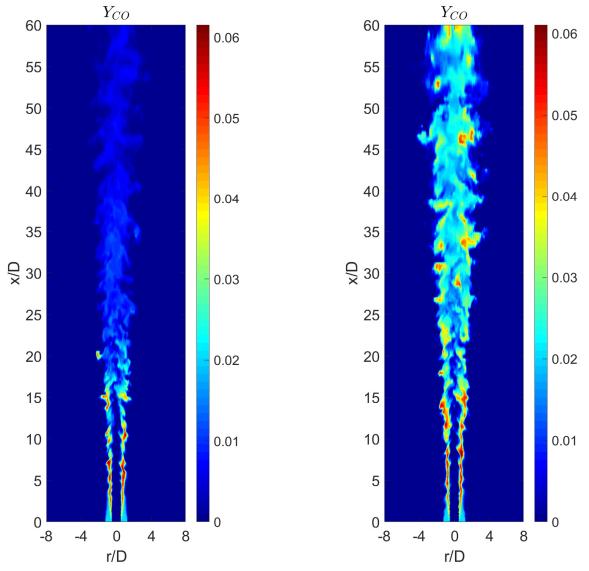

(a) (b)

Fig. 4.17. MCurl: Comparison of instantaneous Y_{CO} between (a) old non-premixed model and (b) multi-regime model with $\beta = 0.5\%$

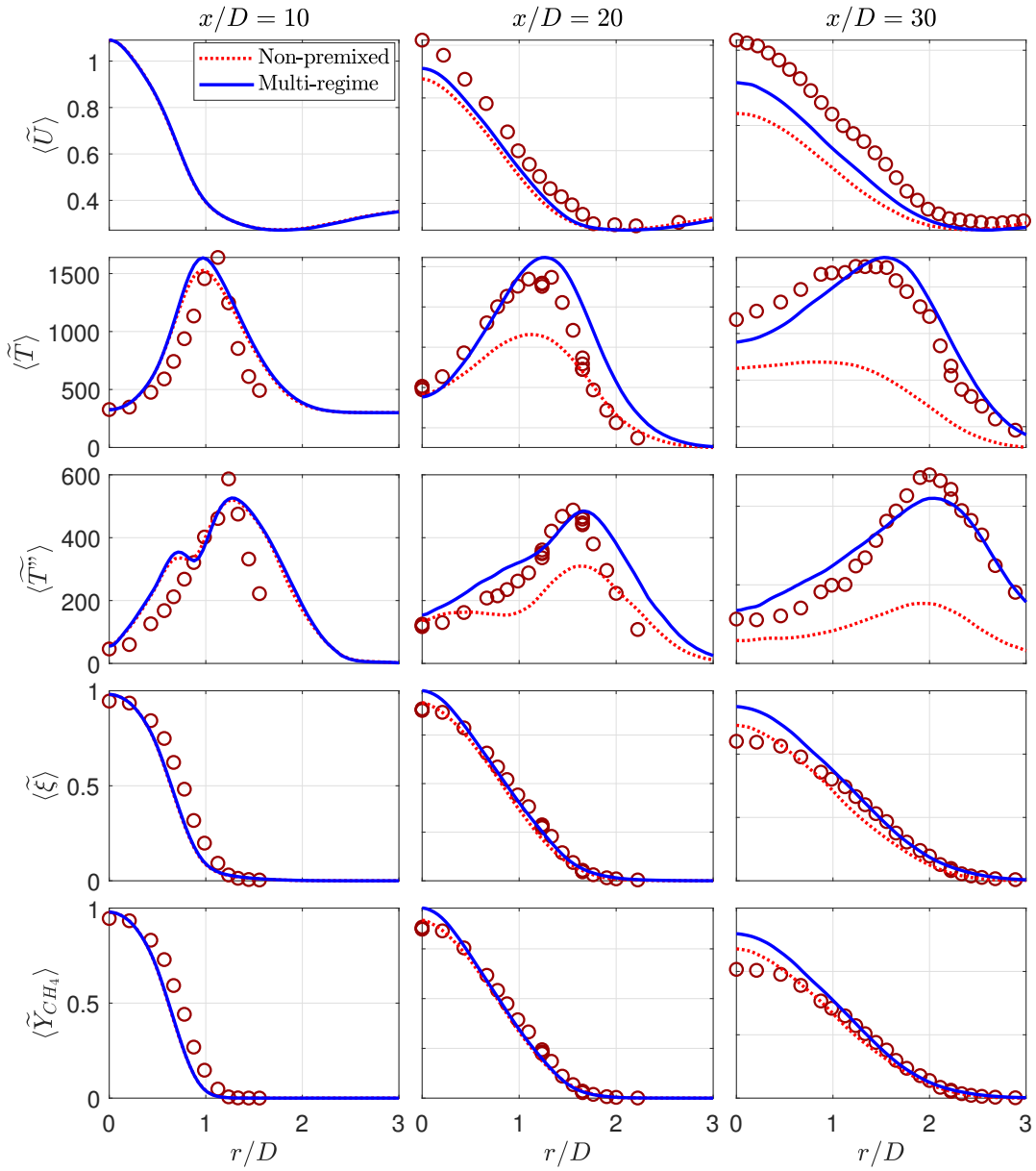

Fig. 4.18. MCurl: Radial profiles of mean axial velocity $\widetilde{U}$, mean temperature $\widetilde{T}$, temperature variance $\widetilde{T''}$, mean mixture fraction $\widetilde{\xi}$ and mass fraction of $\widetilde{Y}_{CH_4}$. Blue solid: multi-regime model and red dotted: non-premixed model.

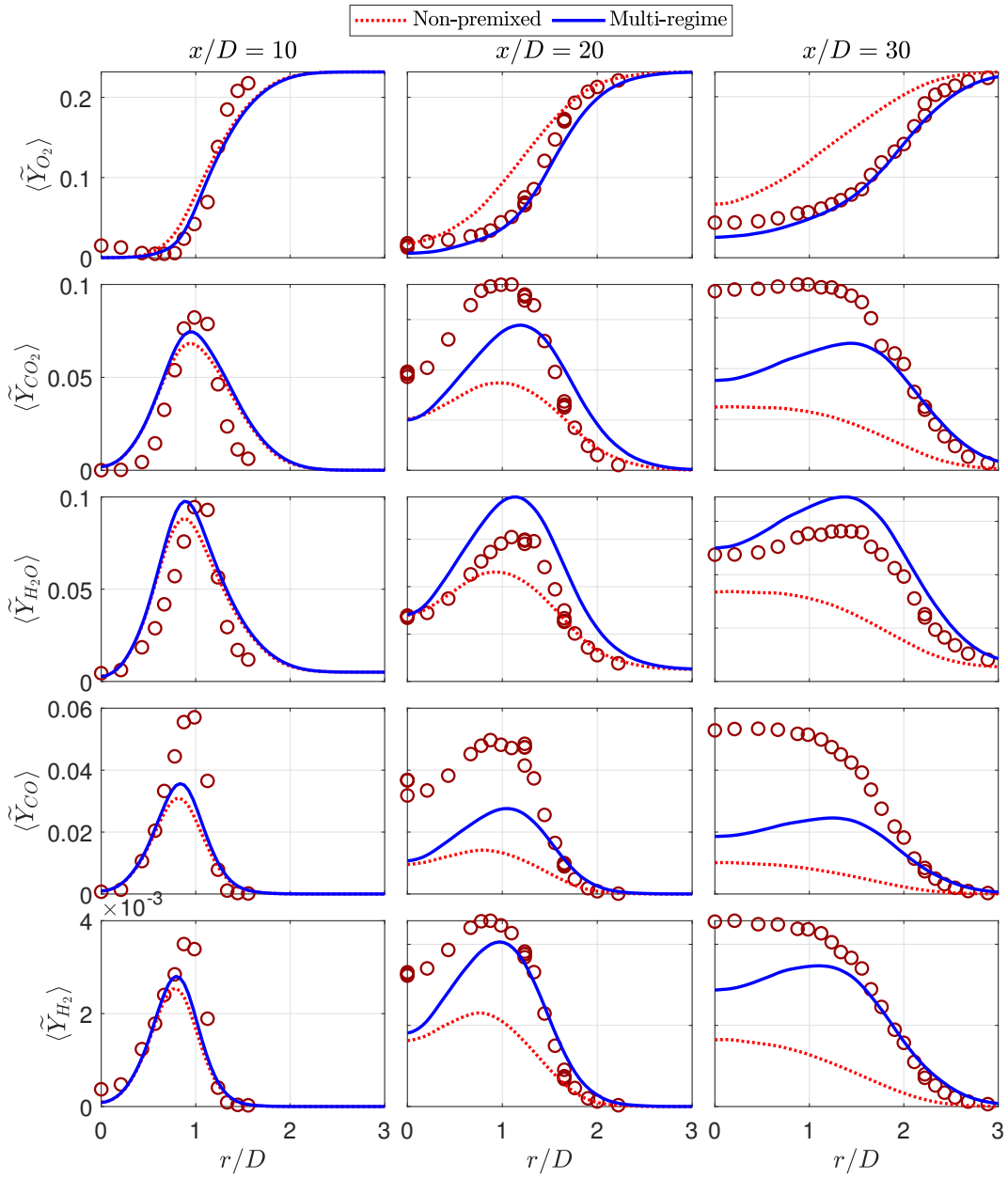

Fig. 4.19. MCurl: Radial profiles of mean mass fractions of $\widetilde{Y}_{O_2}$, $\widetilde{Y}_{CO_2}$, $\widetilde{Y}_{H_2O}$, $\widetilde{Y}_{CO}$ and $\widetilde{Y}_{H_2}$. Blue solid: multi-regime model and red dotted: non-premixed model.

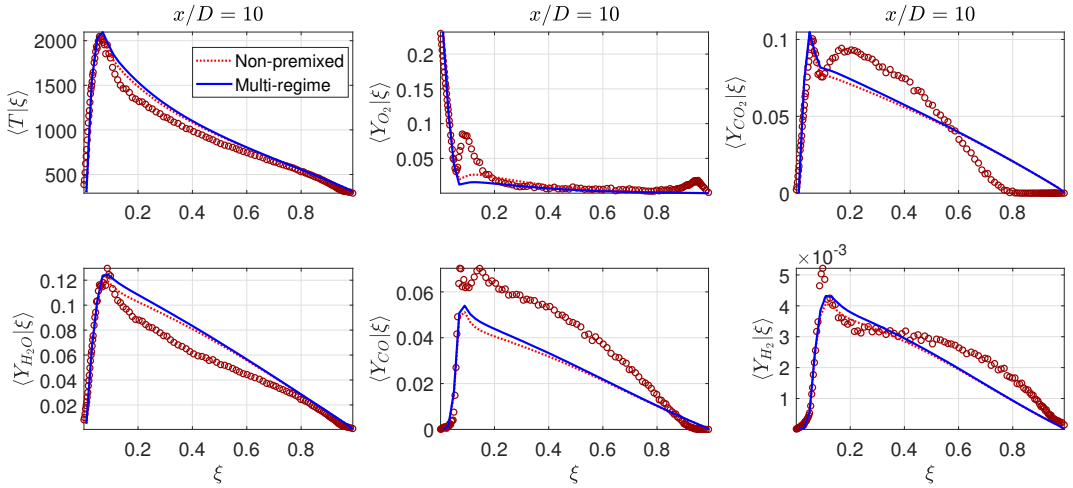

(a)

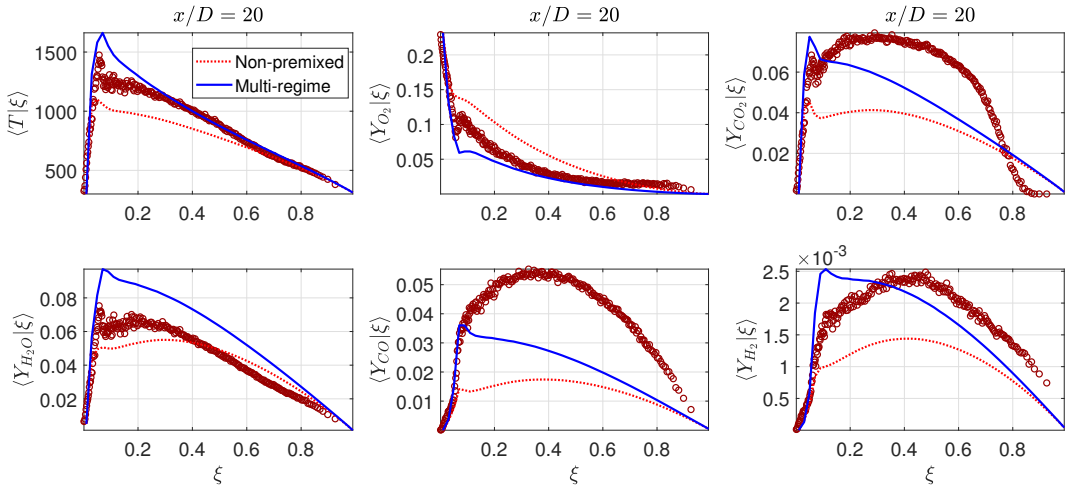

(b)

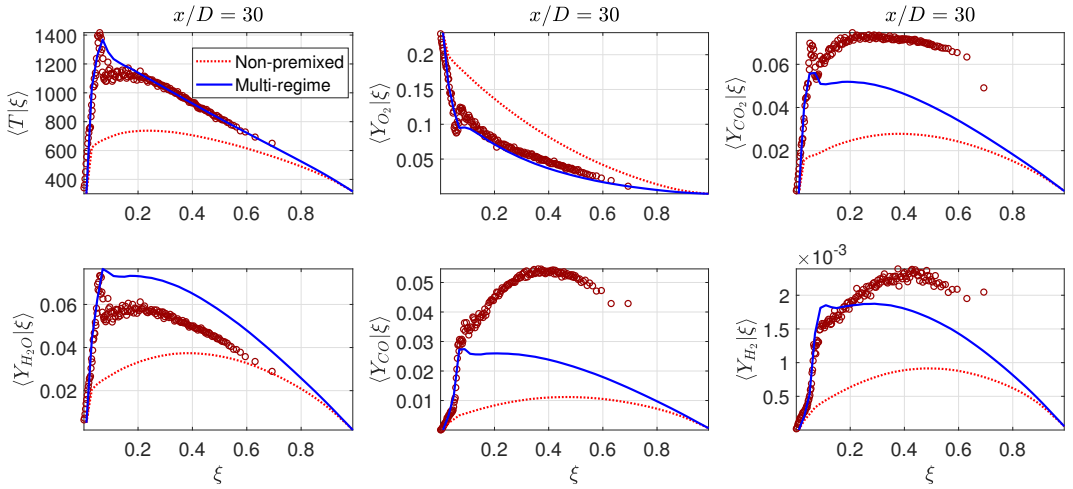

(c)

Fig. 4.20. MCurl: Conditional means of scalars in the mixture fraction space at $x/D = 10, 20$ and 30. Blue solid: multi-regime model and red dotted: non-premixed model.

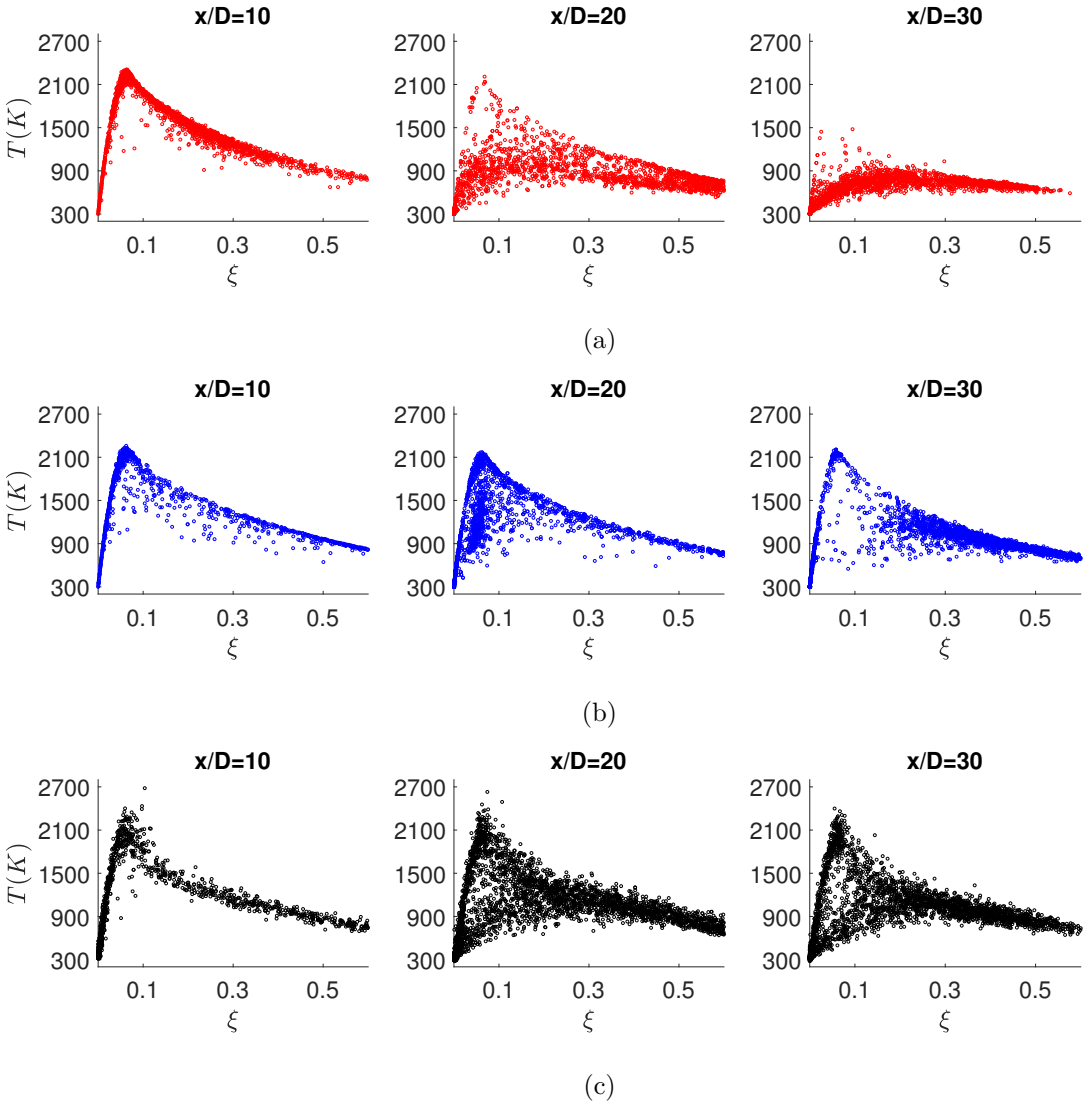

Fig. 4.21. MCurl: Temperature vs mixture fraction particle scatter plot at $x/D = 10, 20, 30$ for (a) non-premixed model, (b) multi-regime model and (c) experimental data.

IEM Mixing Model

Figures 4.22, 4.23 and 4.24 show a qualitative comparison of the instantaneous contours of scalars between the old non-premixed model and new multi-regime model using the IEM mixing model. We observe similar, though minor, improvements from the non-premixed model as seen using the MCurl mixing model. This can also be observed from radial profiles of mean quantities as shown in Figures 4.25 and 4.26 as well as conditional mean profiles in mixture fraction space as shown in Figure 4.27. Though we see improvements in the predictions, the multi-regime model using IEM model is not as accurate as using the MCurl model as seen in the previous section. The particle scatter plots shown in Figure 4.28 also shows that the multi-regime model as well as the non-premixed model using IEM shows extinction at downstream locations as compared to the experimental data. This behavior can be possibly attributed due to the non-localness property of IEM mixing model [45].

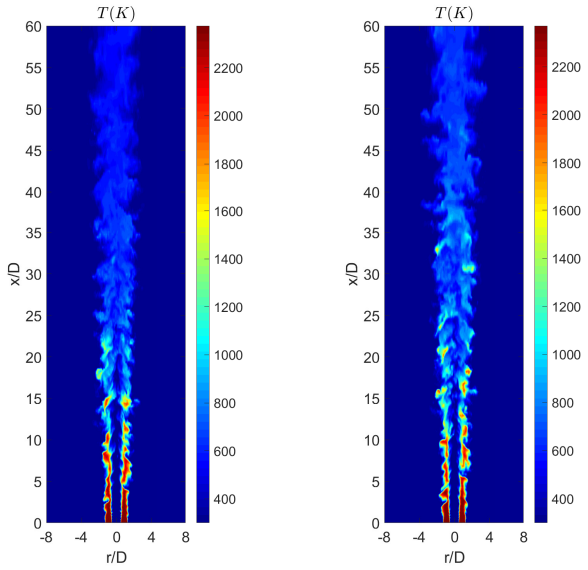

(a) (b)

Fig. 4.22. IEM: Comparison of instantaneous temperature between (a) non-premixed model and (b) multi-regime model with $\beta = 0.5\%$.

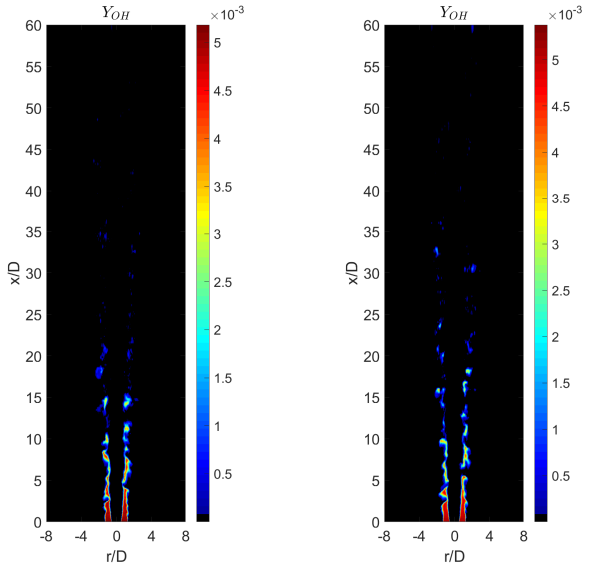

(a) (b)

Fig. 4.23. IEM: Comparison of instantaneous Y_{OH} between (a) old non-premixed model and (b) multi-regime model with $\beta = 0.5\%$

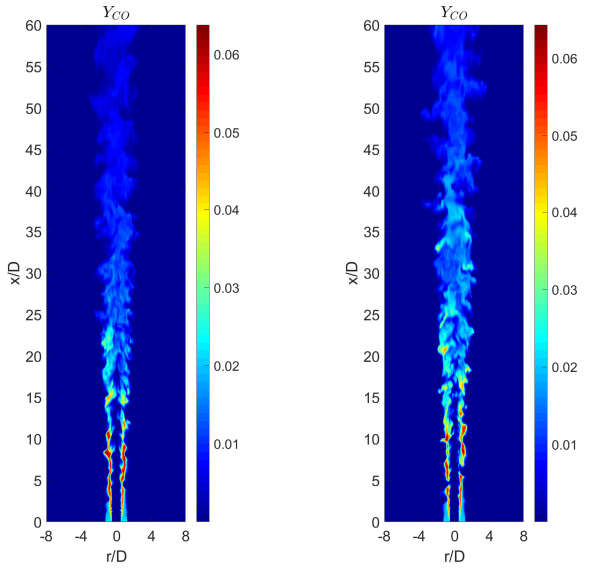

(a) (b)

Fig. 4.24. IEM: Comparison of instantaneous Y_{CO} between (a) old non-premixed model and (b) multi-regime model with $\beta = 0.5\%$

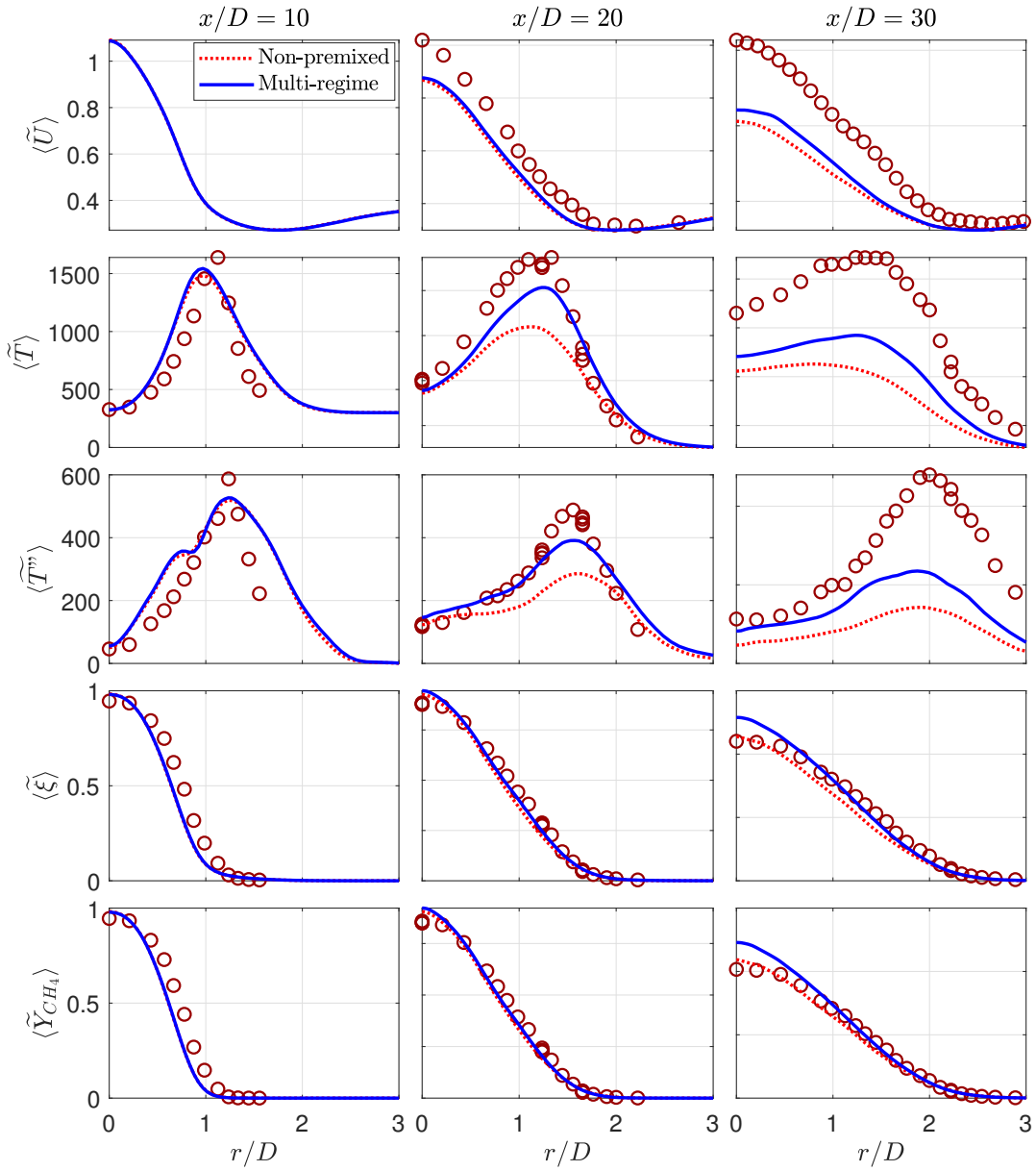

Fig. 4.25. IEM: Radial profiles of mean axial velocity $\widetilde{U}$, mean temperature $\widetilde{T}$, temperature variance $\widetilde{T''}$, mean mixture fraction $\widetilde{\xi}$ and mass fraction of $\widetilde{Y}_{CH_4}$. Blue solid: multi-regime model and red dotted: non-premixed model

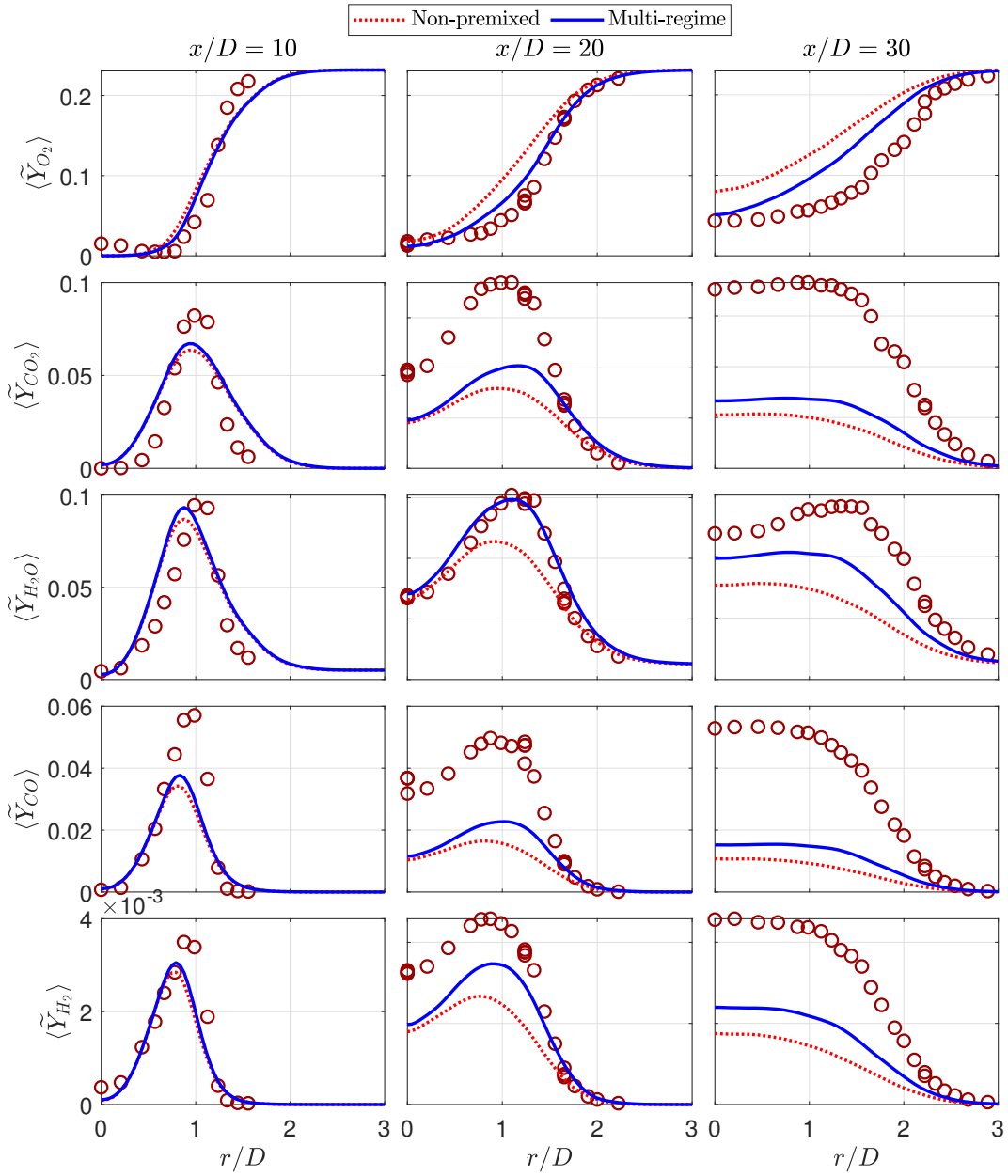

Fig. 4.26. IEM: Radial profiles of mean mass fractions of $\widetilde{Y}_{O_2}$, $\widetilde{Y}_{CO_2}$, $\widetilde{Y}_{H_2O}$, $\widetilde{Y}_{CO}$ and $\widetilde{Y}_{H_2}$. Blue solid: multi-regime model and red dotted: non-premixed model

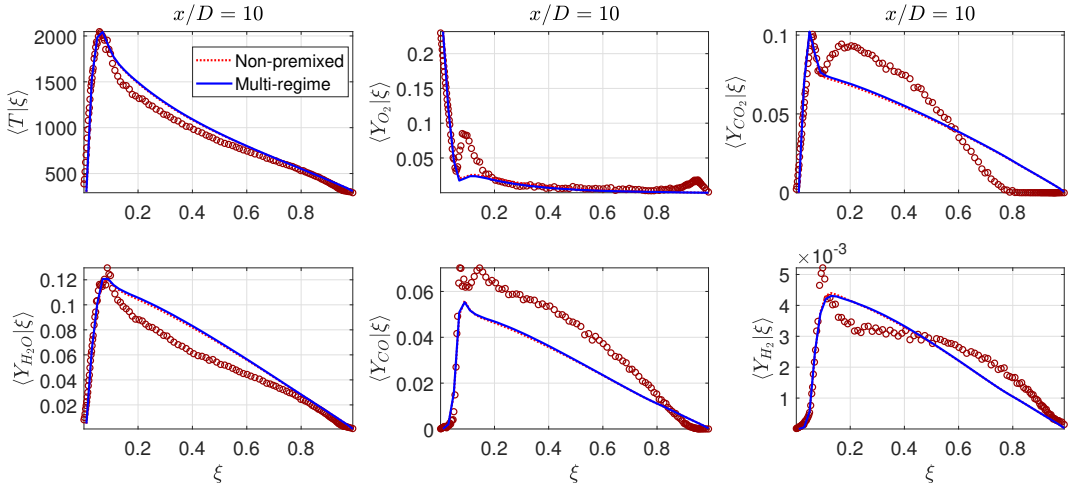

(a)

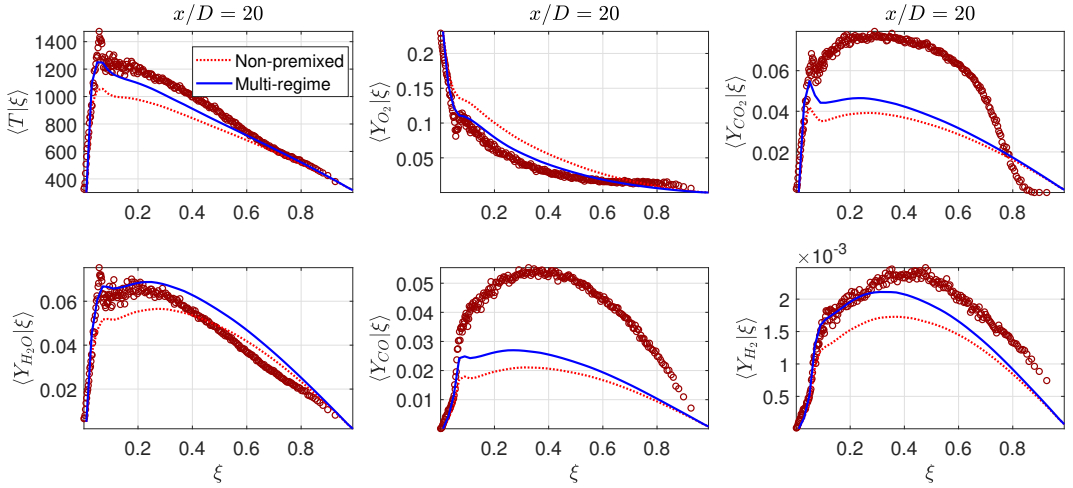

(b)

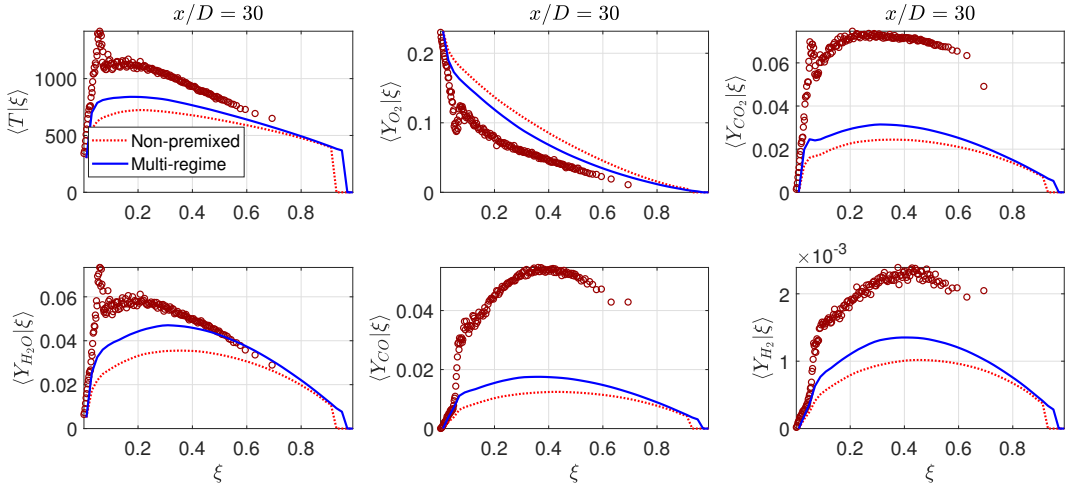

(c)

Fig. 4.27. IEM: Conditional means of scalars in the mixture fraction space at $x/D = 10, 20$ and 30. Blue solid: multi-regime model and red dotted: non-premixed model

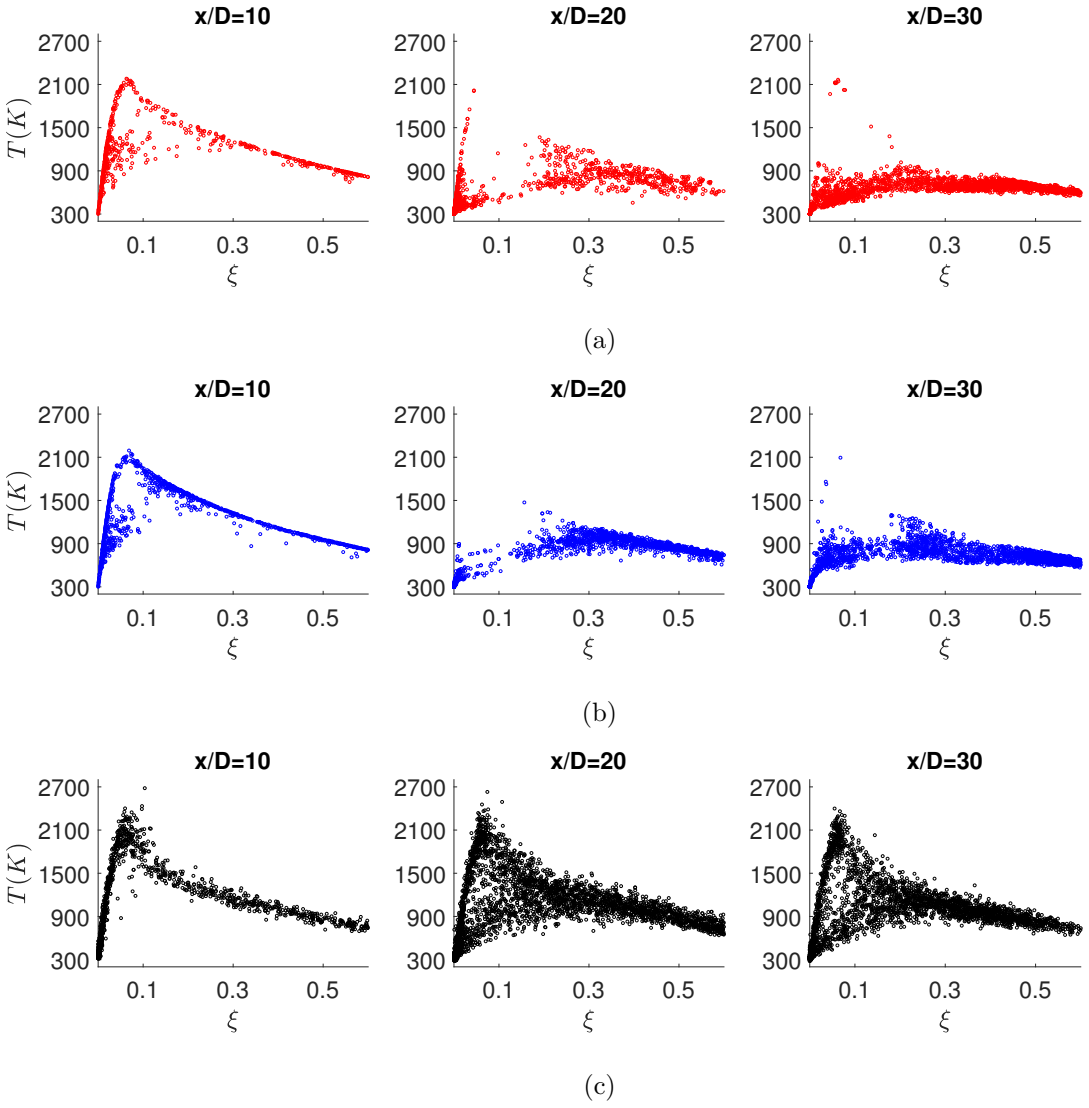

Fig. 4.28. IEM: Temperature vs mixture fraction particle scatter plot at $x/D = 10, 20, 30$ for (a) non-premixed model, (b) multi-regime model and (c) experimental data.

EMST Mixing Model

Figures 4.29. 4.30 and 4.31 show the instantaneous contour plots of scalars. We observe that both the models show very similar combustion fields. Figures 4.32 and 4.33 show the radial profiles of time-averaged quantities. Both the models have very close prediction compared to experimental data, with slight over-prediction by the multi-regime model. Similar trend is observed in conditional mean profiles shown in Figure 4.34. There is not much difference between the model at $x/D = 10$ since the multi-regime model essentially uses the non-premixed PDF model upstream of the flame. EMST mixing model is known to be resistant to extinction due to its localness property [21, 45] and thus, the non-premixed model has good predictions. Difference between the performance of the models can be seen in the particle scatter plot shown in Figure 4.35. At $x/D = 30$, the multi-regime model shows burning while the non-premixed model shows complete extinction.

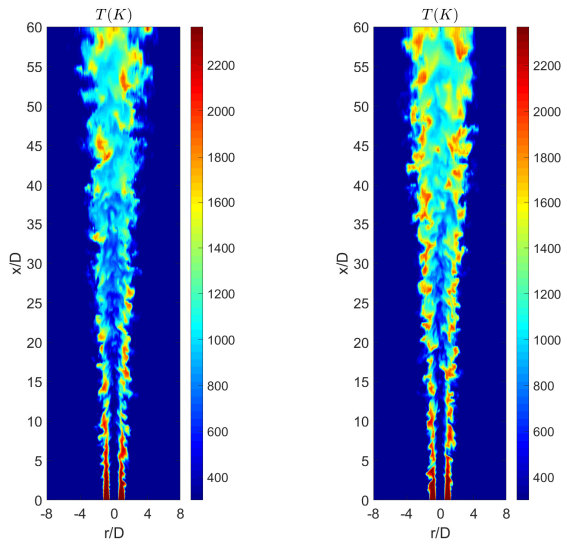

(a) (b)

Fig. 4.29. ESMT: Comparison of instantaneous temperature between (a) non-premixed model and (b) multi-regime model with $\beta = 0.5\%$.

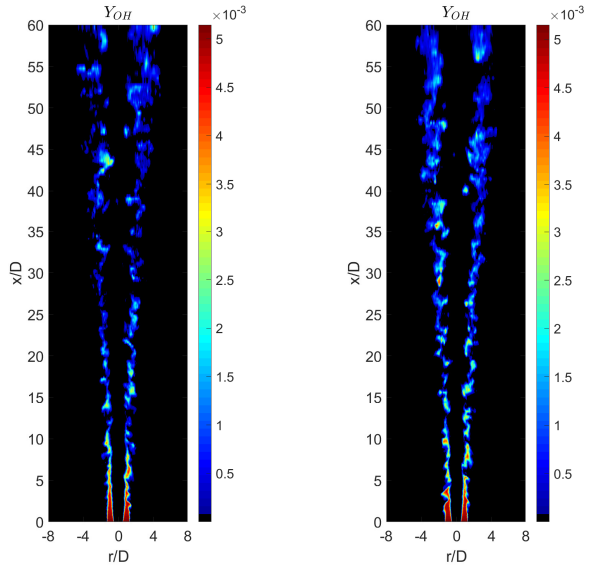

(a) (b)

Fig. 4.30. ESMT: Comparison of instantaneous Y_{OH} between (a) old non-premixed model and (b) multi-regime model with $\beta = 0.5\%$

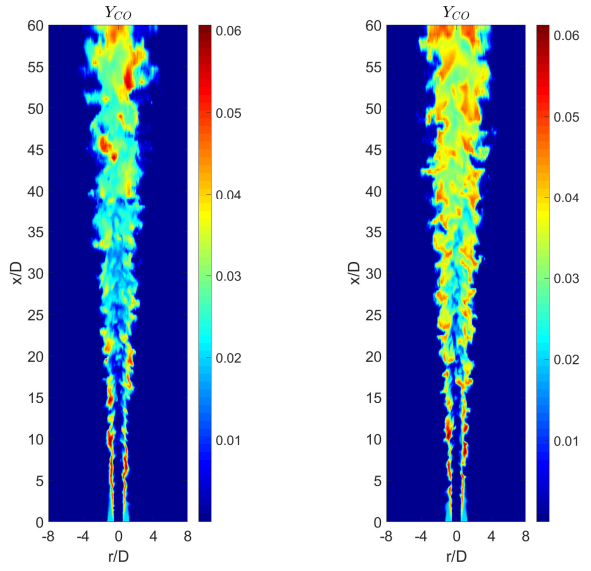

(a) (b)

Fig. 4.31. ESMT: Comparison of instantaneous Y_{CO} between (a) old non-premixed model and (b) multi-regime model with $\beta = 0.5\%$

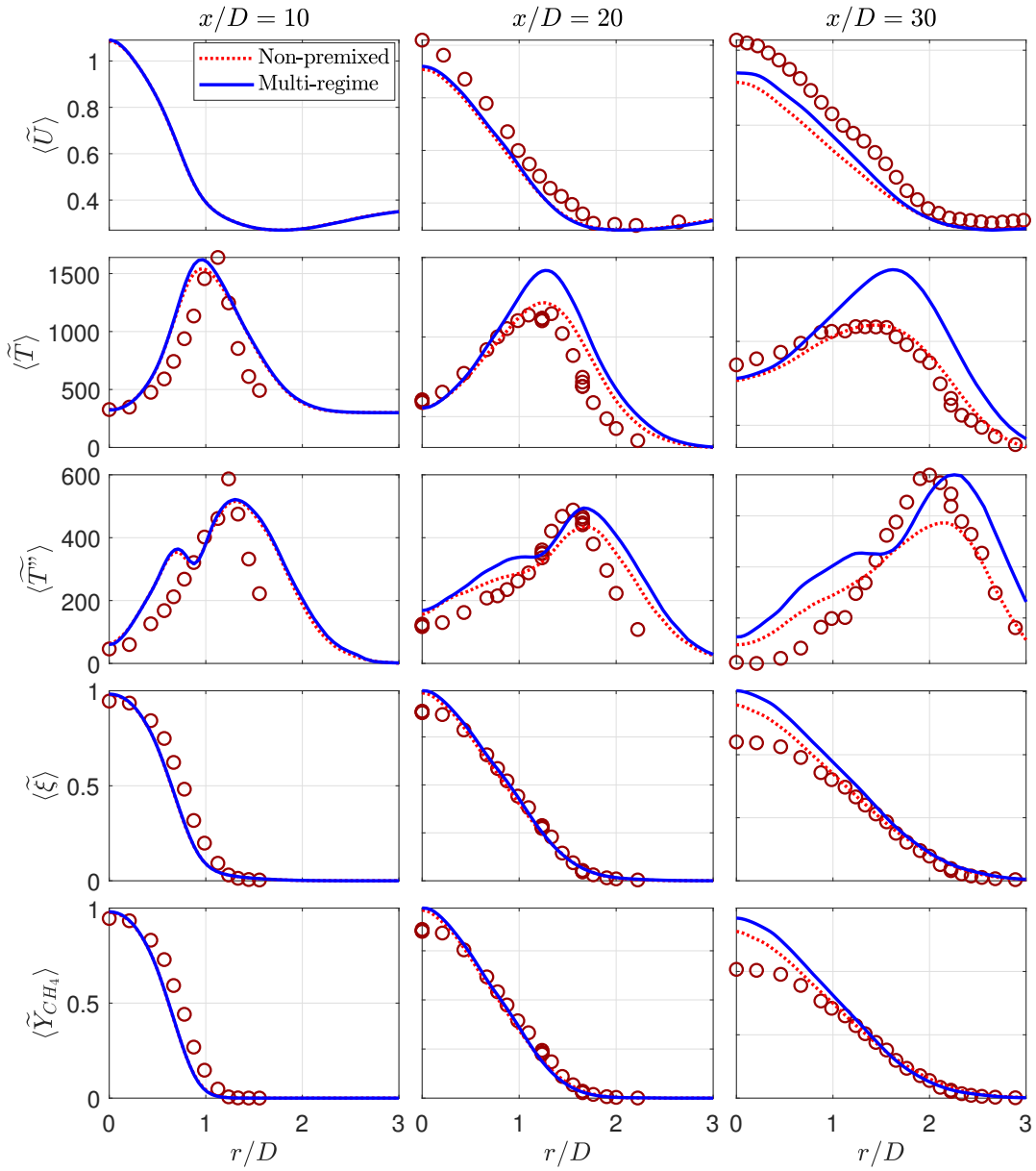

Fig. 4.32. ESMT: Radial profiles of mean axial velocity $\widetilde{U}$, mean temperature $\widetilde{T}$, temperature variance $\widetilde{T''}$, mean mixture fraction $\widetilde{\xi}$ and mass fraction of $\widetilde{Y}_{CH_4}$. Blue solid: multi-regime model and red dotted: non-premixed model

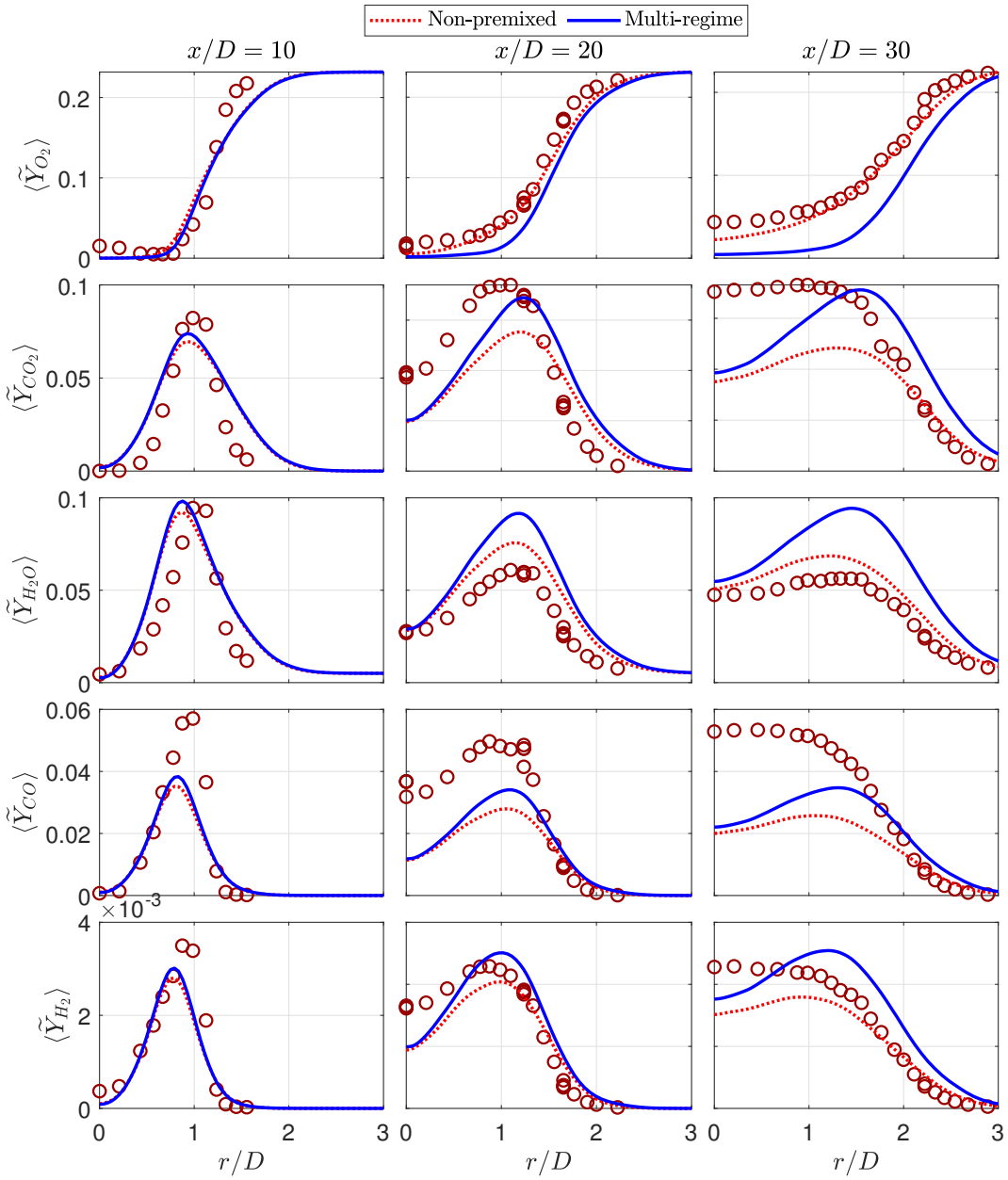

Fig. 4.33. ESMT: Radial profiles of mean mass fractions of $\widetilde{Y}_{O_2}$, $\widetilde{Y}_{CO_2}$, $\widetilde{Y}_{H_2O}$, $\widetilde{Y}_{CO}$ and $\widetilde{Y}_{H_2}$. Blue solid: multi-regime model and red dotted: non-premixed model

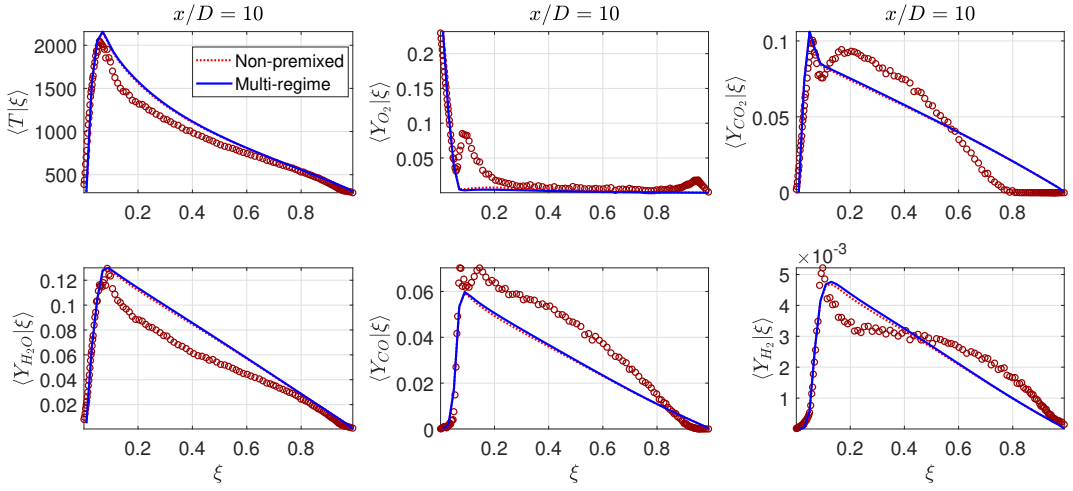

(a)

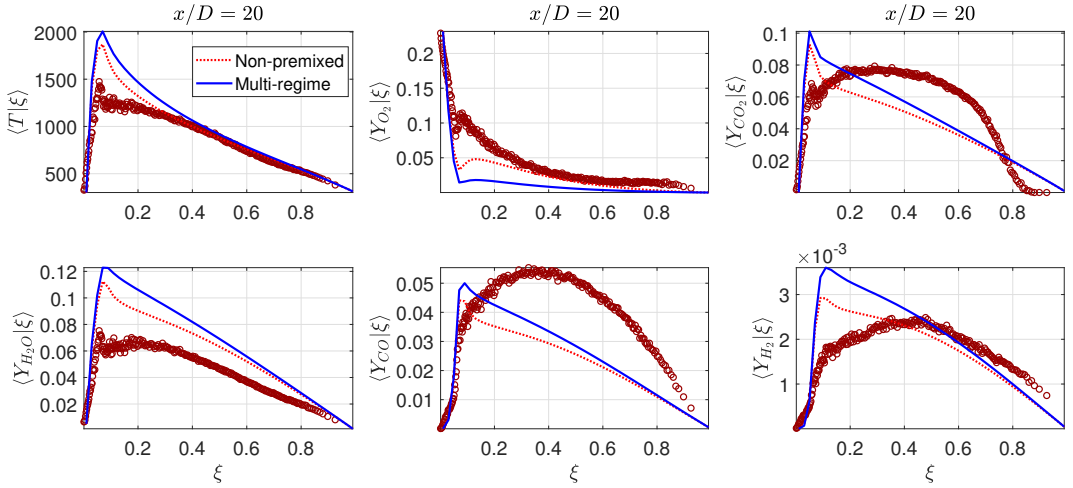

(b)

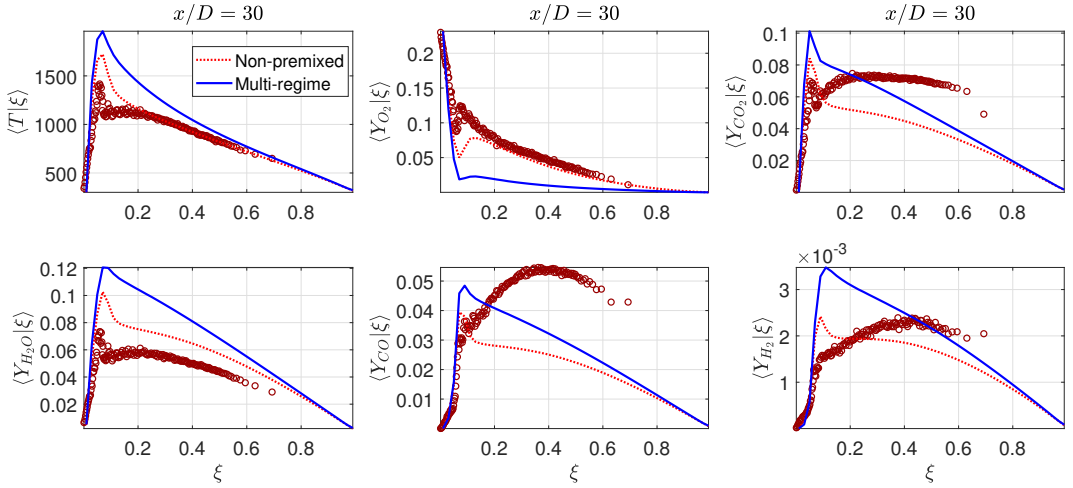

(c)

Fig. 4.34. ESMT: Conditional means of scalars in the mixture fraction space at $x/D = 10, 20$ and 30. Blue solid: multi-regime model and red dotted: non-premixed model

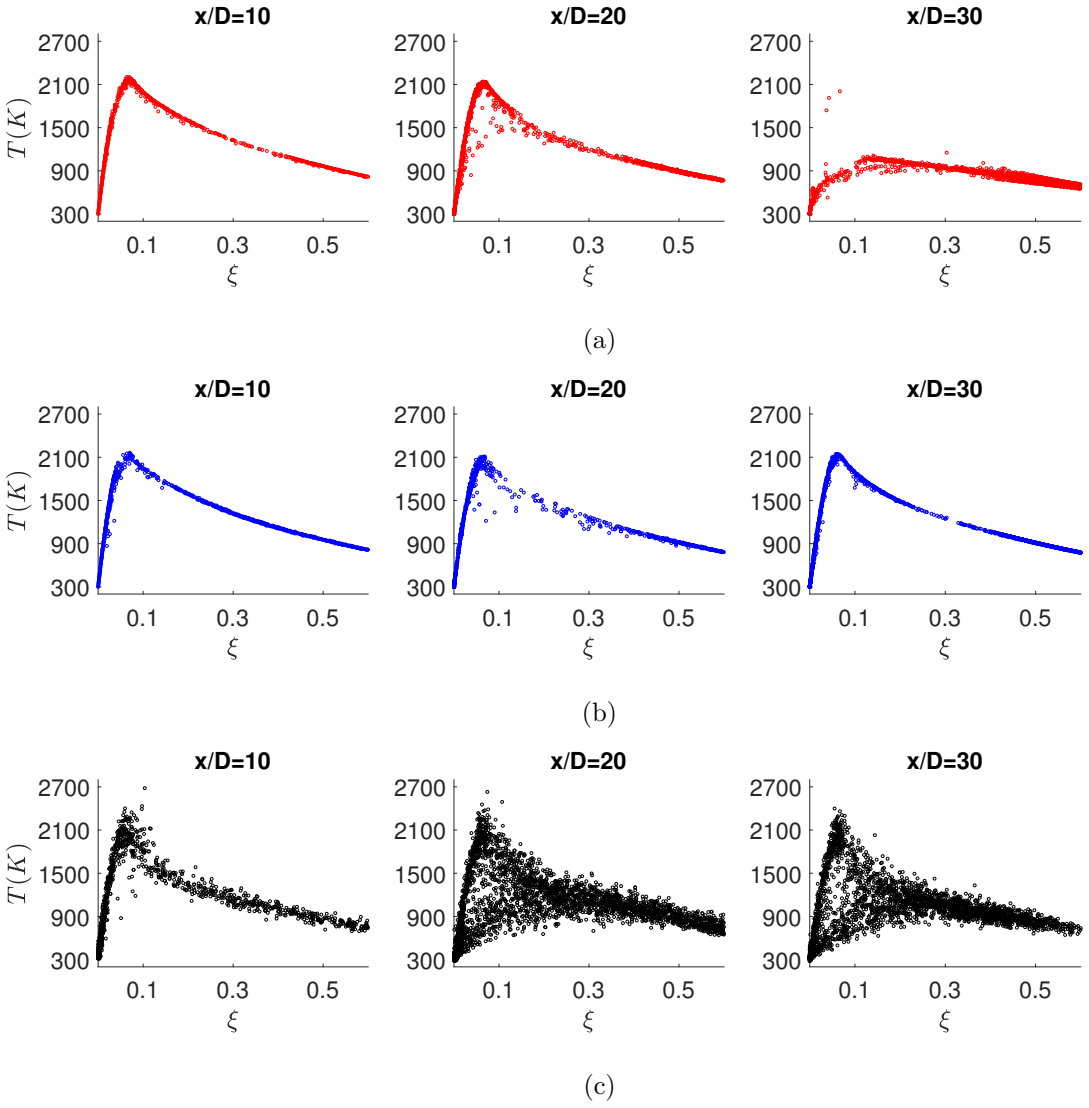

Fig. 4.35. ESMT: Temperature vs mixture fraction particle scatter plot at $x/D = 10, 20, 30$ for (a) non-premixed model, (b) multi-regime model and (c) experimental data.

5. CONCLUSIONS AND FUTURE WORK

5.1 Conclusions

In this study, a mathematical framework was provided for developing a multi-regime combustion model using LES/PDF. The model performance was assessed for the piloted jet flame, Sydney Flame L and compared against the traditional non-premixed PDF model. The following conclusion were made from the study:

- The PDF method developed for non-premixed flames [42, 48] and the PDF method developed for premixed flames [28] are identified as the constructing components of the multi-regime model.

- Flame index [34] was used as a regime identification technique. This traditional flame index definition was found to over-detect premixed combustion regime, especially upstream of the flame. This was primarily caused due to small gradient magnitudes in the field, possibly due to statistical nature of the PDF model, which resulted in wrong detection detection of premixed combustion regime.

- Thus, the flame index definition was refined based on eliminating these small gradients in the calculation for flame index. A gradient threshold parameter β was identified to calculate flame index for gradient magnitudes greater than $\beta\%$ of maximum gradient magnitude in the entire domain for fuel and oxidizer independently. This proposed refinement was found to be more accurate in predicting the regimes than the traditional definition.

- Having identified a range of 0.25% to 1% as suitable for β, three values were chosen in this study: $0.25\%, 0.5\%, 1\%$. A parametric study was performed for Flame L using these values. A value of $\beta = 0.5\%$ was found to have the most accurate prediction.

- For Sydney Flame L, the traditional non-premixed PDF model using MCurl mixing model results in significant extinction downstream of the flame. It tends to under predict the quantities when compared to the experimental data.

- The multi-regime model using $\beta = 0.5\%$ is compared against the non-premixed model for three three mixing models: MCurl, IEM and EMST. For MCurl model, the multi-regime model results in much better predictions than the non-premixed model. For IEM model, the multi-regime model produces similar better predictions. This improvement is minor due to the non-localness property of IEM. The multi-regime model using EMST tends to over-predict quantities than the non-premixed model since EMST mixing model is known to resist extinction in flames.

5.2 Future Work

Much of multi-regime modeling efforts were concentrated using the flamelet-type models. This study uses the coupled LES/PDF to develop a multi-regime model, which has never been done before. The LES/PDF multi-regime model can be improved by improving the existing non-premixed as well as premixed PDF models. Additionally, other regime identification techniques can be explored to obtain a more accurate prediction of combustion modes in the domain. More values for the parameter β can be used to get a broader understanding of the limitations of using the traditional flame index in the PDF context. More explorations can be made to understand the difference in performance of the multi-regime model using different mixing models.

Numerical simulations of the pulsed jet flames [42] shows the presence of an upper branch and lower branch after a pulse is applied to the flame. Studies done by [67] shows that simulations do not capture the two branches joining after the pulse. The current multi-regime model can be used to accurately capture the joining of the two

branches of the pulsed jet flame. Thus, this multi-regime model for PDF methods can be explored further to develop for more general combustion applications.

REFERENCES

REFERENCES

[1] "Global energy demand rose by 2.3% in 2018, its fastest pace in the last decade," Mar. 2019. [Online]. Available: https://www.iea.org/newsroom/news/2019/march/global-energy-demand-rose-by-23-in-2018-its-fastest-pace-in-the-last-decade.html

[2] BP Energy, "BP energy outlook 2019 edition."

[3] H. H. Hu, "Computational fluid dynamics," in *Fluid Mechanics*. Elsevier, 2012, pp. 421–472.

[4] D. Veynante and L. Vervisch, "Turbulent combustion modeling," *Progress in energy and combustion science*, vol. 28, no. 3, pp. 193–266, 2002.

[5] "International workshop on measurement and computaion of turbulent nonopremixed flames." [Online]. Available: https://www.sandia.gov/TNF/abstract.html

[6] S. A. Orszag and G. Patterson Jr, "Numerical simulation of three-dimensional homogeneous isotropic turbulence," *Physical Review Letters*, vol. 28, no. 2, p. 76, 1972.

[7] D. G. Fox and D. K. Lilly, "Numerical simulation of turbulent flows," *Reviews of Geophysics*, vol. 10, no. 1, pp. 51–72, 1972.

[8] B. E. Launder and B. Sharma, "Application of the energy-dissipation model of turbulence to the calculation of flow near a spinning disc," *Letters in heat and mass transfer*, vol. 1, no. 2, pp. 131–137, 1974.

[9] S. B. Pope, "Turbulent flows," 2001.

[10] ——, "Self-conditioned fields for large-eddy simulations of turbulent flows," *Journal of Fluid Mechanics*, vol. 652, pp. 139–169, 2010.

[11] C. D. Pierce and P. Moin, "Progress-variable approach for large-eddy simulation of non-premixed turbulent combustion," *Journal of fluid Mechanics*, vol. 504, pp. 73–97, 2004.

[12] K. Bray, M. Champion, P. Libby, and N. Swaminathan, "Finite rate chemistry and presumed pdf models for premixed turbulent combustion," *Combustion and Flame*, vol. 146, no. 4, pp. 665–673, 2006.

[13] D. Spalding, "Mixing and chemical reaction in steady confined turbulent flames," in *Symposium (International) on Combustion*, vol. 13, no. 1. Elsevier, 1971, pp. 649–657.

[14] S. B. Pope, "Pdf methods for turbulent reactive flows," *Progress in energy and combustion science*, vol. 11, no. 2, pp. 119–192, 1985.

[15] A. Y. Klimenko, "Multicomponent diffusion of various admixtures in turbulent flow," *Fluid dynamics*, vol. 25, no. 3, pp. 327–334, 1990.

[16] H. Pitsch and H. Steiner, "Large-eddy simulation of a turbulent piloted methane/air diffusion flame (sandia flame d)," *Physics of fluids*, vol. 12, no. 10, pp. 2541–2554, 2000.

[17] H. Wang and Y. Chen, "Pdf modelling of turbulent non-premixed combustion with detailed chemistry," *Chemical engineering science*, vol. 59, no. 16, pp. 3477–3490, 2004.

[18] Y. Yang, H. Wang, S. B. Pope, and J. H. Chen, "Large-eddy simulation/probability density function modeling of a non-premixed co/h2 temporally evolving jet flame," *Proceedings of the Combustion Institute*, vol. 34, no. 1, pp. 1241–1249, 2013.

[19] J. Xu and S. B. Pope, "Pdf calculations of turbulent nonpremixed flames with local extinction," *Combustion and Flame*, vol. 123, no. 3, pp. 281–307, 2000.

[20] E. R. Hawkes, R. Sankaran, J. C. Sutherland, and J. H. Chen, "Scalar mixing in direct numerical simulations of temporally evolving plane jet flames with skeletal co/h2 kinetics," *Proceedings of the combustion institute*, vol. 31, no. 1, pp. 1633–1640, 2007.

[21] P. Zhang, A. R. Masri, and H. Wang, "Studies of the flow and turbulence fields in a turbulent pulsed jet flame using les/pdf," *Combustion Theory and Modelling*, vol. 21, no. 5, pp. 897–924, 2017.

[22] R. Barlow and J. Frank, "Effects of turbulence on species mass fractions in methane/air jet flames," in *Symposium (International) on Combustion*, vol. 27, no. 1. Elsevier, 1998, pp. 1087–1095.

[23] V. Moureau, P. Minot, H. Pitsch, and C. Bérat, "A ghost-fluid method for large-eddy simulations of premixed combustion in complex geometries," *Journal of Computational Physics*, vol. 221, no. 2, pp. 600–614, 2007.

[24] K.-J. Nogenmyr, C. Fureby, X.-S. Bai, P. Petersson, R. Collin, and M. Linne, "Large eddy simulation and laser diagnostic studies on a low swirl stratified premixed flame," *Combustion and Flame*, vol. 156, no. 1, pp. 25–36, 2009.

[25] M. Anand and S. Pope, "Calculations of premixed turbulent flames by pdf methods," *Combustion and Flame*, vol. 67, no. 2, pp. 127–142, 1987.

[26] R. Lindstedt and E. Vaos, "Transported pdf modeling of high-reynolds-number premixed turbulent flames," *Combustion and Flame*, vol. 145, no. 3, pp. 495–511, 2006.

[27] M. Stöllinger and S. Heinz, "Evaluation of scalar mixing and time scale models in pdf simulations of a turbulent premixed flame," *Combustion and Flame*, vol. 157, no. 9, pp. 1671–1685, 2010.

[28] H. Wang, T. Pant, and P. Zhang, "Les/pdf modeling of turbulent premixed flames with locally enhanced mixing by reaction," *Flow, Turbulence and Combustion*, vol. 100, no. 1, pp. 147–175, 2018.

[29] P. Kioni, B. Rogg, K. Bray, and A. Linán, "Flame spread in laminar mixing layers: the triple flame," *Combustion and Flame*, vol. 95, no. 3, pp. 276–290, 1993.

[30] [Online]. Available: https://www.cfd-online.com/Wiki/CombustionThe_Partially-Premixed_Regime

[31] Y.-C. Chen and R. W. Bilger, "Experimental investigation of three-dimensional flame-front structure in premixed turbulent combustion: Ii. lean hydrogen/air bunsen flames," *Combustion and flame*, vol. 138, no. 1-2, pp. 155–174, 2004.

[32] Y. Mizobuchi, J. Shinjo, S. Ogawa, and T. Takeno, "A numerical study on the formation of diffusion flame islands in a turbulent hydrogen jet lifted flame," *Proceedings of the Combustion Institute*, vol. 30, no. 1, pp. 611–619, 2005.

[33] K. Luo, H. Pitsch, M. Pai, and O. Desjardins, "Direct numerical simulations and analysis of three-dimensional n-heptane spray flames in a model swirl combustor," *Proceedings of the Combustion Institute*, vol. 33, no. 2, pp. 2143–2152, 2011.

[34] H. Yamashita, M. Shimada, and T. Takeno, "A numerical study on flame stability at the transition point of jet diffusion flames," in *Symposium (International) on Combustion*, vol. 26, no. 1. Elsevier, 1996, pp. 27–34.

[35] P. Domingo, L. Vervisch, and K. Bray, "Partially premixed flamelets in les of nonpremixed turbulent combustion," *Combustion Theory and Modelling*, vol. 6, no. 4, pp. 529–551, 2002.

[36] P. Domingo, L. Vervisch, and J. Réveillon, "Dns analysis of partially premixed combustion in spray and gaseous turbulent flame-bases stabilized in hot air," *Combustion and Flame*, vol. 140, no. 3, pp. 172–195, 2005.

[37] B. Fiorina, O. Gicquel, L. Vervisch, S. Carpentier, and N. Darabiha, "Approximating the chemical structure of partially premixed and diffusion counterflow flames using fpi flamelet tabulation," *Combustion and flame*, vol. 140, no. 3, pp. 147–160, 2005.

[38] E. Knudsen and H. Pitsch, "A general flamelet transformation useful for distinguishing between premixed and non-premixed modes of combustion," *Combustion and flame*, vol. 156, no. 3, pp. 678–696, 2009.

[39] ——, "Capabilities and limitations of multi-regime flamelet combustion models," *Combustion and Flame*, vol. 159, no. 1, pp. 242–264, 2012.

[40] P.-D. Nguyen, L. Vervisch, V. Subramanian, and P. Domingo, "Multidimensional flamelet-generated manifolds for partially premixed combustion," *Combustion and Flame*, vol. 157, no. 1, pp. 43–61, 2010.

[41] A. Masri, R. Bilger, and R. Dibble, "The local structure of turbulent non-premixed flames near extinction," *Combustion and flame*, vol. 81, no. 3-4, pp. 260–276, 1990.

[42] H. Wang, M. Juddoo, S. H. Starner, A. R. Masri, and S. B. Pope, "A novel transient turbulent jet flame for studying turbulent combustion," *Proceedings of the Combustion Institute*, vol. 34, no. 1, pp. 1251–1259, 2013.

[43] J. Villermaux and J. Devillon, "Représentation de la coalescence et de la redispersion des domaines de ségrégation dans un fluide par un modele dinteraction phénoménologique," in *Proceedings of the 2nd International symposium on chemical reaction engineering*, vol. 26. Elsevier New York, 1972, pp. 1–13.

[44] J. Janicka, W. Kolbe, and W. Kollmann, "Closure of the transport equation for the probability density funcfion of turbulent scalar fields," *Journal of Non-Equilibrium Thermodynamics*, vol. 4, no. 1, pp. 47–66, 1979.

[45] S. Subramaniam and S. Pope, "A mixing model for turbulent reactive flows based on euclidean minimum spanning trees," *Combustion and Flame*, vol. 115, no. 4, pp. 487–514, 1998.

[46] J. Smagorinsky, "General circulation experiments with the primitive equations: I. the basic experiment," *Monthly weather review*, vol. 91, no. 3, pp. 99–164, 1963.

[47] D. K. Lilly, "A proposed modification of the germano subgrid-scale closure method," *Physics of Fluids A: Fluid Dynamics*, vol. 4, no. 3, pp. 633–635, 1992.

[48] H. Wang and S. B. Pope, "Large eddy simulation/probability density function modeling of a turbulent ch4/h2/n2 jet flame," *Proceedings of the Combustion Institute*, vol. 33, no. 1, pp. 1319–1330, 2011.

[49] L. Valiño, "A field monte carlo formulation for calculating the probability density function of a single scalar in a turbulent flow," *Flow, turbulence and combustion*, vol. 60, no. 2, pp. 157–172, 1998.

[50] Q. Tang, W. Zhao, M. Bockelie, and R. Fox, "Multi-environment probability density function method for modelling turbulent combustion using realistic chemical kinetics," *Combustion Theory and Modelling*, vol. 11, no. 6, pp. 889–907, 2007.

[51] A. Kazakov and M. Frenklach, "Reduced reaction sets based on gri-mech 1.2," *University of California at Berkeley, Berkeley, CA, http://www. me. berkeley. edu/drm*, 1994.

[52] M. Frenklach, H. Wang, C. Yu, M. Goldenberg, C. Bowman, R. Hanson, D. Davidson, E. Chang, G. Smith, D. Golden *et al.*, "Gri-mech 1.2," *University of California at Berkeley, Berkeley, CA, accessed Sept*, vol. 21, p. 2017, 1995.

[53] S. B. Pope, "Computationally efficient implementation of combustion chemistry using in situ adaptive tabulation," 1997.

[54] S. Pope, "The vanishing effect of molecular diffusivity on turbulent dispersion: implications for turbulent mixing and the scalar flux," *Journal of Fluid Mechanics*, vol. 359, pp. 299–312, 1998.

[55] P. Nooren, H. Wouters, T. Peeters, D. Roekaerts, U. Maas, and D. Schmidt, "Monte carlo pdf modelling of a turbulent natural-gas diffusion flame," 1997.

[56] S. S. Girimaji and Y. Zhou, "Analysis and modeling of subgrid scalar mixing using numerical data," *Physics of Fluids*, vol. 8, no. 5, pp. 1224–1236, 1996.

[57] C. D. Pierce and P. Moin, "A dynamic model for subgrid-scale variance and dissipation rate of a conserved scalar," *Physics of Fluids*, vol. 10, no. 12, pp. 3041–3044, 1998.

[58] R. R. Cao, H. Wang, and S. B. Pope, "The effect of mixing models in pdf calculations of piloted jet flames," *Proceedings of the combustion institute*, vol. 31, no. 1, pp. 1543–1550, 2007.

[59] Y. Gao, N. Chakraborty, and N. Swaminathan, "Algebraic closure of scalar dissipation rate for large eddy simulations of turbulent premixed combustion," *Combustion Science and Technology*, vol. 186, no. 10-11, pp. 1309–1337, 2014.

[60] T. Dunstan, Y. Minamoto, N. Chakraborty, and N. Swaminathan, "Scalar dissipation rate modelling for large eddy simulation of turbulent premixed flames," *Proceedings of the Combustion Institute*, vol. 34, no. 1, pp. 1193–1201, 2013.

[61] Y. Gao, N. Chakraborty, and N. Swaminathan, "Dynamic closure of scalar dissipation rate for large eddy simulations of turbulent premixed combustion: A direct numerical simulations analysis," *Flow, Turbulence and Combustion*, vol. 95, no. 4, pp. 775–802, 2015.

[62] C. Vagelopoulos, F. Egolfopoulos, and C. K. Law, "Further considerations on the determination of laminar flame speeds with the counterflow twin-flame technique," in *Symposium (international) on combustion*, vol. 25, no. 1. Elsevier, 1994, pp. 1341–1347.

[63] J. Lamouroux, M. Ihme, B. Fiorina, and O. Gicquel, "Tabulated chemistry approach for diluted combustion regimes with internal recirculation and heat losses," *Combustion and flame*, vol. 161, no. 8, pp. 2120–2136, 2014.

[64] H. Wu and M. Ihme, "Compliance of combustion models for turbulent reacting flow simulations," *Fuel*, vol. 186, pp. 853–863, 2016.

[65] A. Masri, R. W. Dibble, and R. S. Barlow, "The structure of turbulent nonpremixed flames revealed by raman-rayleigh-lif measurements," *Progress in Energy and Combustion Science*, vol. 22, no. 4, pp. 307–362, 1996.

[66] "Piloted flame database." [Online]. Available: http://web.aeromech.usyd.edu.au/thermofluids/piloted.php

[67] J. Tao, "Numerical simulations of turbulent pulsed jet flame," Master's thesis, Purdue University, 2018.